View metadata, citation and similar papers at core.ac.uk
brought to you by CORE
provided by Repositório Institucional da UFSC

UNIVERSIDADE FEDERAL DE SANTA CATARINA
DEPARTAMENTO DE ENGENHARIA MECÂNICA

Luís Paulo Laus

DETERMINAÇÃO DA EFICIÊNCIA DE MÁQUINAS COM BASE EM TEORIA DE HELICOIDES E GRAFOS: APLICAÇÃO EM TRENS DE ENGRENAGENS E ROBÔS PARALELOS

Florianópolis

2011

Luís Paulo Laus

DETERMINAÇÃO DA EFICIÊNCIA DE MÁQUINAS COM BASE EM TEORIA DE HELICOIDES E GRAFOS: APLICAÇÃO EM TRENS DE ENGRENAGENS E ROBÔS PARALELOS

Tese submetida ao Programa de Pós-Graduação em Engenharia Mecânica para a obtenção do Grau de Doutor em Engenharia Mecânica.
Orientador: Prof. Daniel Martins, Dr. Eng.
Coorientador: Prof. Henrique Simas, Dr. Eng.

Florianópolis

2011

Catalogação na fonte pela Biblioteca Universitária
da
Universidade Federal de Santa Catarina

L388d Laus, Luís Paulo
Determinação da eficiência de máquinas com base em teoria de helicoides e grafos [tese] : aplicação em trens de engrenagens e robôs paralelos / Luís Paulo Laus ; orientador, Daniel Martins. - Florianópolis, SC, 2011.
195 p.: il., grafs., tabs.

Tese (doutorado) - Universidade Federal de Santa Catarina, Centro Tecnológico. Programa de Pós-Graduação em Engenharia Mecânica.

Inclui referências

1. Engenharia mecânica. 2. Engrenagens. 3. Cinemática. 4. Eficiência. 5. Transmissão. 6. Robôs - Sistemas de controle. I. Martins, Daniel. II. Universidade Federal de Santa Catarina. Programa de Pós-Graduação em Engenharia Mecânica. III. Título.

CDU 621

Luís Paulo Laus

DETERMINAÇÃO DA EFICIÊNCIA DE MÁQUINAS COM BASE EM TEORIA DE HELICOIDES E GRAFOS: APLICAÇÃO EM TRENS DE ENGRENAGENS E ROBÔS PARALELOS

Esta Tese foi julgada aprovada para a obtenção do Título de "Doutor em Engenharia Mecânica", e aprovada em sua forma final pelo Programa de Pós-Graduação em Engenharia Mecânica.

Florianópolis, 15 de agosto de 2011.

Prof. Júlio César Passos, Dr.
Coordenador do Curso

Prof. Henrique Simas, Dr. Eng.
Coorientador

Banca Examinadora:

Prof. Daniel Martins, Dr. Eng.
Presidente

Prof. Auteliano Antunes dos Santos Júnior, Dr. Eng.
Relator

Prof. Aníbal Alexandre Campos Bonilla, Dr. Eng.

Prof. Rodrigo de Souza Vieira, Dr.

Prof. Edson Roberto de Pieri, Dr.

To my parents, Wilson (*in memorian*) and Neide, and to my wife Fabiana.

ACKNOWLEDGEMENTS

First and foremost I would like to express my sincere gratitude to Mr. T. H. Davies. He, who does not like to be called Professor, has acted as one guiding, inspiring, supporting, encouraging and sometimes, when needed, even pushing me. I am also immensely grateful to his lovely wife Marigold who is always so gentle and sweet.

The time I have spent in UK, the thinks I have learnt and the people I have met shall never be forgotten. In particular I would like to thank Prof. Mike Jackson for receiving me in Loughborough University. I am extremely grateful for the friends, Matthew Chamberlain, Tussanai Parthornratt, Senthan Mathavan, Phil Ogun, David Liddell, Vianney Lara-Prieto, Sultan Shair and his lovely wife Diana Shair, and many others that I hope to meet again. The World is a better place because of you.

I appreciate the patience and support from the colleagues, particularly, Roberto Simoni, Andrea Piga, Anelize Zomkowski Salvi, Julio Golin, Daniel Ponce Saldias, and Carlos Rodrigues Rocha. For the help with CAD model, I am thankful to Prof. Dr. Altamir Dias and the interns Helena Albino and Izabele Saorin.

I wish to express my gratitude to my supervisor, Prof. Dr. Daniel Martins, and co-supervisor Prof. Dr. Henrique Simas, and the whole university staff.

My gratitude also extends to institutions that have supported my work: UFSC (Federal University of Santa Catarina) for accepting me as doctoral student; UTFPR (Federal University of Technology – Paraná) for granting me a leave; the Brazilian Federal Agency for Support and Evaluation of Graduate Education - CAPES *(Coordenação de Aperfeiçoamento de Pessoal de Nível Superior*) for providing a grant; Loughborough University for receiving me as visiting student. To all the colleagues with UTFPR who have carried a heavy burden in my absence, I would like to say thank you very much. I am partially grateful to the members of the automation group of the Academic Department of Mechanics: Leandro Magatão, Paulo Humberto Ferrazza, Marcelo W. W. Zibetti, Luiz Carlos de Abreu Rodrigues, Celso Salamon, Francisco Gödke, Ruy Nakayama, and João Antonio Palma Setti.

I wish to thank my parents, Neide Bassetti Laus and Wilson Gomes Laus (*in memoriam*). They have bore me, raised me, supported me, taught me, and loved me.

In finally, and most importantly, my beloved wife Fabiana, I thank you for all patience and support with all my heart and love.

Science is nothing but perception.

Plato

RESUMO

Nesta tese o problema da determinação da eficiência mecânica de máquinas é resolvido através da adaptação do Método de Davies. O método proposto é baseado nas teorias de grafos e helicoides e pode ser aplicado a qualquer máquina. Trens de engrenagens e robôs paralelos são usados como exemplos. O Método de Davies é modificado para incluir acoplamentos ativos que permitem que potência entre e saia da rede de acoplamentos. Com esta modificação, é possível modelar atrito como análogo da resistência elétrica, fontes de torque como fontes de corrente e fontes de velocidade como fontes de tensão. Os modelos de atrito podem incluir efeitos que dependem da velocidade e da carga. Fontes de perda, como atrito de engrenamento, atrito em mancais, selos e acoplamentos, podem ser levados em conta. São apresentados exemplos e os resultados são comparados com estudos anteriores encontrados na literatura.

No Capítulo 1 são definidos os objetivos e o escopo do trabalho. É explicado que a tese é dividida em duas grandes áreas tratando da determinação da eficiência de: 1) trens de engrenagens complexos e 2) máquinas complexas com ênfase em robôs paralelos. É apresentada a revisão bibliográfica destas duas áreas e listadas as contribuições feitas a essas áreas e ao Método de Davies.

Uma revisão do Método de Davies é apresentada no Capítulo 2. Nesse capítulo também é apresentada a notação e discutido como as ações externas a uma rede de acoplamento podem ser levadas em conta usando o Método de Davies. A forma com que essas ações externas são internalizadas difere dos métodos apresentados previamente na literatura.

O Capítulo 3 trata da determinação analítica da eficiência de trens de engrenagens complexos. São apresentadas definições com destaque para o fluxo de potência real e virtual. A distinção entre esses fluxos é feita com base na incidência da entrada e saída no elo de referência do trem de engrenagens, o que constitui a principal diferença entre as definições apresentadas aqui e as encontradas na literatura. O caráter estacionário do elo de referência, comumente usado por outros pesquisadores para distinguir esses dois conceitos, é refutado por ser arbitrário e ambíguo. A noção amplamente difundida de que a ação responsável pelas perdas em um engrenamento é um torque puro – portanto um helicoide de ação de passo infinito – é formalizada e provada usando teoria de

helicoides para os casos onde os eixos das engrenagens se cruzam ou são paralelos. O escopo do trabalho é, portanto, limitado a esses dois casos. É apresentado como este *torque de atrito*, em alusão à *força de atrito*, pode ser modelado.

São apresentados três exemplos. O primeiro exemplo é introdutório e tem por objetivo ilustrar a notação e a construção das matrizes. Este exemplo é dividido em três subexemplos: no primeiro é considerado o atrito de Coulomb no engrenamento apenas; no segundo é incluído atrito de Coulomb nos mancais; e no terceiro é considerado o atrito de Coulomb no engrenamento bem como atrito viscoso no engrenamento e nos mancais. A introdução de modelos de atrito dependentes da magnitude da velocidade requer uma alteração nas equações de Davies similar à introdução de fontes dependentes na elétrica. É importante notar que o trem de engrenagens usado é simples o bastante para que as equações obtidas sejam verificadas intuitivamente.

No segundo exemplo é analisado um trem epicicloidal de engrenagens. Nesse exemplo os efeitos de rede de acoplamento se fazem mais perceptíveis. O fluxo de potência virtual é usado para determinar a relação de motora/movida de cada par de engrenamento o que é importante para estabelecer a relação entre o coeficiente de atrito ζ e a eficiência ordinária de cada par η. Também é mostrado que a eficiência global depende da entrada e da saída (uma troca de entrada e saída pode implicar em alterações na equação final) e de relações geométricas do mecanismo, ou seja, de relações entre os raios primitivos. Assim, quatro equações são obtidas. O exemplo termina com a questão de raio primitivo e número de dentes.

No terceiro e último exemplo deste capítulo é obtida uma equação para a eficiência do trem de engrenagens cônicas de Humpage. O objetivo principal do exemplo é mostrar a aplicação do método desenvolvido a trens de engrenagens cônicas. A questão de multiplicidade de soluções é mais complexa nesse caso que no exemplo anterior: são três condições geométricas que, combinadas com a questão de entrada e saída, levam a um total de dezesseis equações para a eficiência global. É bastante provável que esta seja a primeira vez que se obtém uma equação para eficiência desse trem de engrenagens. Essa equação é validada com resultados numéricos obtidos na literatura.

O Capítulo 4 trata da determinação da eficiência de máquinas complexas. O método desenvolvido é geral e pode ser aplicado em máquinas complexas com cadeia cinemática aberta e fechada. Considerar perdas em uma cadeia cinemática requer que os acoplamentos sejam modelados de forma mais próxima à construção real da máquina. É mos-

trado em detalhes como juntas prismáticas e cilíndricas são tratadas. Dois exemplos são apresentados. No primeiro exemplo um mecanismo biela-manivela é usado para mostrar como as matrizes e equações são montadas e é discutida na prática a questão de localização das forças. No segundo exemplo é calculada a eficiência de um manipulador espacial de três graus de liberdade chamado de 3-UPU. É descrito em detalhes como o manipulador é modelado com ênfase no modelo dos acoplamentos. O problema de determinar a eficiência da 3-UPU é muito complexo para ser tratado por *software* de processamento simbólico, como nos casos anteriores, o que demandou a criação de um *software* específico para simular a execução de tarefas por esse manipulador.
Duas tarefas foram simuladas. A primeira consiste em levantar uma carga constante, em linha reta e com velocidade constante. O objetivo desta tarefa é avaliar a eficiência do manipulador. É uma tarefa simples, reprodutível em outras máquinas o que favorece a comparação de resultados, e não ocorrem inversões do sentido de movimentos. A forte dependência da eficiência de máquinas complexa com a tarefa sendo executada é evidenciada pela variação da potência dos atuadores ao longo da execução da tarefa. É mostrado que simplificações comuns na literatura levam a resultados irreais.
A segunda tarefa tem por objetivo avaliar o método empregado e consiste em mover uma carga constante através de uma trajetória elíptica. O comportamento obtido é exatamente o que se espera de um sistema não-linear. Ocorrem várias descontinuidades, pontos cuspidais e mudança de tendência nos gráficos das magnitudes das ações e das potências. Cada um desses fatos está relacionado com mudança de sentido de movimento em alguma junta.
No Capítulo 5 são traçadas as conclusões e discutidos trabalhos futuros. Algum material adicional é fornecido nos apêndices. O Apêndice A trata da eficiência ordinária de um par de engrenagens cilíndricas de dentes retos de perfil evolvente. É obtida uma equação para eficiência e o resultado numérico é comparado com um resultado clássico da literatura. O Apêndice B e C trazem as tabelas descrevendo os helicoides de ação e movimento do segundo e terceiro exemplos do Capítulo 3. O Atrito em mancais cilíndricos é discutido e modelado no Apêndice D. Finalmente, as relações duais entre as equações de Davies são discutidas no Apêndice E que traz também alternativas para a montagem das matrizes de ações e movimentos normalizados de rede bem com um método para determinar todas as ações e movimentos da rede com base em um conjunto mínimo dessas ações e movimentos.
A principal contribuição é a extensão do uso do Método de Davies

para casos onde a perda de potência deve ser considerada. Mais especificamente:
• o problema de internalização de ações foi resolvido de forma mais direta e com menor impacto sobre o modelo do sistema que os métodos anteriormente apresentados na literatura;
• o método obtido é geral e não requer considerações particulares a cada caso além do modelo de atrito;
• a analogia com o estudo de redes elétricas é reforçada com a inclusão de fontes e elementos dissipativos;
• os análogos às fontes de correntes não estão mais relacionados exclusivamente às ações super-restritas da cadeia cinemática;
• o espaço nulo das matrizes de rede é usado para determinar os conjuntos de variáveis candidatas a variáveis primárias dos modelos cinemático e estático;
• potência e fluxo de potência são definidos e comparados com as definições anteriores encontradas na literatura;
• a noção de um sistema de coordenadas estacionário é substituída pela de um sistema de coordenadas de referência atrelado a um corpo comum à entrada e saída;
• é apresentado um método sistemático para o cálculo de fluxo de potência;
• a ideia amplamente aceita de que a ação responsável pela perda de potência em um engrenamento é um torque puro é formalizada e demonstrada usando Teoria de Helicoides;
• o uso de valor médio para potência é adaptado do conceito similar da Engenharia Elétrica;
• é deduzida uma equação para eficiência do trem de engrenagens cônicas de Humpage;
• uma vez que a eficiência depende da entrada e saída bem como das dimensões dos componentes, foi desenvolvido um método para reusar a fórmula de eficiência deduzida para um caso para os demais possíveis casos;
• é proposto um método para estimar a eficiência de máquinas paralelas (e.g. robôs paralelos) mesmo antes da efetiva construção;
• o método considera as ações nos acoplamento de forma mais exata que os métodos anteriores e por isso é considerado mais exato;
• este método é baseado na propagação de ações e movimentos pela rede o que o distingue de métodos variacionais e de energia.

Palavras-chave: eficiência, trens de engrenagens cônicas e cilíndricas, transmissões, eficiência de máquinas complexas, eficiência de robôs paralelos, perda de potência

ABSTRACT

Title: **Machine Efficiency Determination Using Graph and Screw Theories : Application to Gear Trains and Parallel Robots**.

The problem about determination of the mechanical efficiency of machines is solved by a new method based on graph and screw theories. The proposed method can be applied to any machine. Gear trains and parallel robots are used as examples. The well known Davies' method is modified to include active couplings that allow power to enter or leave a coupling network. With this modification, it is possible to model friction as analogous of electrical resistance, torque sources as current sources, and velocities sources as voltage sources. The friction models can include load and speed-dependent effects. Loss sources such as gear meshing friction, bearing friction and seal friction can be taken into account. Examples are presented and the results compared with those of previous studies.

Keywords: efficiency, bevel gear train, gear train, transmission, complex machine efficiency, parallel robot efficiency, power lost

LIST OF FIGURES

LIST OF TABLES

NOMENCLATURE

$\lvert\cdot\rvert$	absolute value operator
$\dagger$	Moore-Penrose pseudoinverse of a matrix
$\bullet$	inner product of action screw by motion screw
α	pressure angle
a, b, ...	general-purpose variables normally used to shorten long expressions
$[\boldsymbol{A}]_{d\times C}$	action matrix of a coupling network in terms of C_N primary variables
$[\boldsymbol{A}]_{d\times e}$	condensed version of $[\boldsymbol{A}]_{d\times C}$ with one column for each coupling
$\left[\hat{\boldsymbol{A}}_D\right]_{d\times C}$	unit action matrix of the direct couplings
$[\boldsymbol{A}_i]_{n-1\times e}$	reduced incidence matrix of G_C
$[\boldsymbol{A}_l]_{d\,l}$	vector of the $d\,l$ action system components for all l circuits
$\left[\hat{\boldsymbol{A}}_N\right]_{d\,k\times C}$	network unit action matrix of a coupling network N
b_i	coefficient of viscous friction
$[\boldsymbol{B}]_{l\times e}$	circuit matrix of G_C
$[\boldsymbol{B}_M]_{l\times F}$	circuit matrix of G_M
C	gross degree of constraint of a coupling network $= \sum c$
c	gross degree of constraint of a direct coupling
C_N	net degree of constrain of a coupling network
d	minimum order of the screw system to which all motion and action screws under consideration belong, $1 \leq d \leq 6$

$\operatorname{diag}(\cdot)$	diagonal matrix of a vector
$[\boldsymbol{D}_A]_{d\,k+g+s\times C}$	augmented action matrix
e	number of couplings in a coupling network and edges of G_C
η	overall efficiency of a coupling network
$\eta_{i\,j}$	ordinary efficiency of a gear coupling when gear i drives gear j
F	gross degree of freedom of a coupling network $= \sum f$
f	gross degree of freedom of a direct coupling
F_N	net degree of freedom of a coupling network
g	number of constitutive equations
$\mathfrak{g}$	general function
G_A	action graph
G_C	coupling graph
G_M	motion graph
h	screw pitch
ISA	instantaneous screw axis
k	number of independent cutsets of graph G_C
l	number of independent circuits (loops) of graph G_C
$[\boldsymbol{M}]_{d\times F}$	motion matrix of a coupling network in terms of F_N primary variables
$[\boldsymbol{M}]_{d\times e}$	a condensed version of $[\boldsymbol{M}]_{d\times F}$ with one column for each coupling
$\left[\hat{\boldsymbol{M}}_D\right]_{d\times F}$	unit motion matrix of the direct couplings
$[\boldsymbol{M}_i]_{d\times n-1}$	absolute motion matrix of a coupling network

$[\boldsymbol{M}_k]_{d\,k}$	vector of the $d\,k$ motion system components for all k cutsets
$\left[\hat{\boldsymbol{M}}_N\right]_{d\,l\times F}$	network unit motion matrix of a coupling network N
N	coupling network
n	number of links in a coupling network and nodes of G_C
$\mathcal{N}$	normal pressure distribution law
$\boldsymbol{\nu}$	dependent sources vector
$\mathcal{P}$	power expended by an action screw on a motion screw
$\vec{P}$	moment vector at the origin
$\vec{p}$	angular velocity vector
$[\boldsymbol{\Psi}]_C$	vector of magnitudes of action screws
$[\boldsymbol{\psi}]_F$	vector of magnitudes of motion screws
$\vec{Q}$	force vector
$\vec{q}$	linear velocity vector of the point on a link instantaneously at the origin
$[\boldsymbol{Q}]_{k\times e}$	cutset matrix of coupling graph G_C
$[\boldsymbol{Q}_A]_{k\times C}$	cutset matrix of action graph G_A
r_i	radius of gear i
$\vec{\rho}$	position vector
ϱ_i^{a}	action screw magnitude of coupling i
ϱ_i^{m}	motion screw magnitude of coupling i
$\{r,\, s,\, t;\, u,\, v,\, w\}$	motion screw components in axis formation
$\{R,\, S,\, T;\, U,\, V,\, W\}$	action screw components in ray formation
s	number of dependent sources

$\vec{\sigma}$	position vector
$\operatorname{sign}(\cdot)$	sign or signum function of a real value
$\$_i^{\mathbf{a}}$	action screw of coupling i
$\$_i^{\mathbf{m}}$	motion screw of coupling i
$\hat{\$}_i$	normalised screw of coupling i
t	time
$\mathcal{W}$	mechanical work
z_i	number of teeth of gear i

CONTENTS

1 INTRODUCTION

If we knew what it was we were doing, it would not be called research, would it?

Albert Einstein

While commonly neglected because it is difficult to model and poorly understood, friction is present to some degree in all mechanical systems [1]. Although friction may be a desirable property, as it is for brakes, it is also responsible for power loss that reduces efficiency. The literature relevant to friction is very widely scattered; important ideas are to be found in journals of controls, tribology, lubrication engineering, acoustics, and general engineering and physics [2].

In multibody systems, friction modelling presents two aspects: the local model and the global effects. The local model is studied by tribology, a vigorous branch of science [2]. The global effects are usually studied in the specific field that made use of the friction model. In this thesis, two fields are treated: gear trains and parallel robots.

The parallel robots focus rests on the mechanical structure of the manipulator. Therefore, the machines studied herein are not necessarily robots and a broader term, like parallel complex machines, might be used. Nevertheless, the approach followed by others is regarded as of lower accuracy when compared with the method developed herein due to a common simplification that ignores the non-linear behaviour found when complex actions are applied to joints.

Gear trains are studied herein because of their high applicability and, consequently, high economical and environmental interest. A second motive is that there is no general method of easy automation available for efficiency determination. The general method proposed by Chen and Angeles [3] demands *ad-hoc* reasoning even considering the improvements by Chen and Liang [4].

The approach adopted herein uses an adaptation of Kirchhoff's laws to multibody systems based on the representation of a kinematic chain by a graph proposed by Davies [5]. Further contributions to the method by others are reported in Chapter 2.

As it must become clear throughout the text, efficiency determination requires friction models that are very specific for each intended

application. Moreover, the available data differs from one case to another. Simple or ordinary gear train efficiency is usually available and it can be used in the overall efficiency expression. For bearings, only the geometry and material are normally known. Therefore, the problem of gear train and robot efficiency are treated independently. More specific introduction with literature review are presented in Sections 1.1 and 1.2.

1.1 GEAR TRAINS EFFICIENCY

It is well known that the mechanical efficiency of gear trains is usually much lower than that of a simple (or ordinary) gear pair. The main reason for this is the power recirculation [6]. Many methods have been proposed for gear train analysis and synthesis, each with its own limitations. For efficiency analysis, perhaps the two most serious limitations are the need for *ad-hoc* reasoning and the lack of generality. The great majority of the available methods do not apply to bevel gear trains [7]. In this thesis, an approach based on a combination of graph and screw theories is proposed. Through the application of this method, the analytical expression for efficiency is obtained based on a short and systematic description of the gear train. The process is automated using a computer algebra system. The gear trains analysed have only one degree of freedom.

1.1.1 Previous studies on gear train efficiency

In his classical work of 1949, Buckingham [8] provides formulae for estimating the efficiency of a simple (or ordinary) gear pair considering geometrical and material aspects of the meshing teeth. However, the systemic effect that explains why the efficiency of a complex gear train is so low is not addressed. One of the earliest studies on gear train efficiency computation was carried out by Macmillan [9]. His method, and many other later methods, is based on the assumption that the torques and power flow are independent of the motion of the observer who measures them. Tuplin [10] explained that the low efficiency achieved by an epicyclic gear reducer is due to the high torque at the output combined with high relative speed.

An atlas for gear train efficiency computation based on power flow diagrams similar to graphs was assembled by Glover [11]; but no

details regarding the method adopted are provided. This omission has also been noted by other researchers [12].

Network theory, as well as graph theory, has been applied to epicyclic gear train analysis [13]. Perhaps the most important result of graph theory applied to gear train analysis is the theorem developed by Buchsbaum and Freudenstein [14] that relates the gear pairs to a spanning tree of the graph. The same authors also showed that in geared kinematic chains, the number of turning (revolute) pairs exceeds the number of gear pairs by the degree of freedom of the mechanism obtained from the chain.

A graph based procedure for kinematics and statics analysis addressing power flow has been proposed by Freudenstein and Yang [15]. A method for force analysis based on power flow has been presented by Saggere and Olson [16]. Pennestrì and Freudenstein [12] proposed a table-based algorithm for computation of the efficiency of epicyclic spur gear trains.

The first method that does not rely on power flow was proposed by Castillo Granado [17]. Application of his method is restricted to parallel axes gear trains, in which the driven/driver relationship of each gear pair can be determined using the sensitivity of the speed ratio. The ratios between inputs and outputs can be determined by a number of methods including that of Davies [18].

Experimental and theoretical results are compared by Mantriota and Pennestrì [19]. Their work is one of the few studies that use a friction model instead of ordinary efficiency. In the present thesis, the relationship between these two features is elucidated.

White [6] recognises the importance of power flow recirculation and proposes a method for identifying arrangements to avoid it in the synthesis of two-stage epicyclic gear trains.

Numerical efficiency analysis of cylindrical and bevel gear trains is performed by Nelson and Cipra [7]. Their method is one of the rare approaches which addresses bevel gears, but it is limited to gear trains whose input and output axes are collinear. The same authors also analysed the spur gear train used by Tuplin [10] and Pennestrì and Freudenstein [12], but their findings are considered to be discrepant by Chen and Angeles [3].

The concept of virtual power flow and virtual power ratio are introduced by Chen and Angeles [3] and used for efficiency determination. The uncertainty regarding the correct number of equations, and the need for *ad-hoc* reasoning in the application of the virtual power ratio disfavour the automatic utilisation of the method.

In a recent paper, the Chen and Angeles [3] method is improved by the use of sources and some simplifications [4].

All of the aforementioned research used some equivalent form of the kinematic equation proposed by Davies [20, 21], but with the number of dimensions equal to one. Consequently, the network equations contain only the summing and subtraction of the angular speed variables; the speed ratio equations must be assembled separately to attain the total number of equations. However, using a higher number of dimensions, all equations required can be obtained using an integrated network approach. Similar conclusion can be reached for statics.

1.1.2 Objectives

The primary objective is to obtain a new method to determine the global efficiency of a generic gear train in terms of the efficiency of each gear coupling, namely the ordinary efficiency, whilst allowing the inclusion of other power loss sources into the model. These loss sources can model the power lost in bearings or seals, for instance, and may or may not be expressed in terms of their efficiency.

A secondary objective is to express the global efficiency in terms of coefficient of frictions or other frictional parameters. This allows the use of arbitrarily complex friction models, but requires the knowledge of the frictional parameters.

In keeping with the scope limits, the gear trains analysed have only one degree of freedom and gear axes are parallel or intersect. However, the method can be applied to any gear train. There are no geometrical nor topological limitations.

1.2 COMPLEX MACHINES EFFICIENCY

Generally, in robotics, efficiency is considered to be of minor importance and the literature in this area is scarce. One fact that contributes to this scenario is the relatively low power required by a typical serial robot. However, the high load capacity of parallel robots is beginning to modify this perception. Craig [22] estimates that, on average, around 25 % of the motor torque magnitude is spent on overcoming joint friction. Even considering that the average energy use of the parallel manipulator was determined to be 26 % that of the

serial manipulator [23], efficiency may have a crucial role given the high amount of energy involved in some parallel robot applications.

The availability of accurate loss models allows the evaluation of efficiency before the manufacturing of the robot. Thus, efficiency can be used as a decision criterion in the selecting between different parallel robot structures.

The friction models can be divided into two parts: friction action magnitude and geometrical support for the friction action. Friction action magnitude, being a prerequisite for friction modelling, is well covered in the literature [2]. The geometrical considerations and their repercussions on the friction action magnitude have not received the attention they merit, as shown in Section 4.1. The key feature to achieve a realistic model is the accuracy with which the actions are represented.

1.2.1 Previous studies on friction in parallel robots

A small number of authors have addressed the issue of friction in parallel robots. Dupont [1] recognises that the normal forces in robot components vary with joint position, velocity, and acceleration. However, in his prismatic joint model, Dupont [1] attributes the losses exclusively to the rubbing between the screw and nut threads. The friction between the sliding pairs is neglected. Dupont [1], also points out that it is not necessarily correct to use a simple aggregate friction model at each joint to cope with all possible frictional effects.

Tischler, Lucas and Samuel [24] use the equation (3) (see Table 1) to model friction in multi-loop linkages. A motion graph [20, 21] was used and external actions are internalised by adding paths to the graph. This choice unnecessarily increases the number of variables. Tischler, Lucas and Samuel [24] consider the magnitudes of the friction actions as independent quantities found by multiplying the magnitudes of the actions transmitted through a coupling by a coefficient of friction in a linear manner. The process iterates until the solution converges. It seems that Tischler, Lucas and Samuel [24] do not consider that friction action may be highly non-linear as explained in Section 4.1. It is clear that the torque transmitted by the coupling is ignored in the friction model.

Dmitry [25] developed and implemented the method for distributed simulation of mechanical systems. The result is claimed to be an exact, non-iterative algorithm that is applicable to mechanisms

with any joint type and any topology, including branches and kinematic loops. Two examples are provided: a serial robot and a car suspension. Since no friction model was detailed, it is likely that Dmitry [25] also neglects the friction modes discussed in Section 4.1.

The solution of a non-linear set of differential equations, termed *stiff differential equations*, that comes from the modelling process is addressed by Farhat et al. [26]. The friction model used was proposed in a previous paper by the same research group [27] and includes friction only in the actuator, similarly to Dupont's [1] model.

1.2.2 Objectives

The focus of this study is the network effects of friction loss. The objective is the establishment of a general method, easily adapted to any friction model, to evaluate the efficiency of complex machines possibly containing loops in their kinematic chain.

In order to allow the use of arbitrary friction models, the complex actions transmitted by the couplings are taken into account without excessive simplification. Specifically, the effects produced by torques transmitted by couplings, and not only forces as in the case of previous studies, are considered when applying the friction model.

1.3 CONTRIBUTIONS TO SCIENCE AND TECHNOLOGY

This thesis contributes for the accuracy of parallel robot efficiency models and for the generality of gear train efficiency models. Contributions to specific fields are as follows.

1.3.1 Davies' method

The contributions for the Davies' method include:

- Development of a new method for action internalisation that is more straightforward than methods described by Davies; Davies and Laus; and Tischler, Lucas and Samuel [20, 24, 28, 29].
- Inclusion of dissipative elements in the coupling network analogous to electrical resistor.
- Inclusion of active elements in the coupling network analogous to

electrical sources.

- The use of null space for determination of the primary variable candidates.

1.3.2 Gear trains

A new method to determine the efficiency of complex gear trains based on graph and screw theories is presented. This method can be used for obtaining the analytical expression of any gear train where the meshing gear axes are parallel (cylindrical gears) or intersecting (bevel gears). There are no other limitations common to gear train analyses like the need for collinearity of the input and output [7] or parallelisms [17]. Extension to skew axes case is straightforward. Losses in gear meshing and bearing can be included and complex friction model can be used. It is perhaps the first truly generic method made available since *ad-hoc* reasoning is avoided.

Some theoretical contributions include:

- Real and virtual power flow are defined and compared with previous definitions in the literature.
- Use of null space to solve the conceptual problem posed by multiple solutions.
- The notion of stationary frame is refuted.
- A systematic method for power flow computation is presented.
- The generally accepted notion that the action responsible for power loss is a pure torque is formalised and proved using screw theory.
- The average (or RMS) idea for mechanical systems is adapted from its analogue on electrical network theory.

Three examples are presented and, probably for the first time, an equation for Humpage bevel gear overall efficiency is published. A coefficient of torque friction is defined and related with simple or ordinary efficiency.

Since efficiency equations are dependent on the gear train input/output and gear dimensions, a method for reuse the efficiency formula devised for one situation to obtain the formula for the other situations was developed and presented herein.

1.3.3 Parallel robots

The method for gear train efficiency determination is extended to parallel robots or parallel complex machines efficiency analysis resulting in an increase in model accuracy when compared with previous works [1, 24, 26, 27].

It is noted that, in complex machines, the efficiency is dependent upon the specific task. Therefore, the concept of an overall efficiency valid for all situations is futile.

Friction in prismatic and cylindrical pairs can be modelled by the method described in Chapter 4 with the advantage that, when considering the correct location of the transmitted forces, a higher accuracy may be achieved.

The method presented in this work wider the application of the equations presented by Davies [20, 21] to the case where power lost has to be considered. It represents an option to the use of energy and variational methods to evaluate the efficiency of machines with closed kinematic chain.

1.4 THESIS OUTLINE

A quick review of Davies' equations including a literature survey is presented in Chapter 2. Also in that chapter, the notation and action internalisation are addressed. In Chapter 3 the efficiency gear trains are covered and a truly generically method for efficiency computation is proposed. The efficiency of complex machines is treated in Chapter 4. Conclusions are given in Chapter 5. It was considered during the elaboration of this document that readers might be interested in gear trains or parallel robots, but seldom in both issues. For this reason, a minimal redundancy between Chapters 3 and 4 was intentionally left.

The instantaneous efficiency analysis of an involute spur gear train is given in Appendix A. Motion and action tables for some examples of Chapter 3 are given in Appendices B and C. Friction in cylindrical journal bearings is discussed and modelled in Appendix D. Finally, the dual relationship between equations (56) and (19), the available alternatives for assembling the network unit motion and action matrices, and topological relationships that allow the determination of all network motion and actions from a minimal set are given in Appendix E.

2 LITERATURE REVIEW, NOTATION, AND ACTION INTERNALISATION

The Lord had the wonderful advantage of being able to work alone.

Kofi Annan

In this chapter, Davies' equations are reviewed, which includes a brief literature review. The notation for screws is presented with emphasis in power computation. Finally, a new approach for internalisation of action external to a coupling network is introduced.

2.1 DAVIES' EQUATIONS

The adaptation of Kirchhoff's laws to multibody systems is based on the representation of a coupling network by a graph, called a *coupling graph*, in which every link (body) is represented by a node and every direct coupling between links by an edge. Thus, the edge variables model the actions transmitted by the coupling (through variable) and the motions allowed by the coupling (across variable). These variables differ from their electrical counterparts in two aspects. Firstly, every motion and every action is geometrically a screw requiring d coordinates where $1 \leq d \leq 6$. Secondly, a coupling can transmit/allow up to d independent actions/motions. For a network of links and couplings the equivalent of the Kirchhoff voltage and current laws are provided by Davies [5]. Another two equations based on virtual power are also presented by Davies [20, 21]. These four equations, reproduced in Table 1, provide relationships between the magnitudes of the motions (first order kinematics) that pairs of links can experience which are attributable to underconstraints, and between the magnitudes of actions that may exist which are attributable to overconstraints. In Sections 3.3.3 and 3.4.1.1 the use of equations (2) and (1), respectively, is exemplified in detail.

The solution of equation (1) is analogous to the solution of the network equations of an electrical network containing only interconnected voltage sources. Likewise, the solution of equation (2) is analogous to the solution of the network equations of an electrical

network containing only interconnected current sources. Herein, to the best of the author's knowledge the mechanical analogue of the electrical resistance is introduced for the first time in mechanical network equations (1-4) to model the power loss attributable to friction.

The alternatives for assembling the network unit motion and action matrices ($\hat{\boldsymbol{M}}_N$ and $\hat{\boldsymbol{A}}_N$) are presented in Appendix E.

2.1.1 Literature review

Davies [5] adapted Kirchhoffs circulation law for potential difference to the purpose of finding a set of independent instantaneous screws associated with any two links in a kinematic chain when the configuration of the kinematic chain is given. The procedure leads to a constraint matrix formulation and the rank calculation and is applicable to any kinematic chain: it does not require special cases to be identified [30]. In a set of three papers on mechanical networks, Davies [31, 32, 33] addressed: passivity and redundancy of mobile and immobile mechanical networks [31]; a formulae for the degrees of mobility and redundancy [32]; and network actions [33]. Later, he discussed couplings, coupling networks and their graphs attempting to normalise some definition [28]. Freedom and constraint in coupling networks and virtual power were treated in reference [21]. Duality was addressed in references [34, 35] and Tellegen's Theorem in [29].

Other researchers have applied Davies' equations. Baker [36] used these equations in the study on lack of structural rigidity. Baker and Hon-Cheung [37] revised some studies on kinematics of planar and spatial mechanism. Baker [38] continued this work on Bennett linkages. Later on, Baker [39] correlated the chemical conformational analysis methods with those of spatial kinematic chains. Huang, Tao and Fang [40] applied the concept of reciprocal screws in 3-dof spatial parallel robots. Bulca [41] used Davies' equations for workspace analysis of mechanism. Tischler, Lucas and Samuel [24] used the equation (3) on modelling friction in multi-loop linkages. Tischler, Samuel and Hunt [18] employed Davies' equations in the development of concept of variety of a kinematic chain and explained how this concept can be used to select a suitable kinematic chain for a specific motion task. Zoppi, Zlatanov and Molfino [42] have considered the Davies' method the standard for obtaining the passive joint speeds in terms of those of the active joints. They also propose a general method for passive joint speed elimination from the velocity equations.

Table 1 – Four equations that express constraints on motions and actions that can exist within mechanical coupling networks

Motion analysis	Action analysis
An adaptation of Kirchhoff's voltage law $\left[\hat{\boldsymbol{M}}_N\right]_{d\,l\times F}\,[\boldsymbol{\psi}]_F = [\mathbf{0}]_{d\,l}$ (1)	An adaptation of Kirchhoff's current law $\left[\hat{\boldsymbol{A}}_N\right]_{d\,k\times C}\,[\boldsymbol{\Psi}]_C = [\mathbf{0}]_{d\,k}$ (2)
Virtual actions and power $\left[\hat{\boldsymbol{A}}_N^T\right]_{C\times d\,k}\,[\boldsymbol{M}_k]_{d\,k} = [\mathbf{0}]_C$ (3)	Virtual motions and power $\left[\hat{\boldsymbol{M}}_N^T\right]_{F\times d\,l}\,[\boldsymbol{A}_l]_{d\,l} = [\mathbf{0}]_F$ (4)

In the "Prof. Raul Guenther Robotics Laboratory" at the Federal University of Santa Catarina, the works connected to Davies' equations have initiated with the study on hierarchical kinematic analysis of robots [43,44]. Campos Bonilla [45] employed the equations in differential kinematic of robots culminating in the *Davies' method*. Cooperative robot kinematics was treated by Dourado [46]. Santos [47] has studied the movement of a submarine robot using artificial intelligence and hybrid systems. The Davies' method was used by Cruz [48] for smoothing velocities and accelerations discontinuities in trajectory generation. Simas [49] has developed a collision avoidance method for trajectory generation. Gear trains have been addressed by Cazangi [50]. Erthal [51] has studied automotive suspensions.

2.2 SCREW NOTATION AND POWER

The notation introduced by Davies [20, 21, 29, 35] is adopted herein again with some extensions. The minimum order of the screw system to which all motion and action screws under consideration belong is the dimension d ($1 \leq d \leq 6$); k and l are the numbers of independent cutsets and circuits (loops); and C and F, the gross degrees of constraint and freedom, are the sums of the degrees of constraint c and freedom f of all couplings, respectively. Each column of $\hat{\boldsymbol{M}}_N$ contains the motion screw coordinates of one of the f independent unit motion screws that span the f-system of motion screws characteristic of a coupling. Likewise, each column of $\hat{\boldsymbol{A}}_N$ contains the action screw coordinates of one of the c independent unit action screws. The vectors $\boldsymbol{\psi}$ and $\boldsymbol{\Psi}$ contain the magnitudes of the motion and action screws respectively.

A force vector $\vec{Q} = \{U, V, W\}$ and a moment vector $\vec{P} = \{R, S, T\}$ at the origin represent an action screw $\$^{\mathbf{a}}$. An angular velocity vector $\vec{p} = \{r, s, t\}$ and a linear velocity vector $\vec{q} = \{u, v, w\}$ of the point on a link instantaneously at the origin represent a motion screw $\$^{\mathbf{m}}$. An action screw $\$^{\mathbf{a}} = \{R, S, T; U, V, W\}$ is said to be written in ray formation[1] and a motion screw $\$^{\mathbf{m}} = \{r, s, t; u, v, w\}$ in axis formation[2]. The relationship between the first and second parts of a screw is called *pitch*, h, and has unit of length. A pure force and

[1] The first part, moment vector $\vec{P} = \{R, S, T\}$, is dependent on the *ray*, a vector from the origin to any point on the line of action.

[2] The first part, angular velocity vector $\vec{p} = \{r, s, t\}$, defines the direction of the *axis*.

a pure angular velocity have zero pitch, $h = 0$. A pure torque and a pure linear velocity have infinite pitch, $h \to \infty$. A combination of torque and force is called *wrench*. Likewise, a combination of linear and angular velocity is called *twist*. If the screw pitch is finite, the direction of the *instantaneous screw axis* (ISA) is given by $\hat{p}$, the unit vector of $\vec{p}$, for a motion screw or by $\hat{Q}$, the unit vector of $\vec{Q}$, for an action screw, and the location of the ISA can be determined by both vectors. If, however, the pitch is infinite, its direction is given by $\hat{q}$ or $\hat{P}$ and the location is undetermined. The ISA of an action screw with finite pitch is often called the *line of action*.

Sometimes it is convenient to express a screw as a magnitude multiplied by a normalised screw, that is, $\$ = \varrho\,\hat{\$}$, where ϱ is the magnitude and $\hat{\$}$ is a normalised screw (a purely geometrical entity). Superscripts **a**, for action, and **m** for motion, are added when needed. The magnitude ϱ is a real number and has magnitude of force or torque (only if the action screw is a pure torque, $h \to \infty$) for action screws and angular or translational speed (only if the motion is a pure translation, $h \to \infty$) for motion screws. Commonly, the magnitude of a particular screw aligned with one of the canonical axes is denoted by the coordinate label. For example, the magnitude of a pure force transmitted by coupling C and aligned in parallel to the x-axis is denoted by U_C instead of $\varrho^{\mathbf{a}}_C$. This practice helps to quickly identify the geometrical support of the screws.

Among the reasons for introducing this notation, explained in [21], is the claim that the power $\mathcal{P}$ expended by an action screw $\$^{\mathbf{a}}$ on a motion screw $\$^{\mathbf{m}}$ is easily remembered as the inner product:

$$\mathcal{P} = \$^{\mathbf{a}} \bullet \$^{\mathbf{m}} = r\,R + s\,S + t\,T + u\,U + v\,V + w\,W\,. \tag{5}$$

The same expression, using Hunt's [52] adaptation of Plücker line coordinates, is:

$$\mathscr{L}_1\,\mathscr{P}^*_2 + \mathscr{M}_1\,\mathscr{Q}^*_2 + \mathscr{N}_1\,\mathscr{R}^*_2 + \mathscr{L}_2\,\mathscr{P}^*_1 + \mathscr{M}_2\,\mathscr{Q}^*_1 + \mathscr{N}_2\,\mathscr{R}^*_1$$

where the subscripts 1 and 2 may denote action or motion indistinctly.

2.3 ACTION INTERNALISATION

The equations (2) and (3) that provide analysis of actions do so for internal actions that could exist as a consequence of overconstraint

[20, 21] . The equations do not provide values for internal actions attributable to active couplings external to the coupling network unless those active couplings, or equivalent passive couplings, are internalised. One didactic approach for action internalisation is discussed in details in [20]. The disadvantage of this approach is that the coupling network has to be modified so the kinematic and static analyses are performed on different networks. Another possibility is the use of parallel pure active and passive coupling as in [29]. In this work, pure active and passive coupling are combined together creating a new kind of active coupling.

Consider, for example, the rotative electric motor shown schematically in Fig. 1 and consisting of a stator and a rotor mechanically coupled by bearings and magnetically coupled by a magnetic field. This motor can be represented by a coupling graph G_C that contains two nodes related to the motor stator and the rotor and, according to approach used in [29], two edges in parallel, one related to the revolute coupling formed by the bearings and the other to the magnetic coupling, as shown in Fig. 2a. The revolute coupling is capable of transmitting five independent actions (assuming $d = 6$) related to the degrees of constraint. The actions transmitted by the magnetic coupling is a torque aligned with the motor axis and it is not related to any degree of constraint; that is why it is represented by a dashed line in Fig. 2a.

In the action graph G_A the action transmitted by a coupling is split in independent actions as shown in Fig. 2b. In an attempt of reconstructing the coupling graph G_C based on action graph G_A the parallel edges are collapsed together as in Fig. 2c. So, it is possible to consider the electric motor as a different kind of coupling capable of transmitting six independent actions. Five actions, akin to the revolute coupling ones, prevent all relative movements with the exception of the rotation around the motor axis; the sixth independent action does not prevent the movement, but provide a torque also around the motor axis. When the action graph G_A is constructed departing from Fig. 2c, the edge will be split up into six parallel edges depending on the actual action screw dimension. Note that the first five independent actions are represented by screws reciprocal to the screw that represents the degree of freedom. This is not true for the sixth and consequently the inner product of the action and motion screws will not be necessary null. This product will be a positive scalar if energy is instantaneously entering the coupling network and negative if it is leaving.

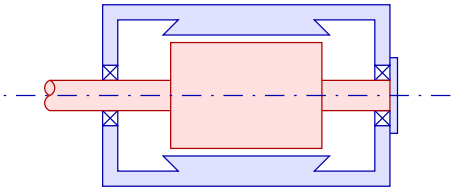

Figure 1 – Schematic representation of a electric motor

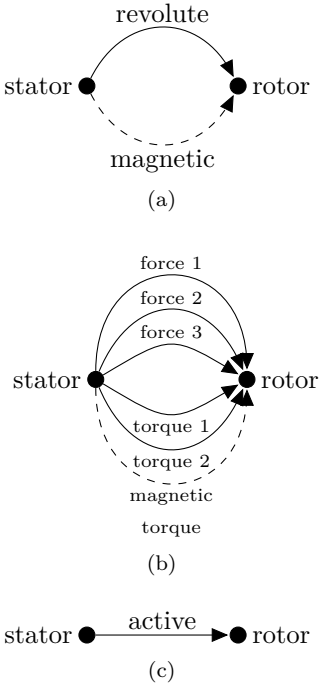

Figure 2 – Graphs that represent the electric motor: (a) coupling graph, (b) action graph, and (c) compact coupling graph

3 EFFICIENCY OF GEAR TRAINS

A few months in the laboratory can save a few hours in the library.

Frank H. Westheimer

It is well known that the mechanical efficiency of gear trains is usually much lower than that of a simple (or ordinary) gear pair. The main reason for this is the power recirculation [6]. Many methods have been proposed for gear train analysis and synthesis, each with its own limitations. For efficiency analysis, perhaps the two most serious limitations are the need for *ad-hoc* reasoning and the lack of generality. The great majority of the available methods do not apply to bevel gear trains [7]. In this thesis, an approach based on a combination of graph and screw theories is proposed. Through the application of this method, the analytical expression for efficiency is obtained based on a short and systematic description of the gear train. The process is automated using a computer algebra system. The method can be applied to any gear train architecture not requiring axes collinearity, parallelisms or other geometrical constraint. The provided examples are of one degree of freedom gear trains, but extension to two or more degrees of freedom is possible.

The method is based on power flow analysis, therefore power and power flow are both defined in Section 3.1. In Section 3.2, friction torque models are defined in terms of action screws. Section 3.3 presents the first example with two main goals: introducing the notation, and providing an insight into the method. In Section 3.4.1 a parallel axes (cylindrical) epicyclic gear train is analysed and the same result reported by Tuplin [10] and Pennestrì and Freudenstein [12] with the corrections suggested by Chen and Angeles [3] is obtained herein. In Section 3.5 the efficiency analysis of an intersecting axes (bevel) epicyclic gear train is presented. Some final remarks concerning the application of the proposed method is given in Section 3.6 and the conclusions are drawn in Section 3.7.

3.1 POWER AND POWER FLOW

In the study of complex gear train efficiency, it is customary to express the overall efficiency in terms of the ordinary efficiency of each gear coupling η_{ij}. The ordinary efficiency would be the efficiency achieved by the gear pair if the carrier, the link that keeps the distance between gear centres constant, was held fixed and the planetary gear pair transformed into a simple (or ordinary) gear pair [17]. The ordinary efficiency is dependent on which gear drives and which is driven for each gear pair. Two techniques have been applied to determine the role of each gear: power flow [3, 6, 7, 9, 16, 19, 53, 54, 55, 56, 57, 58, 59] and sensitivity [17, 58, 60]. Sensitivity renders a very simple way of computing the overall efficiency, but it is applicable only when shaft axes are parallel[1]. Therefore, for the benefit of generality, power flow is used in this work.

Power flows either into or out of the network through couplings. Therefore, in this work, couplings, not links, are said to be the inputs or outputs of a network. In ideal gear trains, power leaves the network exclusively through outputs to which loads are connected. In real gear trains however, power losses may occur causing power to leave the network in couplings not connected to external loads.

Definition 1. *Transferable power*, or just *power*, is the amount of power that enters or leaves the network through a coupling as predicted by equation (5) when using the edge variables associated with that coupling.

The power transferred from link to link without leaving the network is said to flow through the network across couplings.

Definition 2. *Power flow* is the amount of power that is transferred from one link to another across a coupling as measured by an observer that moves along with the reference frame.

The actions are independent of the reference frame, but the motions are not. Thus, the main difference between Definitions 1 and 2 is the motion reference frame. In principle, it is possible to have one set power flow calculated with respect to each link in the network. The common approach is to consider one link stationary and attach the reference frame to this link. Notwithstanding, in network analysis, the notion of a stationary link is unnecessary since

[1] J.M. del Castillo, private communication.

all motions (through variables) are relative; although this practice may help with visualisation. What makes one link so particular that it is said to be stationary is explained by the concept of *port*, adapted by Davies [28] from electrical network theory. External power sources and sinks are connected to the network through ports, called inputs and outputs. Power lost due to imperfections also leaves the network through couplings, but these coupling are not considered to be ports according to the definition by Davies [28].

Definition 3. *Real power flow* is the power flow measured by an observer that moves along with the reference frame attached to a link common to the input and output ports.

Examples of links common to the input and output ports are: link 0 in Fig. 5, link 1 in Fig. 7, and link 5 in Fig. 9.

Using graph theory nomenclature, the input and output edges (couplings) are both incident with the node (link) to which the reference frame is attached.

Definition 3 is meaningless for complex machines like robots in which it is not possible to find a link common to all inputs and outputs. For transmission systems, however, this definition does make sense because, in general, a common link can be found even if multiple inputs and outputs are present as in differentials.

Definition 4. *Virtual power flow* is the power flow measured with respect to a frame that is not common to the input and output.

The real power flow of Definition 3 expresses the real amount of power transferred from link to link since it is related to the inputs and outputs of the system. The virtual power flow of Definition 4 deals with an amount of power that appears to be transferred through the network, but it is deprived of real connotation. It is possible to find a virtual power flow greater than the input power, which is physically impossible for a dissipative network[2] like gear trains. Nevertheless, virtual power flow allows the computation of power losses based on ordinary efficiencies.

The definitions of power flow given herein differ from those found in the literature [3,6,7,9,16,19,53,54,55,56,57,58,59] since other authors consider the stationary nature of the reference frame as the main feature through which to distinguish real from virtual power flow. However,

[2]This allegation can be proved using Tellegen's Theorem; interested readers should refer to references [29, 61]. It is also supported by the second law of thermodynamics.

this feature is somewhat arbitrary. Herein, a more objective criterion is proposed: the incidence of the input and output in relation to the reference link.

Real power flow can be used to determined the power flow direction of each gear pair so that the role (driver/driven) of each gear in a gear pair is established. Besides revealing the driver/driven gear relationship, virtual power flow also renders the amount of power loss in terms of the ordinary efficiency of gear pairs if the carrier is used as a motion reference.

Definition 5. *Overall efficiency* of a gear train is the ratio of work output to work input.

Definition 5 is very common in the literature [8]. In a power or average power constant situation, power or average power can be used in the place of work in Definition 5.

3.1.1 Systematic method for power flow computation

The screw theory based technique adopted in this work yields the computation of power flow in two steps.

Firstly, the motion matrix $\boldsymbol{M}$, which contains one motion screw[3] per column, is converted into an absolute motion matrix $\boldsymbol{M}_i$. "Absolute" actually means that all motions are computed with respect to one particular link i, the reference[4]. This use for the word "absolute" is common in electrical network theory. Thus, each column of the absolute motion matrix $\boldsymbol{M}_i$ contains a motion screw that describes the motions of the respective link with respect to the reference link i and this matrix is given by

$$[\boldsymbol{M}_i]_{d\times n-1} = -\,[\boldsymbol{M}]_{d\times e}\,\left[\boldsymbol{A}_i^{\dagger}\right]_{e\times n-1} \tag{6}$$

where n is the number of links and the number of nodes of G_C, e is the number of couplings and the number of edges of G_C, and

$$\left[\boldsymbol{A}_i^{\dagger}\right]_{e\times n-1} = \left([\boldsymbol{A}_i]_{n-1\times e}\right)^T \left([\boldsymbol{A}_i]_{n-1\times e}\,\left([\boldsymbol{A}_i]_{n-1\times e}\right)^T\right)^{-1} \tag{7}$$

[3] Each motion screw of $\boldsymbol{M}$ describes the relative motion of two directed coupled links.

[4] The reference link is used to compute the time derivatives in the sense that the observer who measures the motions moves along with the reference link. The screw coordinates of all screws are expressed with respect to the same reference frame. This frame is arbitrarily located and also moves along with the reference link.

is the Moore-Penrose pseudoinverse of matrix $\boldsymbol{A}_i$, the reduced incidence matrix of G_C obtained by removing the row respective to the reference link i from the incidence matrix of G_C.

The rank of $\boldsymbol{A}_i$ is known to be $n-1$, so the existence of the inverse in equation (7) is guaranteed. Moreover, the incidence matrix, and consequently its reduced form, contains only the integers 0 and ± 1 demanding little effort for pseudoinverse computation. Therefore, the elements of $\boldsymbol{A}_i^{\dagger}$ are rational numbers and, consequently, the motion screws in the columns of $\boldsymbol{M}_i$ are linear combination of the motion screws in the columns of $\boldsymbol{M}$ being the weights rational numbers. Noteworthily, the $\det\left(\boldsymbol{A}_i\ (\boldsymbol{A}_i)^T\right)$ is equal to the maximum number of spanning trees of G_C [62].

The columns of $\boldsymbol{M}_i$ are analogous to node voltages in an electrical network and those of $\boldsymbol{M}$ to branch (or edge[5]) voltages. Moreover, the motion screws in the columns of $\boldsymbol{M}_i$ observe the same order that the rows of the reduced incidence matrix $\boldsymbol{A}_i$ of G_C and are associated with the same respective links.

The second part constitutes computing the inner product of each motion screw in $\boldsymbol{M}_i$ and the respective action screws in the actions matrix $\boldsymbol{A}$. Again, the reduced incidence matrix $\boldsymbol{A}_i$ comes in handy: every non-null element $a_{i\,j}$ of $\boldsymbol{A}_i$ indicates a column i of $\boldsymbol{M}_i$ and a column j of $\boldsymbol{A}$, which are multiplied, using equation (5), to obtain the power flow from/to link i across the coupling j. A positive power moves or flows in the edge direction and a negative power in the opposite direction to that of the edge.

Depending on the selected link i, this method can render the real or virtual power flow. The application of this method is exemplified in Section 3.4.1.4.

3.2 FRICTION TORQUES IN BEVEL AND CYLINDRICAL GEARS

When building a mathematical model for gear train efficiency computation, many authors assume explicitly or implicitly that the action related to friction and responsible for friction losses is a pure torque [3, 7, 8, 10, 12, 15, 16, 17, 19, 55, 56, 58, 60, 63, 64]. Although this is true for almost all practical needs, this assumption requires some further examination since no mathematical proof was found in the literature review.

[5] In graph theory the concept of a *branch* is related to trees, in electrical network theory the same word is used for what is called *edge* in graph field.

Losses produced by gearing have many causes, for instance, imperfectly shaped teeth, incorrect shaft alignment, lubrication, micro-sliding, micro-deformation, and windage [55]. In most cases, the appreciable effect of these losses is a torque aligned with the rotation axis around which one gear twists with respect to the other gear. In allusion to friction forces, these torques are called *friction torques*. The same kind of torque is also present in bearings and seals [65]. In this section, the actions directly related to friction are modelled. For the sake of completeness, the common assumption related to torque friction is stated herein as a theorem and some discussion is provided along with the proof.

Theorem 1. *If the shaft axes of a gear pair intersect (bevel gears) or are parallel (cylindrical gears), the equivalent friction action is a pure torque, i.e., an infinite pitch action screw.*

Proof. A simple, yet generic, gear set is composed of two gears (e.g., gears[6] 1 and 2 in Fig. 3) and a frame that keeps the geometrical relationship between the gear shafts constant. The joints between this frame and the gears are revolute and the motions allowed by these joints are zero pitch screws, labelled $\$_A^{\mathbf{m}}$ and $\$_B^{\mathbf{m}}$ in Fig. 3. The gear-to-gear relative movement is described by a third screw $\$_C^{\mathbf{m}}$, that is, one gear twists with respect to the other gear around $\$_C^{\mathbf{m}}$ (see Fig. 3). According to the theorem of three axes in kinematics [68, p. 39], the three screws share the same line as a common perpendicular [66, p. 16], which is conveniently vertical in Fig. 3, and they are generators of the same cylindroid. If the two gear shafts are skew, as shown in Fig. 3, $\$_C^{\mathbf{m}}$ have a non-zero pitch, namely h_C. If both gear shafts intersect or are parallel, the pitch h_C is zero and the cylindroid degenerates to a plane.

The action transmitted from one gear to the other is a force through a single contact point G in Fig. 4. The velocity of point G is

$$\vec{q}_G = \vec{p}_C \times \vec{\sigma} + \vec{p}_C \times \vec{\rho} + h_C \, \vec{p}_C \tag{8}$$

where $\vec{\sigma}$ is the position vector of the contact normal $n-n$ with respect to the motion screw $\$_C^{\mathbf{m}}$ (along the common perpendicular to $n-n$ and $\$_C^{\mathbf{m}}$), $\vec{\rho}$ is the position vector of G along $n-n$, and $\vec{p}_C$ is the angular velocity of one gear with respect to the other.

The friction force at point G is anti-parallel to $\vec{q}_G$. If the gear shafts are parallel or intersect, the pitch h_C is null so the friction force

[6] In Fig. 3, the gears are represented schematically by two hyperboloids since the gear shafts are skew. Refer to references [66] or [67] for details.

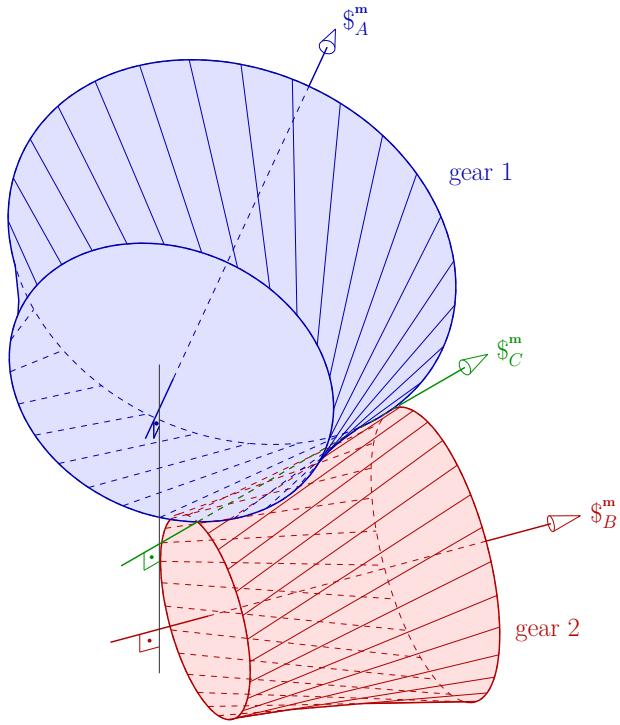

Figure 3 – Generic gear pair: $\$_A^{\mathbf{m}}$ and $\$_B^{\mathbf{m}}$ are screws along the gear shaft axis, $\$_C^{\mathbf{m}}$ is the screw axis around which one gear twists with respect to the other

lies in a plane orthogonal to $\$_C^{\mathbf{m}}$ (refer to equation (8) remembering that the $\$_C^{\mathbf{m}}$ direction is given by $\vec{p}_C$). Therefore, this force produces a torque around $\$_C^{\mathbf{m}}$, but it has no component aligned with $\$_C^{\mathbf{m}}$. As a consequence, the power produced by the friction force is due to the angular motion only and the friction force can be replaced by a friction torque aligned with $\$_C^{\mathbf{m}}$, meaning parallel to $\vec{p}_C$, with suitable magnitude.

□

The hypothesis of Theorem 1 excludes the case where the shaft axes of a gear pair are skew. In this case, a friction force component may also be considered. Treatment of this particular case is not included in this thesis; noteworthily, it is similarly absent in the literature.

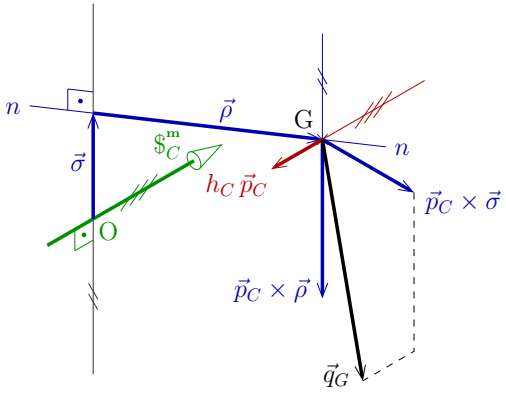

Figure 4 – Gear coupling contact point velocity $\vec{q}_G$ and its components (adapted from Phillips [66])

3.2.1 Friction models

Generalising, the infinite pitch action screw $\$_{L\,i}^{\mathbf{a}}$ that represents the friction torque related to losses in coupling i has the same direction as $\$_i^{\mathbf{m}}$ and can be written as

$$\$_{L\,i}^{\mathbf{a}} = \varrho_{L\,i}^{\mathbf{a}} \begin{bmatrix} \hat{p}_i \\ \vec{0} \end{bmatrix} \tag{9}$$

where $\hat{p}_i$ is the angular velocity of coupling i, $\vec{0}$ is the null vector, and the action screw magnitude $\varrho_{L\,i}^{\mathbf{a}}$ can be dependent on the action transmitted by the coupling, the relative motion, and the coefficient of friction.

Equation (9) can be used for bearing or gear couplings. Table 2 brings some possibilities for the magnitude $\varrho_{L\,i}^{\mathbf{a}}$ according to the friction model adopted. Greater model variety is discussed by Armstrong-Hélouvry, Dupont and Wit [2]. In Table 2, $\varrho_{T\,i}^{\mathbf{a}}$ is the magnitude of the action transmitted by coupling i, ζ_i is the coefficient of friction with a unit of length and numerical value that incorporates every possible cause of loss that is not dependent on speed magnitude; b_i is the coefficient of viscous friction; and $\mathfrak{g}$ is a general function.

The Coulomb and viscous models can be combined. For constant operational speeds, the most common approach for gear friction modelling is to use the Coulomb friction model with the coefficient

Table 2 – Friction torque magnitudes according to different friction models

Friction Model	$\varrho^{\mathbf{a}}_{L\,i}$	#
Coulomb	$-\left\lvert\varrho^{\mathbf{a}}_{T\,i}\right\rvert \operatorname{sign}\left(\varrho^{\mathbf{m}}_{i}\right) \zeta_i$	(10)
Viscous (linear)	$-b_i \left\lvert\varrho^{\mathbf{m}}_{i}\right\rvert$	(11)
Viscous (quadratic)	$-b_i \left(\varrho^{\mathbf{m}}_{i}\right)^2$	(12)
Viscous (cubic)	$-b_i \left(\varrho^{\mathbf{m}}_{i}\right)^3 \operatorname{sign}\left(\varrho^{\mathbf{m}}_{i}\right)$	(13)
Viscous (generic)	$-\mathfrak{g}\left(\varrho^{\mathbf{m}}_{i}\right)$	(14)
General	$-\mathfrak{g}\left(\varrho^{\mathbf{a}}_{T\,i},\, \varrho^{\mathbf{m}}_{i}\right)$	(15)

of friction adapted according to the operational speed.

The coefficient of friction ζ_i of a gear coupling is usually expressed in terms of the efficiency $\eta_{i\,j}$ of the inverted mechanism, i.e., the mechanism obtained when the link that keeps the distance between gears is considered as a motion reference. When expressed in this manner, ζ_i does not yield the instantaneous friction torque, but an average torque. Moreover, the sign of ζ_i is positive and ζ_i has a maximum value equal to the lever arm length when the gear efficiency is zero. Local analysis aimed at obtaining the expression of the coefficient of friction ζ_i as a function of constructive, material or operational parameters is beyond the scope of this work. However, an example is presented in Appendix A which is similar to the method described by Buckingham [8]. Realistic values can be obtained via Tooth Contact Analysis (TCA) [69, 70].

If the direction of the power flow is known, the absolute value operator ($\lvert\cdot\rvert$) and the function $\operatorname{sign}(\cdot)$ can be omitted in Table 2 provided that a minus sign is used accordingly.

One advantage of the network approach used in this work is that all friction torques propagate throughout the network and their effects are systematically considered wherever necessary. One clear example is the influence on the bearing reaction forces caused by the friction torques.

3.3 SIMPLE GEAR TRAIN MODEL

A simple, or ordinary, gear train is used to illustrate the concepts presented in the previous sections. It is also exemplified how power flow direction must be interpreted to obtain the efficiency expression.

The simple gear train represented schematically in Fig. 5 has three links: a frame 0, and two gears 1 and 2. In Fig. 5 the letters A, B, and C identify features such as bearings and tooth contacts. For a gear train to be useful, one gear must be connected to some sort of motor, a torque source, and the other gear to a load, a torque sink. These torques, external to the network, are internalised (see Section 2.3) considering the revolute pairs, labelled A and B in Fig. 5, as active couplings.

Equations (2) and (3) which provide analysis of actions do so for internal actions that could exist as a consequence of overconstraint. The equations do not provide values for internal actions attributable to active couplings external to the gear train unless those active couplings, or equivalent passive couplings, are internalised. If the active couplings are internalised, it becomes difficult to distinguish the internal actions attributable to these active couplings from those attributable to the existing overconstraint [20, 29]. This difficulty can be overcome by making some simplifying assumptions that allow the existing overconstraint to be ignored. These assumptions, however, do not reduce the accuracy of the final results.

3.3.1 Simplifying assumptions and screw system

To ignore overconstraint it is sufficient to assume that:

1. The gear train occupies negligible axial length so that all forces lie in the plane $z = 0$.

2. All gears are thin spur gears making tooth contacts at points on the y-axis.

Further simplifications are made for other reasons. It is assumed that the pressure angle α is zero. Without this assumption the term $\cos\alpha$ would appear in every expression and would then be eliminated. After making these simplifications the only actions that can exist are forces with lines of action parallel to the x-axis in the plane $z = 0$ and torque directed parallel to the z-axis. Thus, geometrically, the actions are

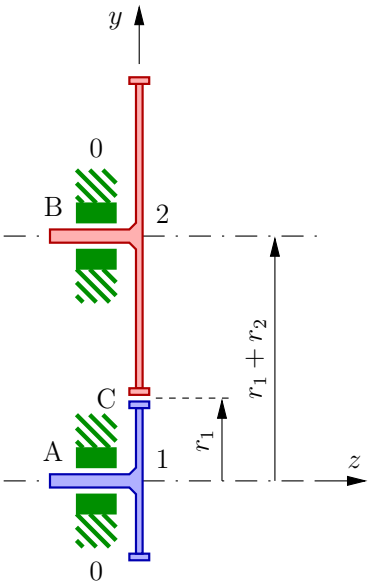

Figure 5 – Simple cylindrical gear train

screws that belong to the 2nd special 2-system of screws according to Hunt's [52] classification. The motions are angular velocities about axes parallel to the z-axis in the plane $x = 0$. Thus the motion screws also belong to a 2nd special 2-system of screws, but a system with ISAs that lie in a different plane to the ISAs of the action system.

3.3.2 Motion analysis

Motion analysis of the system described in this section does not require the use of equation (1) and can be performed by, e.g., application of the theorem of three axes in kinematics [68, p. 39]; so only a few remarks and the final result are provided herein.

The topology of the gear train shown schematically in Fig. 5 is represented by a coupling graph shown in Fig. 6a. The small line crossing the edge C indicates that this coupling is a gear coupling while the other couplings are of revolute type.

Coupling C has a single degree of freedom represented by an angular velocity whose ISA is parallel to the z-axis and passes through point C in Fig. 5. A similar situation is found for couplings A and

B. Thus, geometrically, the motions are screws that belong to the 2nd special 2-system of screws according to Hunt's [52] classification.

The motions allowed have magnitudes t_A, t_B and t_C. These motions are depicted in Table 3 where r_1 and r_2 are the pitch radii of gears 1 and 2. This gear train has a unitary net degree of freedom and any of the magnitudes listed in Table 3 can be selected as a primary variable. Arbitrarily selecting t_A, the angular speed of gear 1 with respect to the frame 0 in Fig. 5, as a primary variable, the motion matrix, that contains one two-dimensional motion screw per column, is written as

$$\boldsymbol{M} = \begin{array}{c} \\ t \\ u \end{array} \begin{array}{c} \begin{array}{ccc} \$_A^{\mathbf{m}} & \$_B^{\mathbf{m}} & \$_C^{\mathbf{m}} \end{array} \\ \begin{bmatrix} r_2 & -r_1 & -r_1 - r_2 \\ 0 & -r_1\ (r_1 + r_2) & -r_1\ (r_1 + r_2) \end{bmatrix} \end{array} \begin{array}{c} \\ \\ \dfrac{t_A}{r_2} \end{array} \tag{16}$$

where row labels t and u on the left of the matrix indicate the respective screw coordinate, and column labels $\$_A^{\mathbf{m}}$, $\$_B^{\mathbf{m}}$, and $\$_C^{\mathbf{m}}$ on the top of matrix indicate the respective motion screw.

3.3.3 Action analysis

The degrees of constraint of couplings A, B and C are represented by forces parallel to the x-axis through points A, B and C, respectively. Thus, geometrically, the actions are screws that belong to the 2nd special 2-system of screws, but a system with ISAs that lie in a different plane to the ISAs of the motion system. These transmitted actions have magnitudes U_A, U_B and U_C.

The introduction of an external source and sink in the coupling network is reflected in the coupling graph by the addition of two edges, A' and B', in Fig. 6b. Their respective torques have magnitudes T_A and T_B. Likewise, the introduction of a power loss due to friction is accompanied by the addition of edge C' in Fig. 6c and its associated friction torque T_C. The graph in Fig. 6c is called action graph G_A and it has one edge for every independent action that can take place in the gear train of Fig. 5. These actions are depicted in Table 4 where r_1 and r_2 are the pitch radii of gears 1 and 2. Collapsing the parallel edges of the action graph results in the coupling graph of Fig. 6a. The unit

Table 3 – Motions spanning the systems of motions allowed by the couplings in Fig. 5

Coupling Label, type	Planar Location		Rotational or Translational Velocity (direction)	Magnitude	Unit motion screw coordinates in axis formation	
					Angular Velocity	Velocity of the point at the origin
	y	z			t	u
A, revolute	0	0	Rotational (z)	t_A	1	0
B, revolute	$r_1 + r_2$	0	Rotational (z)	t_B	1	$r_1 + r_2$
C, gear	r_1	0	Rotational (z)	t_C	1	r_1

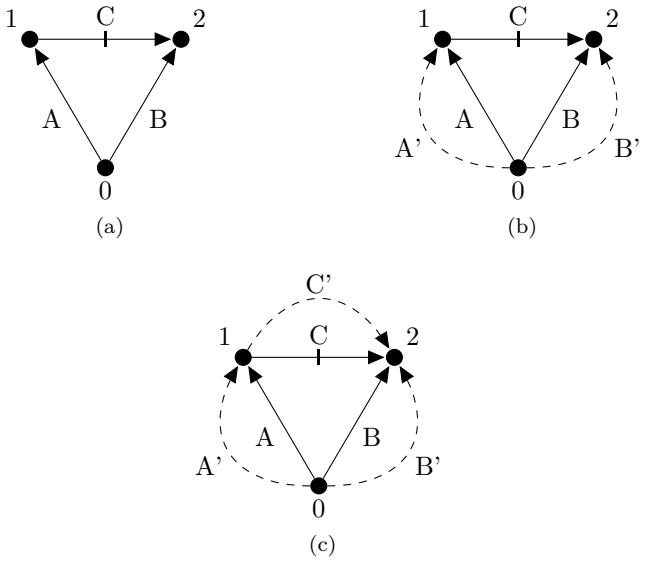

Figure 6 – Simple gear train graphs: (a) original coupling graph G_C, (b) inclusion of external power source and sink, (c) inclusion of frictional power sink, G_A

action matrix of the direct couplings is assembled from Table 4 as

$$\hat{\boldsymbol{A}}_D = \begin{array}{c} \\ T \\ U \end{array} \begin{array}{c} \begin{array}{cccccc} T_A & U_A & T_B & U_B & T_C & U_C \end{array} \\ \left[\begin{array}{cccccc} 1 & 0 & 1 & -r_1 - r_2 & 1 & -r_1 \\ 0 & 1 & 0 & 1 & 0 & 1 \end{array}\right] \end{array}. \tag{17}$$

where the column associated with T_C originates from the application of the row corresponding to t_C of Table 3 in equation (9).

Using edges A and B as branches of the spanning tree, the cutset matrix of action graph G_A in Fig. 6c is written as

$$\boldsymbol{Q}_A = \begin{array}{c} \\ A \\ B \end{array} \begin{array}{c} \begin{array}{cccccc} A & A' & B & B' & C & C' \end{array} \\ \left[\begin{array}{cccccc} 1 & 1 & 0 & 0 & -1 & -1 \\ 0 & 0 & 1 & 1 & 1 & 1 \end{array}\right] \end{array}. \tag{18}$$

The network unit action matrix is assembled from equations (17) and

(18) as

$$\left[\hat{\boldsymbol{A}}_N\right]_{d\,k\times C} = \begin{bmatrix} \left[\hat{\boldsymbol{A}}_D\right]_{d\times C} & [\boldsymbol{Q}_1]_{C\times C} \\ \left[\hat{\boldsymbol{A}}_D\right]_{d\times C} & [\boldsymbol{Q}_2]_{C\times C} \\ & \vdots \\ \left[\hat{\boldsymbol{A}}_D\right]_{d\times C} & [\boldsymbol{Q}_k]_{C\times C} \end{bmatrix}_{d\,k\times C} \tag{19}$$

where $[\boldsymbol{Q}_i]_{C\times C} = \text{diag}\left([\boldsymbol{Q}_A]_i\right)$ are diagonal matrices ($i = 1, 2, \ldots, k$). The diagonal elements of $[\boldsymbol{Q}_i]_{C\times C}$ are those of row i of $[\boldsymbol{Q}_A]_{k\times C}$. Thus

$$\hat{\boldsymbol{A}}_N = \begin{array}{c} \\ T \\ U \\ T \\ U \end{array} \begin{array}{c} \begin{array}{cccccc} T_A & U_A & T_B & U_B & T_C & U_C \end{array} \\ \begin{bmatrix} 1 & 0 & 0 & 0 & -1 & r_1 \\ 0 & 1 & 0 & 0 & 0 & -1 \\ 0 & 0 & 1 & -r_1 - r_2 & 1 & -r_1 \\ 0 & 0 & 0 & 1 & 0 & 1 \end{bmatrix} \end{array}. \tag{20}$$

3.3.4 Constitutive equations

Equation (20) carries only topological information; element characteristics are not present. Equations that express the element characteristics are called *constitutive equations* [71]. For instance, the sole constitutive equation of this system is expressed using equation (10) in Table 2 with magnitude of the transmitted action $\left|\varrho^{\mathrm{a}}_{T_C}\right| = |U_C| = \text{sign}\,(U_C)\; U_C$ and magnitude of motion $\varrho^{\mathrm{m}}_{C} = t_C$ as

$$T_C = -\zeta_C\; \text{sign}\,(U_C)\; U_C\; \text{sign}\,(t_C) \tag{21}$$

where ζ_C is the coefficient of friction with dimension of length that converts the transmitted action of magnitude U_C to a friction torque of magnitude T_C.

The coefficient of friction ζ_C can be obtained from experimental data or from mathematical models as in Appendix A. This coefficient can also be expressed in terms of the gear pair efficiency as in Section 3.3.5.

The augmented action matrix $\boldsymbol{D}_A$ which models the relationship between actions in the network is obtained by introducing equation (21)

Table 4 – Actions spanning the systems of actions that can be transmitted by the couplings of Fig. 5

Coupling Label, type	Planar Location		Force or Torque (direction)	Magnitude	Unit action screw coordinates in ray formation	
					Moment at origin	Force
	y	z			T	U
A, revolute	0	0	Torque (z)	T_A	1	0
			Force (x)	U_A	0	1
B, revolute	$r_1 + r_2$	0	Torque (z)	T_B	1	0
			Force (x)	U_B	$-r_1 - r_2$	1
C, gear	r_1	0	Torque (z)	T_C	1	0
			Force (x)	U_C	$-r_1$	1

in matrix form into equation (20) as

$$\boldsymbol{D}_A = \begin{array}{c} \\ T \\ U \\ T \\ U \\ c.e. \end{array} \begin{array}{c} \begin{array}{cccccc} T_A & U_A & T_B & U_B & T_C & U_C \end{array} \\ \left[\begin{array}{cccccc} 1 & 0 & 0 & 0 & -1 & r_1 \\ 0 & 1 & 0 & 0 & 0 & -1 \\ 0 & 0 & 1 & -r_1 - r_2 & 1 & -r_1 \\ 0 & 0 & 0 & 1 & 0 & 1 \\ \hdashline 0 & 0 & 0 & 0 & 1 & c\,\zeta_C \end{array}\right] \end{array} \tag{22}$$

where $c = \text{sign}\,(U_C)\ \text{sign}\,(t_C)$, and the label *c.e.* indicates that the last row originates from a constitutive equation.

Matrix $\boldsymbol{D}_A$ is used in place of $\hat{\boldsymbol{A}}_N$ in equation (2) and its null space, also called kernel, is

$$\text{Null}\,(\boldsymbol{D}_A) = \begin{bmatrix} 1 \\ -\frac{1}{r_1 + c\,\zeta_C} \\ \frac{r_2 - c\,\zeta_C}{r_1 + c\,\zeta_C} \\ \frac{1}{r_1 + c\,\zeta_C} \\ \frac{c\,\zeta_C}{r_1 + c\,\zeta_C} \\ -\frac{1}{r_1 + c\,\zeta_C} \end{bmatrix} \tag{23}$$

where, again, $c = \text{sign}\,(U_C)\ \text{sign}\,(t_C)$.

The action vector $\boldsymbol{\Psi}$, the solution of equation (2), is proportional to the vector in equation (23). The chosen proportionality constant is the primary variable T_A, but this choice is somewhat arbitrary. Therefore, from the last element of the vector in equation (23),

$$U_C = \frac{-T_A}{r_1 + \zeta_C\ \text{sign}\,(U_C)\ \text{sign}\,(t_C)} \tag{24}$$

and, since the sign of ζ_C is positive and, in a practical situation[7], $\zeta_C < r_1$, the denominator in equation (24) will always be positive. Consequently, the sign of U_C will be the opposite of the sign of T_A, thus $\text{sign}\,(U_C) = -\,\text{sign}\,(T_A)$. Also, from equation (16), $\text{sign}\,(t_C) = -\,\text{sign}\,(t_A)$.

The action matrix $\boldsymbol{A}$ that contains the action screws transmitted

[7] Practical limits for the coefficient of friction ζ_i are dependent on geometrical considerations as, e.g., in Appendix A.

through the network is obtained by multiplying the screws in the unit action matrix of the direct couplings $\hat{\boldsymbol{A}}_D$, given by equation (17), by the respective magnitudes. The action magnitudes are given by the product of the augmented action matrix $\boldsymbol{D}_A$ null space, given by equation (23), by the action primary variable T_A. In matrix form, the actions matrix is given by

$$[\boldsymbol{A}]_{2\times 6} = \hat{\boldsymbol{A}}_D \ \mathrm{diag}\left(\mathrm{Null}\left(\boldsymbol{D}_A\right)\right) \ T_A \, . \tag{25}$$

The condensed version of the matrix in equation (25) is obtained by adding together the columns related to the same coupling as

$$[\boldsymbol{A}]_{2\times 3} = \begin{matrix} \\ T \\ U \end{matrix} \begin{matrix} \$_A^{\mathbf{a}} \\ \end{matrix} \begin{matrix} \$_B^{\mathbf{a}} \\ \end{matrix} \begin{matrix} \$_C^{\mathbf{a}} \\ \end{matrix} \begin{bmatrix} 1 & -1 & 1 \\ -\frac{1}{r_1 + a\,\zeta_C} & \frac{1}{r_1 + a\,\zeta_C} & -\frac{1}{r_1 + a\,\zeta_C} \end{bmatrix} T_A \tag{26}$$

where T_A is the magnitude of the torque transmitted by coupling A (a scalar), t_A is the angular speed of gear 1 with respect to link 0, $a = \mathrm{sign}\left(T_A\right) \mathrm{sign}\left(t_A\right)$, and the identities $\mathrm{sign}\left(U_C\right) = -\mathrm{sign}\left(T_A\right)$ and $\mathrm{sign}\left(t_C\right) = -\mathrm{sign}\left(t_A\right)$ were applied (see the considerations following equation (24)).

3.3.5 Power, power flow, and efficiency

Equations (16) and (26) are important because they can be used to calculate the power that enters or leaves the network in each coupling, the power flow transmitted into the network through each coupling, and the efficiency.

The power that enters or leaves the network through coupling A is

$$\mathcal{P}_A = \$_A^{\mathbf{a}} \bullet \$_A^{\mathbf{m}} = T_A \, t_A \tag{27}$$

where the screws $\$_A^{\mathbf{a}}$ and $\$_A^{\mathbf{m}}$ were taken from equations (16) and (26), respectively. The amount of power $\mathcal{P}_A$ given by equation (27) enters the network if the signs of T_A and t_A coincide and leaves the network otherwise. For couplings B and C:

$$\mathcal{P}_B = \$_B^{\mathbf{a}} \bullet \$_B^{\mathbf{m}} = -T_A \, t_A \, \frac{r_1 \ (r_2 - \zeta_C \ \mathrm{sign}\left(T_A\right) \ \mathrm{sign}\left(t_A\right))}{r_2 \ (r_1 + \zeta_C \ \mathrm{sign}\left(T_A\right) \ \mathrm{sign}\left(t_A\right))} \tag{28}$$

$$\mathcal{P}_C = \$_C^{\mathbf{a}} \bullet \$_C^{\mathbf{m}} = -T_A \, t_A \, \frac{\zeta_C \ (r_1 + r_2) \ \mathrm{sign}\left(T_A\right) \ \mathrm{sign}\left(t_A\right)}{r_2 \ (r_1 \ \mathrm{sign}\left(T_A\right) \ \mathrm{sign}\left(t_A\right) + \zeta_C)} \tag{29}$$

and, independently of the sign of T_A and t_A , $\mathcal{P}_A + \mathcal{P}_B + \mathcal{P}_C = 0$ and $\mathcal{P}_C < 0$ because $0 < \zeta_C < r_1$. $\mathcal{P}_C < 0$ implies that energy always leaves the network through coupling C since this power is lost due to friction.

The power transferred from gear 1 to gear 2, in addition to the power lost in the process, is given by

$$\mathcal{P}_{12} = \$_C^{\mathbf{a}} \bullet \$_A^{\mathbf{m}} = T_A \, t_A \tag{30}$$

where $\$_A^{\mathbf{m}}$ is the motion screw of gear 1 with respect to link 0, the reference, and $\$_C^{\mathbf{a}}$ is the action between gears 1 and 2. The power transferred from gear 2 to gear 1, in addition to the power lost in the process, is

$$\mathcal{P}_{21} = \$_C^{\mathbf{a}} \bullet \$_B^{\mathbf{m}} = T_A \, t_A \, \frac{r_1 \, (r_2 - \zeta_C \, \text{sign}\,(T_A) \, \text{sign}\,(t_A))}{r_2 \, (r_1 + \zeta_C \, \text{sign}\,(T_A) \, \text{sign}\,(t_A))} \, . \tag{31}$$

The ordinary efficiency of the gear coupling is defined by the ratio between the power that the driver gear transfers to the driven gear to the power that the driven gear receives from the driver gear taking into account the power loss; thus it is dependent on the power flow direction.

Two cases are possible. In the first case, gear 1 drives gear 2, therefore, the signs of T_A and t_A are coincident. Coupling A is said to be the input and B the output. For coupling B to be the output it is also necessary that $\zeta_C \leq r_2$, which is true in a practical situation[8].

The efficiency η_{12}, where the subscripts indicate that gear 1 drives gear 2, is given by

$$\eta_{12} = \frac{\mathcal{P}_{\text{driven}}}{\mathcal{P}_{\text{driver}}} = \frac{\mathcal{P}_{21}}{\mathcal{P}_{12}} = \frac{\$_C^{\mathbf{a}} \bullet \$_B^{\mathbf{m}}}{\$_C^{\mathbf{a}} \bullet \$_A^{\mathbf{m}}} = \frac{r_1 \, (r_2 - \zeta_C)}{r_2 \, (r_1 + \zeta_C)} \tag{32}$$

where the screws are taken from equations (16) and (26), and the sign coincidence of T_A and t_A eliminates the sign function of equations (30) and (31).

The numerical value of η_{12} can be estimated [8,69,70], or adopted as, for instance, 0.98 for external meshing and 0.99 for internal meshing as suggested by Glover [11]. Equation (32) can be solved for ζ_C as

$$\zeta_C = \zeta_{12} = \frac{r_1 \, r_2 \, (1 - \eta_{12})}{r_1 + \eta_{12} \, r_2} \tag{33}$$

[8]Practical limits for the coefficient of friction ζ_i are dependent on geometrical considerations as, e.g., in Appendix A.

where the index 12 indicates that this particular value of ζ_C has to be used when T_A and t_A have the same sign or, equivalently, when coupling A is an input.

In the second case, gear 2 drives gear 1 and consequently the signs of T_A and t_A are opposite. The ordinary efficiency of the gear coupling is

$$\eta_{21} = \frac{\mathcal{P}_{\text{driven}}}{\mathcal{P}_{\text{driver}}} = \frac{\mathcal{P}_{12}}{\mathcal{P}_{21}} = \frac{\$_C^{\mathbf{a}} \bullet \$_A^{\mathbf{m}}}{\$_C^{\mathbf{a}} \bullet \$_B^{\mathbf{m}}} = \frac{r_2\ (r_1 - \zeta_C)}{r_1\ (r_2 + \zeta_C)} \tag{34}$$

and

$$\zeta_C = \zeta_{21} = \frac{r_1\, r_2\ (1 - \eta_{21})}{(r_2 + \eta_{21}\, r_1)} \tag{35}$$

can be obtained from equation (34), or by replacing η_{12} with ${\eta_{21}}^{-1}$ in equation (33) and reverting the sign of the result to compensate for the opposite signs of T_A and t_A.

The index 21 indicates that this particular value of ζ_C is to be used when T_A and t_A have opposite signs or, equivalently, when coupling B is an input.

It could be expected that equation (34) would be the reciprocal of equation (32), but the sign of ζ_C is also reverted.

Assuming that power losses are not sufficient to cause changes in the power flow direction, the use of the sign function can be avoided if, in addition, ζ_C is allowed to be negative when the situation requires it to be. These facts are used to devise the global efficiency formula for power flowing in one direction based on a formula derived for power flowing in the opposite direction in more complicated gear trains.

Substituting equations (32) and (34) in equation (28) and taking into account the signs of T_A and t_A, leads to

$$\mathcal{P}_B = -\eta_{12}\, T_A\, t_A \tag{36}$$

$$\mathcal{P}_B = -\frac{T_A\, t_A}{\eta_{21}} \tag{37}$$

which are in accordance with the definition of ordinary efficiency. Equation (37) is used when coupling B is the input and equation (36) when B is the output. The minus sign in equation (37) compensates the different signs of T_A and t_A; and in equation (36) the negative sign implies that energy is leaving the network through this coupling. The chosen primary variables are related to coupling A regardless of which

coupling is the input or output. Thus, the product $T_A\, t_A$ is the input power in equation (36) and output power in (37).

Despite the fact that η_{12} and η_{21} are defined under different circumstances depending on the power flow, their numerical values are the same.

3.3.6 Load-dependent bearing losses

Friction in bearings induces loss which is dependent on the action transmitted by the bearings. In the example, the actions transmitted by the bearings labelled A and B in Fig. 5 are single forces. These forces balance the force transmitted by the gear coupling C and the force created by the friction torque. A coefficient of friction ζ_i relates the force transmitted by the coupling to a torque aligned with the coupling axis. This parameter can be estimated [72] or identified from experimental data. In the latter approach all possible effects, some of which are disregarded in the knowledge-based modelling, can be included. In particular, the alleged small friction force reaction can be accounted for. In this section, following the example of the previous sections, ζ_i is expressed in terms of the bearing efficiency η_i.

For bearings A and B, application of equation (17) in Table 2 leads to

$$T_A^\star = -U_A\, \zeta_A\, \text{sign}\,(U_A)\, \text{sign}\,(t_A) \tag{38}$$

$$T_B^\star = -U_B\, \zeta_B\, \text{sign}\,(U_B)\, \text{sign}\,(t_B) \tag{39}$$

where the superscript $\star$ is used to indicate that these torques are distinct from the external torques applied to the couplings, ζ_A and ζ_B are coefficients of friction that relate the magnitudes U_A and U_B of the reaction forces acting on the bearings with the bearing friction torque magnitudes $T_A^\star$ and $T_B^\star$, and t_A and t_B are the bearing angular speeds.

To accommodate equations (38) and (39), matrix $\boldsymbol{D}_A$ in equation (22) is modified as follows: first the columns related to T_A and T_B

are duplicated, then two rows are added resulting in:

$$\boldsymbol{D}_A = \begin{array}{c} \\ T \\ U \\ T \\ U \\ \hline c.e. \\ c.e. \\ c.e. \end{array} \begin{array}{c} \begin{array}{cccccccc} T_A & T_A^\star & U_A & T_B & T_B^\star & U_B & T_C & U_C \end{array} \\ \left[\begin{array}{cccccccc} 1 & 1 & 0 & 0 & 0 & 0 & -1 & r_1 \\ 0 & 0 & 1 & 0 & 0 & 0 & 0 & -1 \\ 0 & 0 & 0 & 1 & 1 & -r_1 - r_2 & 1 & -r_1 \\ 0 & 0 & 0 & 0 & 0 & 1 & 0 & 1 \\ \hline 0 & 1 & -a\,\zeta_A & 0 & 0 & 0 & 0 & 0 \\ 0 & 0 & 0 & 0 & 1 & -a\,\zeta_B & 0 & 0 \\ 0 & 0 & 0 & 0 & 0 & 0 & 1 & a\,\zeta_C \end{array}\right] \end{array} \tag{40}$$

where $a = \operatorname{sign}(T_A)\,\operatorname{sign}(t_A)$, and the identities

$$\begin{aligned} \operatorname{sign}(U_A) &= -\operatorname{sign}(T_A) \\ \operatorname{sign}(U_B) &= \operatorname{sign}(T_A) \\ \operatorname{sign}(U_C) &= -\operatorname{sign}(T_A) \\ \operatorname{sign}(t_B) &= -\operatorname{sign}(t_A) \\ \operatorname{sign}(t_C) &= -\operatorname{sign}(t_A) \end{aligned} \tag{41}$$

were applied. The identities in equation (41) are valid for all practical situations and they are directly obtained from equations (16) and (23) using a similar argument following equation (24).

The vector of magnitudes of action screws $\boldsymbol{\Psi}$ is proportional to the sole vector in $\boldsymbol{D}_A$ null space given by

$$\operatorname{Null}(\boldsymbol{D}_A) = \begin{bmatrix} 1 \\ -\frac{a\,\zeta_A}{r_1 + a\,(\zeta_A + \zeta_C)} \\ -\frac{1}{r_1 + a\,(\zeta_A + \zeta_C)} \\ \frac{r_2 - a\,(\zeta_B + \zeta_C)}{r_1 + a\,(\zeta_A + \zeta_C)} \\ \frac{a\,\zeta_B}{r_1 + a\,(\zeta_A + \zeta_C)} \\ \frac{1}{r_1 + a\,(\zeta_A + \zeta_C)} \\ \frac{a\,\zeta_C}{r_1 + a\,(\zeta_A + \zeta_C)} \\ -\frac{1}{r_1 + a\,(\zeta_A + \zeta_C)} \end{bmatrix}$$

where $a = \operatorname{sign}(T_A)\,\operatorname{sign}(t_A)$.

Choosing T_A as the primary variable, the actions matrix is

written as

$$\boldsymbol{A}^T = \begin{bmatrix} \$^{\mathbf{a}}_{T_A}{}^T \\ \$^{\mathbf{a}}_{T^\star_A}{}^T \\ \$^{\mathbf{a}}_{U_A}{}^T \\ \$^{\mathbf{a}}_{T_B}{}^T \\ \$^{\mathbf{a}}_{T^\star_B}{}^T \\ \$^{\mathbf{a}}_{U_B}{}^T \\ \$^{\mathbf{a}}_{T_C}{}^T \\ \$^{\mathbf{a}}_{U_C}{}^T \end{bmatrix} = \begin{bmatrix} T & U \\ 1 & 0 \\ -a\,\zeta_A & 0 \\ 0 & -1 \\ r_2 - a\,(\zeta_B + \zeta_C) & 0 \\ a\,\zeta_B & 0 \\ -r_1 - r_2 & 1 \\ a\,\zeta_C & 0 \\ r_1 & -1 \end{bmatrix} \frac{T_A}{r_1 + a\,(\zeta_A + \zeta_C)} \tag{42}$$

where, again, $a = \text{sign}\,(T_A)\,\text{sign}\,(t_A)$. This matrix can be made compact by adding together the action screws related to the same coupling, for example

$$\$^{\mathbf{a}}_A = \$^{\mathbf{a}}_{T_A} + \$^{\mathbf{a}}_{T^\star_A} + \$^{\mathbf{a}}_{U_A} \tag{43}$$

$$\$^{\mathbf{a}}_B = \$^{\mathbf{a}}_{T_B} + \$^{\mathbf{a}}_{T^\star_B} + \$^{\mathbf{a}}_{U_B} \tag{44}$$

where $\$^{\mathbf{a}}_A$ is the wrench of coupling A, $\$^{\mathbf{a}}_{T_A}$ is the external torque applied to coupling A, $\$^{\mathbf{a}}_{T^\star_A}$ is the friction torque whose magnitude is given by equation (38), and $\$^{\mathbf{a}}_{U_A}$ is the bearing reaction force at coupling A. A similar description is valid for equation (44) replacing A with B. However, individual screws are needed for bearing efficiency computation.

Assuming that $T_A\,t_A > 0$, the power that enters coupling A is given by the inner product $\$^{\mathbf{a}}_{T_A} \bullet \$^{\mathbf{m}}_A$ and the difference between this power and the power loss is given by $\$^{\mathbf{a}}_A \bullet \$^{\mathbf{m}}_A$, where $\$^{\mathbf{a}}_A$ is given by equation (43). Thus, the efficiency of coupling A is

$$\eta_A = \frac{\$^{\mathbf{a}}_A \bullet \$^{\mathbf{m}}_A}{\$^{\mathbf{a}}_{T_A} \bullet \$^{\mathbf{m}}_A} = \frac{r_1 + \zeta_C}{r_1 + \zeta_A + \zeta_C} \tag{45}$$

where ζ_C is given by equation (33).

Solving equation (45) for ζ_A gives

$$\zeta_A = \frac{(1 - \eta_A)\,(r_1 + \zeta_C)}{\eta_A}\,. \tag{46}$$

The total power that leaves coupling B is given by the inner product $\$^{\mathbf{a}}_{B} \bullet \$^{\mathbf{m}}_{B}$, where $\$^{\mathbf{a}}_{B}$ is given by equation (44), and the power that is effectively used by the load is given by $\$^{\mathbf{a}}_{T_B} \bullet \$^{\mathbf{m}}_{B}$. Thus, the efficiency of coupling B is given by

$$\eta_B = \frac{\$^{\mathbf{a}}_{T_B} \bullet \$^{\mathbf{m}}_{B}}{\$^{\mathbf{a}}_{B} \bullet \$^{\mathbf{m}}_{B}} = \frac{r_2 - \zeta_B - \zeta_C}{r_2 - \zeta_C} \,. \tag{47}$$

Solving equation (47) for ζ_B gives

$$\zeta_B = (1 - \eta_B)\ (r_2 - \zeta_C) \,. \tag{48}$$

The overall efficiency η is the ratio between the power effectively used by the load and the power that enters the network given by

$$\eta = \frac{-\$^{\mathbf{a}}_{T_B} \bullet \$^{\mathbf{m}}_{B}}{\$^{\mathbf{a}}_{T_A} \bullet \$^{\mathbf{m}}_{A}} = \eta_A\, \eta_B\, \eta_{12} \tag{49}$$

where the screws were taken from equations (16) and (42) and the coefficients of friction from equations (33), (46), and (48).

If $T_A\, t_A < 0$, the fractions in equations (45), (47), and (49) are inverted and the result is the same predicted by equation (49), as expected.

Perhaps the most significant change in this section in relation to the previous section is the use of individual or partial action screws such as $\$^{\mathbf{a}}_{T_A}$ and $\$^{\mathbf{a}}_{T_B}$. These screws are needed because one coupling may have more than one single power source or sink, therefore, requiring a more careful definition of efficiency.

3.3.7 Speed-dependent losses

Assuming a linear friction model, equation (11) (see Table 2) is applied and the following torque magnitudes are expressed in terms of the angular speed as

$$\begin{aligned} T^{\ddagger}_{A} &= -b_A\, t_A\ \mathrm{sign}\,(t_A) \\ T^{\ddagger}_{B} &= -b_B\, t_B\ \mathrm{sign}\,(t_B) \\ T^{\ddagger}_{C} &= -b_C\, t_C\ \mathrm{sign}\,(t_C) \end{aligned} \tag{50}$$

where the superscript ‡ is used to distinguish these torques from the external torques applied to the couplings, t_A is the primary

motion variable, t_B and t_C are obtained from equation (16), and b_i $(i = A, \ldots, C)$ are coefficients of viscous friction and have dimension of mass times length per time, $[\mathrm{MLT}^{-1}]$.

The speed-dependent torques in equation (50) act like dependent sources requiring an adaptation of equation (2) as follows

$$\boldsymbol{D}_A \, \boldsymbol{\Psi} = \left[\begin{array}{c} \mathbf{0} \\ \hdashline \boldsymbol{\nu} \end{array}\right] \tag{51}$$

where $\boldsymbol{\nu}$ is the dependent sources vector.

The first $d\,k$, where d is the order of the action screw system and k is the number of independent cutsets of G_C, rows of matrix $\boldsymbol{D}_A$ are inherited from $\boldsymbol{A}_N$, the next g rows are related to constitutive equations which do not have any term that is exclusively dependent on speed, e.g., equation (21), and the final s rows represent the action-dependent part of the equations which have terms that are only dependent on speed, e.g., those in equations (50). The terms of these last-named equations, which are dependent only on motion, appear in the dependent sources vector $\boldsymbol{\nu}$, e.g., the right-hand side of the equations (50). They are called *dependent sources terms* in analogy to the voltage-dependent current sources found in electrical network theory [73].

Disregarding the load-dependent losses in the bearings, equations (22) and (50) are used to rewrite matrix $\boldsymbol{D}_A$ as

$$\boldsymbol{D}_A = \begin{array}{c} \\ T \\ U \\ T \\ U \\ \hdashline c.e. \\ s.e. \\ s.e. \\ s.e. \end{array} \begin{array}{c} \begin{array}{ccccccccc} T_A & T_A^{\ddagger} & U_A & T_B & T_B^{\ddagger} & U_B & T_C & T_C^{\ddagger} & U_C \end{array} \\ \left[\begin{array}{ccccccccc} 1 & 1 & 0 & 0 & 0 & 0 & -1 & -1 & r_1 \\ 0 & 0 & 1 & 0 & 0 & 0 & 0 & 0 & -1 \\ 0 & 0 & 0 & 1 & 1 & -r_1 - r_2 & 1 & 1 & -r_1 \\ 0 & 0 & 0 & 0 & 0 & 1 & 0 & 0 & 1 \\ \hdashline 0 & 0 & 0 & 0 & 0 & 0 & 1 & 0 & a\,\zeta_C \\ 0 & 1 & 0 & 0 & 0 & 0 & 0 & 0 & 0 \\ 0 & 0 & 0 & 0 & 1 & 0 & 0 & 0 & 0 \\ 0 & 0 & 0 & 0 & 0 & 0 & 0 & 1 & 0 \end{array}\right] \end{array} \tag{52}$$

where $a = \operatorname{sign}(T_A) \operatorname{sign}(t_A)$, and label *s.e.* indicates that the row corresponds to a source equation and *c.e.* to a constitutive equation.

The dependent sources vector $\boldsymbol{\nu}$ is assembled from the right-hand

side of the equation (50) as

$$\boldsymbol{\nu} = \begin{bmatrix} -b_A \\ -b_B \, \frac{r_1}{r_2} \\ -b_C \, \left(\frac{r_1}{r_2} + 1 \right) \end{bmatrix} t_A \, \text{sign}\,(t_A) \tag{53}$$

where equation (16) and the identities (41) were used in the replacement of t_B and t_C and their signs.

Assuming $T_A \, t_A > 0$, choosing T_A as the primary variable, solving equation (51) and using the obtained magnitudes to calculate the action matrix $\boldsymbol{A}$, equation (49) gives the overall efficiency

$$\eta = \frac{T_A \, ((r_2 - \zeta_C) \, r_1 \, r_2) - a \, t_A}{T_A \, {r_2}^2 \, (r_1 + \zeta_C)}$$

where $a = b_A \, (r_2 - \zeta_C) \, r_1 \, r_2 - b_B \, (r_1 + \zeta_C) \, {r_1}^2 - b_C \, r_1 \, (r_1 + r_2)^2$.

The overall efficiency η is dependent on the actual input torque T_A and speed t_A. Note that ζ_C has a dimension of length and is expressed in terms of the ordinary efficiency of the gear coupling C by equation (33).

Following the proposed approach, it is possible to use a more general friction models. In the following sections, however, Coulomb friction is used because it is relatively simple and by far the most used friction model in the literature. Another interesting feature of the Coulomb friction model is that it is non-linear requiring a more general approach than simpler linear friction models.

3.4 POWER FLOW BASED ALGORITHM

In general, friction models are non-linear (see Table 2). Assuming that the speed is constant allows motion computation independent of the actions, which solves part, but not all, of the problems created by the non-linearity.

The friction model might also be dependent on the direction of the transmitted actions as, e.g., in Coulomb friction. Power flow can be used to simplify the analysis process removing the need for sign function in the friction model. Algorithm 1 uses power flow to convert the matter of efficiency determination into a linear problem. The application of this algorithm is discussed and exemplified in the next section.

Algorithm 1 – Gear train efficiency determination using power flow

1. produce a sketch of the gear trains;
2. identify the motion ISAs;
3. identify the transmitted action ISAs;
4. write the direct coupling unitary motions, $\hat{\boldsymbol{M}}_D$, and actions, $\hat{\boldsymbol{A}}_D$, matrices;
5. identify the ports (input and output);
6. establish the coupling graph G_C and one spanning tree of G_C;
7. write the fundamental circuits, $\boldsymbol{B}$, and cutsets, $\boldsymbol{Q}$, matrices of G_C;
8. write the fundamental circuits matrix $\boldsymbol{B}_M$ of motion graph G_M by column replication of $\boldsymbol{B}$ using matrix $\hat{\boldsymbol{M}}_D$ (step 4);
9. write the fundamental cutsets matrix $\boldsymbol{Q}_A$ of action graph G_A by column replication of $\boldsymbol{Q}$ using matrix $\hat{\boldsymbol{A}}_D$ (step 4);
10. rewrite the fundamental cutsets matrix $\boldsymbol{Q}_A$ using only the columns of matrix $\hat{\boldsymbol{A}}_D$ not related to power lost;
11. assemble the network unit motion matrix $\hat{\boldsymbol{M}}_N$ using matrix $\boldsymbol{B}_M$ (step 8) and matrix $\hat{\boldsymbol{M}}_D$ (step 4);
12. select the motion primary variable;
13. determine the motion magnitudes in terms of the primary variable;
14. compute the motion matrix $\boldsymbol{M}$ using matrix $\hat{\boldsymbol{M}}_D$ (step 4) and the magnitudes of step 13;
15. identify the carrier i;
16. convert the motion matrix $\boldsymbol{M}$ into absolute motion matrix $\boldsymbol{M}_i$ with respect to the carrier i.
17. assemble the network unit action matrix $\hat{\boldsymbol{A}}_N$ using matrix $\boldsymbol{Q}_A$ (step 10) and the columns of matrix $\hat{\boldsymbol{A}}_D$ (step 4) not related to power lost;

18. select the action primary variable;
19. determine action magnitudes in terms of the primary variable (lossless model);
20. compute the action matrix $\boldsymbol{A}$ using matrix $\hat{\boldsymbol{A}}_D$ (step 4) and the magnitudes of step 19;
21. compute the virtual power flow with respect to the carrier using the absolute motion matrix $\boldsymbol{M}_i$ (step 16) and the action matrix $\boldsymbol{A}$ (step 20);
22. establish the turning conditions;
23. reassemble the network unit action matrix $\hat{\boldsymbol{A}}_N$ using matrix $\boldsymbol{Q}_A$ (step 9) and the entire matrix $\hat{\boldsymbol{A}}_D$ (step 4);
24. establish the friction action magnitude equations considering the power flow direction;
25. assemble the dependent sources vector $\boldsymbol{\nu}$ using the motion magnitudes (step 13) if necessary;
26. obtain augmented action matrix $\boldsymbol{D}_A$ using equations of step 24 and matrix $\hat{\boldsymbol{A}}_N$ (step 23);
27. determine all action magnitudes in terms of the primary variable (lost model) solving the linear system formed by $\boldsymbol{D}_A$ and $\boldsymbol{\nu}$;
28. compute the action matrix $\boldsymbol{A}$ using matrix $\hat{\boldsymbol{A}}_D$ (step 4) and the magnitudes of step 27;
29. compute the port powers using the motion matrix $\boldsymbol{M}$ (step 14) and the action matrix $\boldsymbol{A}$ (step 28);
30. compute the efficiency as the ratio of port powers;
31. modify the efficiency equation for all turning conditions established in step 22.

In the application of Algorithm 1 some flexibility is allowed and even encouraged, particularly regarding the computation order.

When the motion ISAs are identified in step 2, the friction action ISAs are established using equation (9). Step 22 is performed by detecting changes in the power flow sign. It is necessary to repeat step 16 for all carriers if there are more than one (see Section 3.6.5).

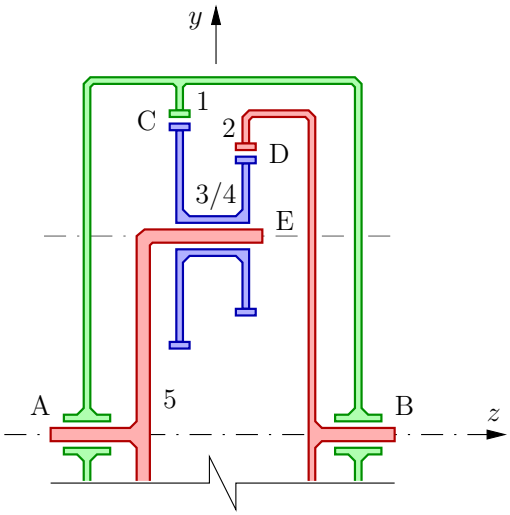

Figure 7 – Epicyclic gear train

3.4.1 Epicyclic gear train model

As a second and more complex example, the epicyclic gear train shown diagrammatically in Fig. 7 is analysed. This gear train has one carrier, link 5, one planet, link 3/4, and two annuli, links 1 and 2. Note that, a single number is associated with a gear, not a link, so link 3/4 comprises gears 3 and 4 and the gear pitch radii are r_3 and r_4, respectively. Characters A-E identify features such as bearings and tooth contacts. The coupling graph G_C is shown in Fig. 8 using the same notation introduced in Section 3.3.

3.4.1.1 Motion analysis

The motions allowed in the network of Fig. 7 are angular velocities about the axes parallel to the z-axis in the plane $x = 0$. Thus, the motion screws belong to a 2^{nd} special 2-system of screws according to Hunt's [52] classification. The unit motion matrix of the

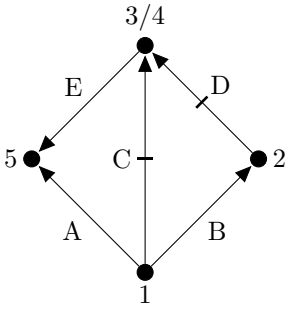

Figure 8 – Epicyclic gear train coupling graphs G_C

direct couplings is assembled from Table 12 in Appendix B as

$$\hat{\boldsymbol{M}}_D = \begin{matrix} \\ t \\ u \end{matrix} \begin{matrix} \begin{matrix} t_A & t_B & t_C & t_D & t_E \end{matrix} \\ \begin{bmatrix} 1 & 1 & 1 & 1 & 1 \\ 0 & 0 & r_1 & r_2 & r_1 - r_3 \end{bmatrix} \end{matrix}. \tag{54}$$

The coupling graph G_C and the motion graph G_M are identical since every coupling has one degree of freedom. The circuit matrices $\boldsymbol{B}$ of G_C and $\boldsymbol{B}_M$ of G_M are written choosing edges D and E as chords. This choice is arbitrary; it determines one of the eight possible spanning trees for G_C. Thus

$$\boldsymbol{B} = \boldsymbol{B}_M = \begin{matrix} \\ D \\ E \end{matrix} \begin{matrix} \begin{matrix} A & B & C & D & E \end{matrix} \\ \begin{bmatrix} 0 & 1 & -1 & 1 & 0 \\ -1 & 0 & 1 & 0 & 1 \end{bmatrix} \end{matrix}. \tag{55}$$

The network unit motion matrix $\left[\hat{\boldsymbol{M}}_N\right]_{d\,l \times F}$ is given by:

$$\left[\hat{\boldsymbol{M}}_N\right]_{d\,l \times F} = \begin{bmatrix} \left[\hat{\boldsymbol{M}}_D\right]_{d \times F} & [\boldsymbol{B}_1]_{F \times F} \\ \left[\hat{\boldsymbol{M}}_D\right]_{d \times F} & [\boldsymbol{B}_2]_{F \times F} \\ & \vdots \\ \left[\hat{\boldsymbol{M}}_D\right]_{d \times F} & [\boldsymbol{B}_l]_{F \times F} \end{bmatrix}_{d\,l \times F} \tag{56}$$

where l is the number of independent circuits (loops) of the cou-

pling graph G_C, $\left[\hat{\boldsymbol{M}}_D\right]_{d\times F}$ is the unit motion matrices of the direct couplings, and $[\boldsymbol{B}_i]_{F\times F} = \operatorname{diag}\left([\boldsymbol{B}_M]_i\right)$ are diagonal matrices $(i = 1, 2, \ldots, l)$. The diagonal elements of $[\boldsymbol{B}_i]_{F\times F}$ are those of row i of $[\boldsymbol{B}_M]_{l\times F}$, the circuit matrix of motion graph G_M. Applying the matrices of equations (54) and (55) in equation (56) leads to

$$\hat{\boldsymbol{M}}_N = \begin{array}{c} \\ t \\ u \\ t \\ u \end{array} \begin{array}{c} \begin{array}{ccccc} t_A & t_B & t_C & t_D & t_E \end{array} \\ \begin{bmatrix} 0 & 1 & -1 & 1 & 0 \\ 0 & 0 & -r_1 & r_2 & 0 \\ -1 & 0 & 1 & 0 & 1 \\ 0 & 0 & r_1 & 0 & r_1 - r_3 \end{bmatrix} \end{array} T_A \tag{57}$$

and the solution of equation (1) is proportional to the null space of $\hat{\boldsymbol{M}}_N$ given by

$$\operatorname{Null}\left(\hat{\boldsymbol{M}}_N\right) = \begin{bmatrix} 1 \\ \frac{(r_1 - r_2)\,(r_1 - r_3)}{r_2\, r_3} \\ 1 - \frac{r_1}{r_3} \\ -\frac{r_1\,(r_1 - r_3)}{r_2\, r_3} \\ \frac{r_1}{r_3} \end{bmatrix}. \tag{58}$$

Arbitrarily choosing t_A as the primary variable, the motion screws allowed by the epicyclic gear trains in Fig. 7 are given by

$$\begin{aligned} [\boldsymbol{M}]_{2\times 5} &= \hat{\boldsymbol{M}}_D \operatorname{diag}\left(\operatorname{Null}\left(\hat{\boldsymbol{M}}_N\right)\right) t_A \\ &= \begin{array}{c} \\ t \\ u \end{array} \begin{array}{c} \begin{array}{ccccc} \$_A^{\mathrm{m}} & \$_B^{\mathrm{m}} & \$_C^{\mathrm{m}} & \$_D^{\mathrm{m}} & \$_E^{\mathrm{m}} \end{array} \\ \begin{bmatrix} r_2\, r_3 & (r_1 - r_2)\,(r_1 - r_3) & -r_2\,(r_1 - r_3) & -r_1\,(r_1 - r_3) & r_1\, r_2 \\ 0 & 0 & -r_1\, r_2\,(r_1 - r_3) & -r_1\, r_2\,(r_1 - r_3) & r_1\, r_2\,(r_1 - r_3) \end{bmatrix} \end{array} \frac{t_A}{r_2\, r_3}. \end{aligned} \tag{59}$$

3.4.1.2 Action analysis ignoring power losses

The action analysis is very similar to the analysis presented in Section 3.3.3 and, if the same assumptions are made in addition to the assumption that there is only one planet, the geometrical classification of the action system is the same. In this particular case T_A and T_B are magnitudes of external torques, T_C and T_D are those of friction

torques, U_A, U_B and U_E are those of reaction forces related to the sole degree of constraint of each revolute coupling, and U_C and U_D are those of forces transmitted by the gear couplings. Ignoring power losses, the analysis is carried out without the actions whose magnitudes are T_C and T_D . So, the action matrix of the direct couplings $\hat{\boldsymbol{A}}_D$ is assembled with only seven columns from the data in Table 13 in Appendix B as

$$\hat{\boldsymbol{A}}_D = \begin{array}{c} \\ T \\ U \end{array} \begin{array}{c} \begin{array}{ccccccc} T_A & U_A & T_B & U_B & U_C & U_D & U_E \end{array} \\ \begin{bmatrix} 1 & 0 & 1 & 0 & -r_1 & -r_2 & r_3 - r_1 \\ 0 & 1 & 0 & 1 & 1 & 1 & 1 \end{bmatrix} \end{array}. \tag{60}$$

From Fig. 8 the cutset matrix, $\boldsymbol{Q}$, of coupling graph G_C is assembled and used to obtain $\boldsymbol{Q}_A$, the cutset matrix of action graph G_A, by means of column replication. Every column of $\boldsymbol{Q}$ is replicated a number of times equal to the number of independent actions transmitted by the respective coupling. Alternatively, the action graph G_A can be drawn as in reference [21] and the matrix $\boldsymbol{Q}_A$ is assembled by inspection. Cutset matrices are written with respect to a spanning tree, which can be chosen arbitrarily and even independently from the spanning tree used for motion analysis. Selecting branches A, B, and C for the G_C spanning tree, leads to

$$\boldsymbol{Q}_A = \begin{array}{c} \\ \mathrm{A} \\ \mathrm{B} \\ \mathrm{C} \end{array} \begin{array}{c} \begin{array}{ccccccc} \mathrm{A} & \mathrm{A} & \mathrm{B} & \mathrm{B} & \mathrm{C} & \mathrm{D} & \mathrm{E} \\ T_A & U_A & T_B & U_B & U_C & U_D & U_E \end{array} \\ \begin{bmatrix} 1 & 1 & 0 & 0 & 0 & 0 & 1 \\ 0 & 0 & 1 & 1 & 0 & -1 & 0 \\ 0 & 0 & 0 & 0 & 1 & 1 & -1 \end{bmatrix} \end{array}. \tag{61}$$

Matrix $\hat{\boldsymbol{A}}_N$ is then assembled using equation (19). The nullity of $\hat{\boldsymbol{A}}_N$ is one, indicating that only one primary variable is needed. Arbitrarily choosing T_A as the primary variable, the solution of equation (2) multiplied by the columns of matrix $\hat{\boldsymbol{A}}_D$ given by equation (60) produces the final result

$$\boldsymbol{A} = \begin{array}{c} \\ T \\ U \end{array} \begin{array}{c} \begin{array}{ccccc} \$_A^{\mathbf{a}} & \$_B^{\mathbf{a}} & \$_C^{\mathbf{a}} & \$_D^{\mathbf{a}} & \$_E^{\mathbf{a}} \end{array} \\ \begin{bmatrix} r_2\, r_3 - r_1\, r_4 & -r_2\, r_3 & r_1\, r_4 & -r_2\, r_3 & r_1\, r_4 - r_2\, r_3 \\ r_2 - r_1 & r_3 & -r_4 & r_3 & r_1 - r_2 \end{bmatrix} \end{array} \frac{T_A}{r_2\, r_3 - r_1\, r_4} \tag{62}$$

where the geometrical identity $r_1 - r_3 = r_2 - r_4$ was used to shorten the expression. The action screws in equation (62) are used to determine

the power flow of the ideal epicyclic gear train.

3.4.1.3 Action analysis considering power losses

The inclusion of friction losses is straightforward. Firstly, equations (60) and (61) have to be modified in order to include the action screws that model the friction torques and the respective edges of G_A. Matrix $\hat{\boldsymbol{A}}_N$ is reassembled using these matrices. The nullity of the new matrix $\hat{\boldsymbol{A}}_N$ is three, indicating that two more equations are needed. These equations relate the friction torque magnitudes to those of the transmitted forces and are given by

$$T_C = \zeta_C \, U_C \tag{63}$$

$$T_D = \zeta_D \, U_D \tag{64}$$

where ζ_C and ζ_D are coefficients of friction, now assumed to be real numbers in order to avoid the use of sign functions in equations (63) and (64).

Matrix $\hat{\boldsymbol{A}}_N$ is then stacked over two rows, those representing equations (63) and (64), to obtain the augmented action matrix $\boldsymbol{D}_A$. Finally, the sole vector of the null space of $\boldsymbol{D}_A$ is applied in equation (25) and columns relative to the same coupling are added together to produce

$$\boldsymbol{A} = \begin{array}{c} \\ T \\ U \end{array} \begin{array}{c} \begin{array}{ccccc} \$_A^a & \$_B^a & \$_C^a & \$_D^a & \$_E^a \end{array} \\ \begin{bmatrix} r_1 - r_3 & \frac{(\zeta_D - r_2)(\zeta_C - r_3)}{\zeta_C - \zeta_D - r_1 + r_2} & -\frac{(\zeta_C - r_1)(\zeta_D + r_4)}{\zeta_C - \zeta_D - r_1 + r_2} & \frac{(\zeta_D - r_2)(\zeta_C - r_3)}{\zeta_C - \zeta_D - r_1 + r_2} & r_3 - r_1 \\ -1 & \frac{\zeta_C - r_3}{\zeta_C - \zeta_D - r_1 + r_2} & 1 - \frac{\zeta_C - r_3}{\zeta_C - \zeta_D - r_1 + r_2} & \frac{\zeta_C - r_3}{\zeta_C - \zeta_D - r_1 + r_2} & 1 \end{bmatrix} \end{array} \frac{T_A}{r_1 - r_3} \tag{65}$$

The action screws in equation (65) are used to determine the power flow of the real epicyclic gear train and the overall efficiency.

3.4.1.4 Virtual power flow

The virtual power flow reveals which gear drives and which is driven in a gear pair, so it is important when deriving efficiency equations. Moreover, ordinary efficiency is the portion of the virtual power flow that actually flows across the gear coupling when the carrier is taken as the reference (see Section 3.4.1.5).

The carrier of the system under analysis is link 5 in Fig. 7 and the motion screws relative to this link can be written with the help of

the reduced incidence matrix $\boldsymbol{A}_5$ constructed by inspecting the graph in Fig. 8 as

$$\boldsymbol{A}_5 = \begin{array}{c} \\ 1 \\ 2 \\ 3/4 \end{array} \begin{array}{c} \begin{array}{ccccc} \mathrm{A} & \mathrm{B} & \mathrm{C} & \mathrm{D} & \mathrm{E} \end{array} \\ \begin{bmatrix} 1 & 1 & 1 & 0 & 0 \\ 0 & -1 & 0 & 1 & 0 \\ 0 & 0 & -1 & -1 & 1 \end{bmatrix} \end{array} \tag{66}$$

where the element $a_{i\,j}$ of $\boldsymbol{A}_5$ is 1 if the edge j starts in node i, -1 if edge j ends at this node, and zero if edge j is not incident with node i. The pseudoinverse of matrix $\boldsymbol{A}_5$ is then computed using equation (7) as

$$\boldsymbol{A}_5^{\dagger} = \begin{array}{c} \\ \mathrm{A} \\ \mathrm{B} \\ \mathrm{C} \\ \mathrm{D} \\ \mathrm{E} \end{array} \begin{array}{c} \begin{array}{ccc} 1 & 2 & 3/4 \end{array} \\ \begin{bmatrix} 5 & 4 & 3 \\ 1 & -4 & -1 \\ 2 & 0 & -2 \\ 1 & 4 & -1 \\ 3 & 4 & 5 \end{bmatrix} \end{array} \frac{1}{8}\,. \tag{67}$$

Application of equation (6) results in

$$\boldsymbol{M}_5 = \begin{array}{c} \\ t \\ u \end{array} \begin{array}{c} \begin{array}{ccc} {}^{5}\$_{1}^{\mathbf{m}} & {}^{5}\$_{2}^{\mathbf{m}} & {}^{5}\$_{3/4}^{\mathbf{m}} \end{array} \\ \begin{bmatrix} 1 & -\frac{r_1\,r_4}{r_2\,r_3} & -\frac{r_1}{r_3} \\ 0 & 0 & r_1 - \frac{{r_1}^2}{r_3} \end{bmatrix} \end{array} t_A\,. \tag{68}$$

Power losses are unlikely to change the power flow direction [12], thus, in the determination of the driver/driven relationship they can be neglected. To prevent the possibility of a mistake, however, it might be wise to verify the overall efficiency equation obtained as described in Section 3.6.2. The main motivation for neglecting power loss is the obtainment of a turning condition of easy interpretation.

Observing the third columns of matrix $\boldsymbol{A}_5$ in equation (66), the virtual power flow through gear coupling C can be computed using the first or third column of matrix $\boldsymbol{M}_5$ in equation (68). If power losses are neglected, the power exchanged by gears 1 and 3 is given by

$$\mathcal{P}_{13} = \$_{C}^{\mathbf{a}} \bullet^{5} \$_{1}^{\mathbf{m}} = \$_{C}^{\mathbf{a}} \bullet^{5} \$_{3/4}^{\mathbf{m}} = T_A\,t_A\,\frac{r_1\,r_4}{r_1\,r_4 - r_2\,r_3} \tag{69}$$

where $\$_{C}^{\mathbf{a}}$ is taken from equation (62).

If $T_A\,t_A > 0$ and $r_1\,r_4 - r_2\,r_3 > 0$ (or simply $r_1 < r_2$ since $r_1 - r_3 = r_2 - r_4$), $\mathcal{P}_{13} > 0$ in equation (69). Consequently, the virtual power flow direction through coupling C is the same as that of edge C of G_C in Fig. 8: from gear 1 to gear 3. In other words, gear 1 drives gear 3 if these conditions are observed. If $T_A\,t_A > 0$ and $r_1 < r_2$, $\$_C^{\mathbf{a}} \bullet^5 \$_1^{\mathbf{m}}$ will be the power flow that leaves link 1 through coupling C and $\$_C^{\mathbf{a}} \bullet^5 \$_{3/4}^{\mathbf{m}}$ will be the power flow that arrives at link 3/4 through coupling C and these quantities are equal only if power losses in coupling C are neglected.

Likewise, the virtual power flow through gear coupling D can be computed using the second or third column of matrix $\boldsymbol{M}_5$ in equation (68) since the respective rows of the fourth column of matrix $\boldsymbol{A}_5$ in equation (66) contain non-null elements. The power exchanged by gears 2 and 4 neglecting power losses is given by

$$\mathcal{P}_{24} = \$_D^{\mathbf{a}} \bullet^5 \$_2^{\mathbf{m}} = \$_D^{\mathbf{a}} \bullet^5 \$_{3/4}^{\mathbf{m}} = -T_A\,t_A\,\frac{r_1\,r_4}{r_1\,r_4 - r_2\,r_3} \tag{70}$$

where $\$_D^{\mathbf{a}}$ is taken from equation (62).

The virtual power flow direction through coupling D will be the opposite to that of edge D of G_C in Fig. 8 if $T_A\,t_A > 0$ and $r_1 < r_2$. In other words, gear 4 drives gear 2 if these conditions are observed.

3.4.1.5 Efficiency

According to Definition 5, the overall efficiency of epicyclic gear trains is the ratio between the output and input power. Temporarily assuming that $T_A\,t_A > 0$ which implies that coupling A is the input and, consequently, coupling B is the output, the overall efficiency is given by

$$\eta = \frac{-\mathcal{P}_B}{\mathcal{P}_A} = \frac{-\$_B^{\mathbf{a}} \bullet \$_B^{\mathbf{m}}}{\$_A^{\mathbf{a}} \bullet \$_A^{\mathbf{m}}} = \frac{(r_2 - r_1)\,(\zeta_D - r_2)\,(\zeta_C - r_3)}{r_2\,r_3\,(\zeta_C - \zeta_D - r_1 + r_2)} \tag{71}$$

where action screws $\$_A^{\mathbf{a}}$ and $\$_B^{\mathbf{a}}$ are taken from equation (65), since power loss is to be considered, motion screws $\$_A^{\mathbf{m}}$ and $\$_B^{\mathbf{m}}$ from equation (59), and the negative sign compensates the fact that output power has a negative sign according to the adopted sign convention. If, however, the input/output relationship is inverted and $T_A\,t_A < 0$, the efficiency will be the reciprocal of the value predicted by equation (71).

The coefficients of friction ζ_C and ζ_D can be determined in terms

of the ordinary efficiencies η_{13} and η_{42}. The ordinary efficiency of a gear coupling is computed dividing the virtual power flow that enters the driven gear by that which leaves the driver gear through the gear coupling. Thus, assuming, also temporarily, that $r_1 < r_2$ and so gear 1 drives gear 3 and gear 4 drives gear 2, the ordinary efficiencies are

$$\eta_{13} = \frac{\$_C^{\mathbf{a}} \bullet^5 \$_{3/4}^{\mathbf{m}}}{\$_C^{\mathbf{a}} \bullet^5 \$_1^{\mathbf{m}}} = \frac{r_1\,(\zeta_C - r_3)}{r_3\,(\zeta_C - r_1)} \tag{72}$$

$$\eta_{42} = \frac{\$_D^{\mathbf{a}} \bullet^5 \$_2^{\mathbf{m}}}{\$_D^{\mathbf{a}} \bullet^5 \$_{3/4}^{\mathbf{m}}} = \frac{r_4\,(\zeta_D - r_2)}{r_2\,(\zeta_D - r_4)} \tag{73}$$

where action screws $\$_C^{\mathbf{a}}$ and $\$_D^{\mathbf{a}}$ are taken from equation (65), and motion screws ${}^5\$_1^{\mathbf{m}}$, ${}^5\$_2^{\mathbf{m}}$, and ${}^5\$_{3/4}^{\mathbf{m}}$ from equation (68). Isolating the coefficients of friction:

$$\zeta_C = \frac{r_1\,r_3 - \eta_{13}\,r_1\,r_3}{r_1 - \eta_{13}\,r_3} \tag{74}$$

$$\zeta_D = \frac{r_2\,r_4 - \eta_{42}\,r_2\,r_4}{r_4 - \eta_{42}\,r_2} \tag{75}$$

and substituting these coefficients of friction in equation (71), the overall efficiency is written as

$$\eta = \frac{\eta_{13}\,\eta_{42}\,(r_1\,r_4 - r_2\,r_3)}{r_1\,r_4 - \eta_{13}\,\eta_{42}\,r_2\,r_3}\,. \tag{76}$$

Equation (76) is valid only when $T_A\,t_A > 0$ and $r_1 < r_2$. If $r_1 > r_2$, the virtual power flow through the gear couplings will reverse direction and equations (72) and (73) will express the reciprocal of the ordinary efficiency. Thus, η_{13} must be replaced by ${\eta_{31}}^{-1}$ and η_{42} by ${\eta_{24}}^{-1}$ in equation (76). The result is shown in equation (77) (see Table 5). If r_1 is kept smaller than r_2, but the input/output are swapped, the product $T_A\,t_A$ will be negative and the power flow will also reverse. Equation (76) will need to be changed in two ways: with the aforementioned replacement and inversion. The result is equation (78). The last case occurs when $T_A\,t_A < 0$ and $r_1 > r_2$. In this case the power flow through the gear couplings will not reverse, but the input/output are swapped and so the actual efficiency will be the reciprocal of that of equation (76), as predicted by equation (79).

Table 5 – Overall efficiency of the epicyclic gear train of Fig. 7 under different conditions

Input	Output	$T_A\, t_A$	$\dfrac{r_1}{r_2}$	η	#
A	B	> 0	< 1	$\dfrac{\eta_{13}\,\eta_{42}\,(r_1\,r_4 - r_2\,r_3)}{r_1\,r_4 - \eta_{13}\,\eta_{42}\,r_2\,r_3}$	(76)
A	B	> 0	> 1	$\dfrac{r_2\,r_3 - r_1\,r_4}{r_2\,r_3 - \eta_{31}\,\eta_{24}\,r_1\,r_4}$	(77)
B	A	< 0	< 1	$\dfrac{r_2\,r_3 - \eta_{31}\,\eta_{24}\,r_1\,r_4}{r_2\,r_3 - r_1\,r_4}$	(78)
B	A	< 0	> 1	$\dfrac{r_1\,r_4 - \eta_{13}\,\eta_{42}\,r_2\,r_3}{\eta_{13}\,\eta_{42}\,(r_1\,r_4 - r_2\,r_3)}$	(79)

Equation (77) in Table 5 is in accordance with the equation

$$\eta = \frac{1}{(\lambda_1 + \lambda_2 - \lambda_1\,\lambda_2)\,(k-1)+1}$$

proposed by Chen and Angeles [3] where $\lambda_1 = 1 - \eta_{31}$, $\lambda_2 = 1 - \eta_{24}$, and

$$k = \frac{r_2\,r_3}{r_2\,r_3 - r_1\,r_4}\,.$$

3.4.1.6 Pitch radius r_i versus number of teeth z_i

It is interesting to note that the formulae of Table 5 will produce the same result if pitch radii r_i $(i = 1, \ldots, 4)$ are replaced by the number of teeth z_i even if the gear pair C and D have different modules. This is so because every term in the efficiency formulae contains the product of two radii, each one from a different meshing pair. Radii, nevertheless, should still be used to select the correct formula.

Consider, for example, that coupling A is the input and the number of teeth are $z_1 = 80$, $z_2 = 60$, $z_3 = 30$, and $z_4 = 35$. The module of the gear pair D must be twice that of C to assure that the radii satisfy the geometrical constraint: $r_1 - r_3 = r_2 - r_4$. Adopting 1 mm for the module of gear pair C, and consequently 2 mm for gear pair D, the radii are found to be: $r_1 = 40\,\text{mm}$, $r_2 = 60\,\text{mm}$,

$r_3 = 15\,\text{mm}$, and $r_4 = 35\,\text{mm}$. The geometrical constraint is respected, $r_1 - r_3 = r_2 - r_4 = 25\,\text{mm}$. Assuming now that $\eta_{13} = \eta_{42} = 0.99$, in keeping with common practice [11], from equation (76) the overall efficiency is found to be $\eta = 0.9462$ even if the numbers of teeth are used instead of radii. Equation (76) is used here because $r_1 < r_2$.

If, however, by mistake the numbers of teeth are used in the comparison ($z_1 > z_2$), equation (77) could be wrongly used producing a result which is greater than the unity, a clear indication of an error.

It is also not recommendable to blindly apply the formulae in Table 5 hoping for a result which is smaller than unity. In this example, equation (78) produces $\eta = 0.9443$ which is close to the correct value of 0.9462, but wrong nevertheless.

3.5 BEVEL GEAR TRAIN MODEL

Bevel gears have found broad application in mechanical engineering, for instance, in helicopter and truck transmission and reducers for transformation of rotation and torque between intersected axes [70]. The major difficulty associated with the calculation of efficiency of these gear trains arises from the non parallelism between axes, which requires special consideration, as in the work by Nelson and Cipra [7]. The application of the work of Castillo Granado [17] is also prevented for the same reason.

The proposed approach, however, encounters no difficulty with these trains if an appropriate screw system is selected. An epicyclic gear using bevel gears, called the Humpage bevel gear, is used herein to illustrate the method application. Interestingly, although the Humpage bevel gear appears frequently in the literature, no efficiency equation was found for it in the review.

3.5.1 Humpage bevel gear

The simplification assumptions detailed in the previous sections are again made herein. However, the non-parallelism of the axes requires an increase in the screw system dimension.

In the Humpage bevel gears schematically illustrated in Fig. 9, the relative motions that can take place are rotations whose ISAs belong to the pencil of lines passing through the origin in the plane $x = 0$. Thus, according to Hunt's [52] classification, all motion screws belong

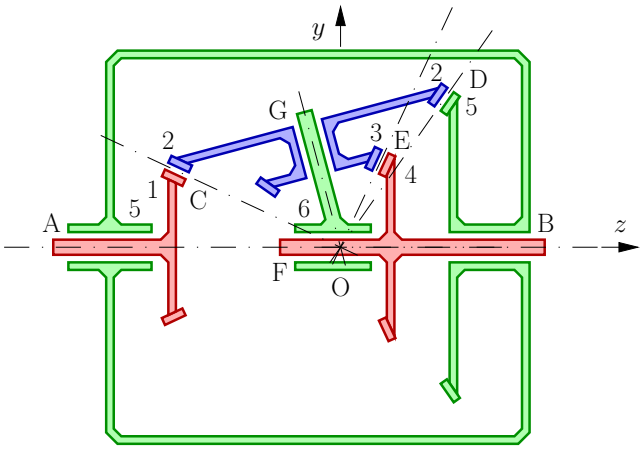

Figure 9 – Humpage bevel gears

to a 1st special 2-system of screws.

The actions transmitted by the couplings and not related to overconstrains are forces parallel to the x-axis and torques directed parallel to plane $x = 0$. Thus, these action screws belong to a 5th special 3-system of screws and can be spanned by the 3-system of screws $\{S, T; U\}$.

The motion screws can be spanned by the 2-system of screws $\{s, t\}$. It is desirable, but not necessary if equation (5) is judiciously applied, to use the same dimension d for both action and motion systems of screws. Thus, the 4th special 3-system of screws $\{s, t; u\}$ is adopted for motions. Consequently, the last coordinate is zero for all motion screws.

Couplings A and B are connected to the external torque source and sink which provide torques whose magnitude are T_A and T_B. It is assumed that coupling A is the input, so $T_A\, t_A > 0$, and the changes needed for the converse case are explained at the end of this section.

Couplings A, B, F, and G are of the revolute type allowing a rotation about the z-axis with the exception of G, which allows a rotation about the axis through the origin with orientation parallel to

the unit vector

$$\hat{p}_G = \begin{matrix} x \\ y \\ z \end{matrix} \begin{bmatrix} 0 \\ -(r_5 - r_1) \\ \sqrt{4\,{r_2}^2 - (r_5 - r_1)^2} \end{bmatrix} \frac{1}{2\,r_2} \tag{80}$$

at the instant that the coupling network is found as shown in Fig. 9.

The action transmitted by each coupling can be spanned by a force parallel to the x-axis and a torque directed parallel to plane $x = 0$. For gear couplings, the force line of action passes through the respective contact point (see equation (138)). For revolute couplings, the force line of action intersects the coupling axis at a chosen point and the most sensible choice is the origin. The torque direction, also for revolute couplings, is orthogonal to the motion ISA allowed by the coupling. For couplings A, B, and F these torques are parallel to the y-axis and for coupling G parallel to the unit vector

$$\hat{P}_G = \begin{matrix} x \\ y \\ z \end{matrix} \begin{bmatrix} 0 \\ \sqrt{4\,{r_2}^2 - (r_5 - r_1)^2} \\ r_5 - r_1 \end{bmatrix} \frac{1}{2\,r_2}\,. \tag{81}$$

Couplings C, D, and E are of the gear type and their motion ISAs pass through the origin O and the respective point in Fig. 9. Also, their friction torques are parallel to the respective motion ISAs.

Using the data available from Table 14 in Appendix C, the unit motion matrix of the direct couplings is assembled as

$$\boldsymbol{M}_D = \begin{matrix} \\ s \\ t \\ u \end{matrix} \begin{bmatrix} t_A & t_B & p_C & p_D & p_E & t_F & p_G \\ 0 & 0 & \frac{a\sqrt{b}\,r_1}{2\,r_2} & \frac{a\sqrt{b}\,r_5}{2\,r_2} & \frac{\sqrt{b}\,r_4}{2\,c} & 0 & -\frac{g}{2\,r_2} \\ 1 & 1 & -\frac{a\,e}{2\,r_2} & \frac{a\,d}{2\,r_2} & \frac{f}{2\,c} & 1 & \frac{\sqrt{b}}{2\,r_2} \\ 0 & 0 & 0 & 0 & 0 & 0 & 0 \end{bmatrix} \tag{82}$$

where

$$
\begin{aligned}
a &= \sqrt{{r_2}^2 + r_1\, r_5} \\
b &= 4\,{r_2}^2 - (r_5 - r_1)^2 \\
c &= \sqrt{({r_3}^2 + {r_4}^2)\ {r_2}^2 - r_2\, r_3\, r_4\ (r_5 - r_1)} \\
d &= 2\,{r_2}^2 - r_5\ (r_5 - r_1) \\
e &= 2\,{r_2}^2 + r_1\ (r_5 - r_1) \\
f &= 2\, r_2\, r_3 - r_4\ (r_5 - r_1)\ .
\end{aligned}
\tag{83}
$$

The unit action matrix of the direct couplings is assembled as

$$
\boldsymbol{A}_D^T = \begin{array}{c} \\ S_A \\ T_A \\ U_A \\ S_B \\ T_B \\ U_B \\ P_C \\ U_C \\ P_D \\ U_D \\ P_E \\ U_U \\ S_F \\ U_F \\ P_G \\ U_G \end{array}
\begin{array}{c}
\begin{array}{ccc} S & T & U \end{array} \\
\left[\begin{array}{ccc}
1 & 0 & 0 \\
0 & 1 & 0 \\
0 & 0 & 1 \\
1 & 0 & 0 \\
0 & 1 & 0 \\
0 & 0 & 1 \\
\frac{\sqrt{b}\, r_1}{2\, a\, r_2} & -\frac{e}{2\, a\, r_2} & 0 \\
-\frac{e}{\sqrt{b}} & -r_1 & 1 \\
\frac{\sqrt{b}\, r_5}{2\, a\, r_2} & \frac{d}{2\, a\, r_2} & 0 \\
\frac{d}{\sqrt{b}} & -r_5 & 1 \\
\frac{\sqrt{b}\, r_4}{2\, c} & \frac{f}{2\, c} & 0 \\
\frac{f}{\sqrt{b}} & -r_4 & 1 \\
1 & 0 & 0 \\
0 & 0 & 1 \\
\frac{\sqrt{b}}{2\, r_2} & -\frac{r_1 - r_5}{2\, r_2} & 0 \\
0 & 0 & 1
\end{array}\right]
\end{array}
\tag{84}
$$

using the data available from Table 15 in Appendix C.

The topology of the coupling network illustrated in Fig. 9 is represented by the coupling graph in Fig. 10. Using any of the 21 possible spanning trees of this coupling graph, the fundamental cutset, $\boldsymbol{Q}$, and circuit, $\boldsymbol{B}$, matrices are written. There is no need to use the same spanning tree for the two matrices, but sometimes it is convenient [50].

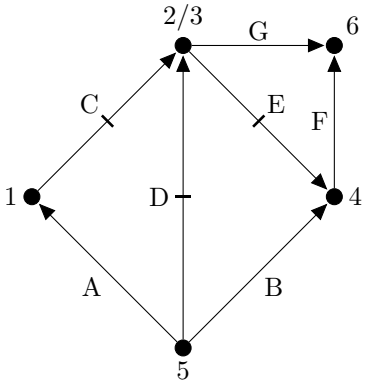

Figure 10 – Humpage bevel gear coupling graph G_C

The fundamental circuit matrix for the motion graph, $\boldsymbol{B}_M$, is identical to that of the coupling graph, $\boldsymbol{B}$. Therefore, the motion analysis can be performed assembling the network unit motion matrix $\hat{\boldsymbol{M}}_N$ using equations (56) and (82) and the circuit matrix $\boldsymbol{B} = \boldsymbol{B}_M$, then solving the system for a primary variable, for example, t_A and finally writing the motion matrix $\boldsymbol{M}$ in terms of the primary variable. This process is exemplified in detail in Section 3.4.1.1.

Two fundamental cutset matrices for the actions graph, $\boldsymbol{Q}_A$, are obtained replicating the columns of $\boldsymbol{Q}$ a number of times equal to the number of independent actions transmitted by the respective coupling. The first one has 13 columns and is used to perform the power flow analysis ignoring power loss. This matrix does not include columns related to the actions whose magnitude are P_C, P_D, and P_E. The other matrix has 16 columns, one for each direct coupling action. This matrix is used to determine the coefficients of friction ζ_C, ζ_D, and ζ_E in terms of the ordinary efficiencies η_{21}, η_{25} and η_{43}, and also the overall efficiency η.

These matrices $\boldsymbol{Q}_A$ are used to assemble two network unit action matrices $\hat{\boldsymbol{A}}_N$ using equations (19) and (84). The two solutions for equation (2) are then found, one of them ignoring power loss and the other considering it. These solutions are magnitudes of all actions in terms of a primary variable, e.g., T_A.

Using the matrix $\boldsymbol{A}_D$ in equation (84) all direct coupling actions are found in terms of the chosen primary variable for the two distinct situations, with and without power loss. This process is exemplified in detail in Section 3.4.1.2 and 3.4.1.1.

3.5.1.1 Virtual power flow and efficiency

To determine the virtual power flow direction it is necessary to ascertain the motion of each gear with respect to the carrier (link 6 in Fig. 9). This can be carried out using the procedure described in Section 3.1.1 and exemplified in Section 3.4.1.4 or by inspection. In this Section, the inspection method is explained and exemplified.

Starting from the reference link, a *path*[9] leading to a specific link is traced on the coupling graph. Normally, multiple paths are possible, and all of them produce the same result. For example, from link 6 to link 2/3 in Fig. 10, four different paths are possible. The shortest path has only edge G, the second shortest path has edges F and E; the third shortest path has edges F, B, and D; and finally the longest path has edges F, B, A, and C.

The motion screw that describes the relative motion of the destination link with respect to the starting link is equal to the algebraic sum of the motion screws associated with the edges belonging to the path. These motion screws have a negative sign when the edge direction is the opposite of the path direction and positive otherwise.

Applying these rules, the motion screws of all links with respect to link 6 are

$$\begin{aligned} {}^6\$_1^{\mathbf{m}} &= -\$_G^{\mathbf{m}} - \$_C^{\mathbf{m}} \\ {}^6\$_{2/3}^{\mathbf{m}} &= -\$_G^{\mathbf{m}} \\ {}^6\$_4^{\mathbf{m}} &= -\$_F^{\mathbf{m}} \\ {}^6\$_5^{\mathbf{m}} &= -\$_G^{\mathbf{m}} - \$_D^{\mathbf{m}} \end{aligned} \tag{85}$$

where $\$_C^{\mathbf{m}}$, $\$_D^{\mathbf{m}}$, $\$_F^{\mathbf{m}}$, and $\$_G^{\mathbf{m}}$ are taken from motion matrix $\boldsymbol{M}$ written in terms of the primary variable. In equation (85), the chosen paths are made evident by the screw index.

Once the motions are known, the power flow through each coupling can be found. Using the action screw computed ignoring power loss, the power flow through coupling C is given by

$$\begin{aligned} \mathcal{P}_{12} &= \$_C^{\mathbf{a}} \bullet^6 \$_1^{\mathbf{m}} = \$_C^{\mathbf{a}} \bullet^6 \$_{2/3}^{\mathbf{m}} \\ &= T_A\, t_A\, \frac{r_5 \left((r_5 - 3\, r_1)\; {r_2}^2 + r_1\; (r_5 - r_1)^2 \right)}{{r_2}^2\; ({r_5}^2 - {r_1}^2)} \end{aligned} \tag{86}$$

where T_A is the input torque and t_A is the input angular speed since

[9] Also called *walk* [74]

coupling A is the input under the hypothesis that $T_A\, t_A > 0$, and $\$^{\mathbf{a}}_C$ is taken from action matrix $\boldsymbol{A}$ written in terms of the primary variable and ignoring power losses. Note that the choice of T_A and t_A as primary variables is an arbitrary one, but it is convenient nevertheless.

If the sign of $\mathcal{P}_{12}$ given by equation (86) is positive, the power flows in the same direction as that of edge C in Fig. 10, meaning that gear 1 drives gear 2. Thus, assuming that the input coupling is established, the power flow direction is dependent only on the relationship between the pitch radii. Making the right-hand side of equation (86) equal to zero, a three dimensional surface in the radii space is defined. This turning condition surface, shown in Fig. 11, separates the regions of the radii space in which the power flow through coupling C has different signs. On crossing from one region to another, the definition for ordinary efficiency is inverted.

Since the goal is not to compute the actual value of the power flow, but rather to ascertain its direction, the expression $\left((r_5 - 3\,r_1)\ {r_2}^2 + r_1\ (r_5 - r_1)^2\right)\ (r_5 - r_1)$ might be used in place of the fraction on the right-hand side of equation (86).

Likewise, the power flow through coupling D can be determined using the motion of gear 2 or 5

$$\begin{aligned}\mathcal{P}_{25} &= \$^{\mathbf{a}}_D \bullet^6 \$^{\mathbf{m}}_5 = \$^{\mathbf{a}}_D \bullet^6 \$^{\mathbf{m}}_{2/3} \\ &= T_A\, t_A\, \frac{r_5\ (r_1\, r_3 + r_2\, r_4)\ \left((r_1 - 3\,r_5)\ {r_2}^2 + r_5\ (r_5 - r_1)^2\right)}{{r_2}^2\ (r_2\, r_4 - r_3\, r_5)\ ({r_5}^2 - {r_1}^2)}\end{aligned} \tag{87}$$

where ${}^6\$^{\mathbf{m}}_5$ and ${}^6\$^{\mathbf{m}}_{2/3}$ are given by equation (85) and $\$^{\mathbf{a}}_D$ is taken from action matrix $\boldsymbol{A}$. In this case, the turning condition surface is defined in an $\mathbb{R}^5$ space by the equation

$$\left((r_1 - 3\,r_5)\ {r_2}^2 + r_5\ (r_5 - r_1)^2\right)\ (r_5 - r_1)\ (r_2\, r_4 - r_3\, r_5) = 0\,.$$

The power flow through coupling E, as with every gear coupling, can be determined by two gear motions as

$$\begin{aligned}\mathcal{P}_{43} &= \$^{\mathbf{a}}_E \bullet^6 \$^{\mathbf{m}}_4 = \$^{\mathbf{a}}_E \bullet^6 \$^{\mathbf{m}}_{2/3} \\ &= T_A\, t_A\, \frac{r_5\ \left(r_4\ \left((r_5 - r_1)^2 - 2\,{r_2}^2\right) - r_3\, r_2\ (r_5 - r_1)\right)}{r_2\ (r_5 - r_1)\ (r_2\, r_4 - r_3\, r_5)}\end{aligned} \tag{88}$$

where ${}^6\$^{\mathbf{m}}_4$ and ${}^6\$^{\mathbf{m}}_{2/3}$ are given by equation (85) and $\$^{\mathbf{a}}_E$ is taken from

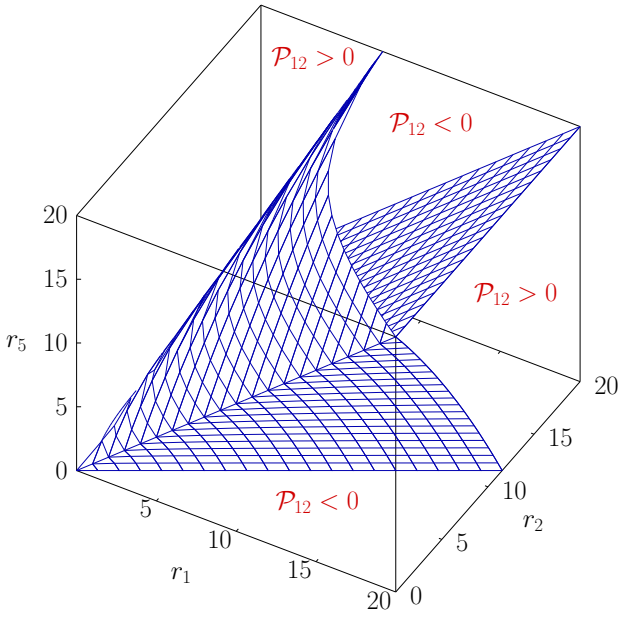

Figure 11 – Turning condition surfaces for gear coupling C for $T_A\, t_A > 0$, $\mathcal{P}_{12}$ is given by equation (86)

action matrix $\boldsymbol{A}$. In this case, the turning condition surface is also defined in an $\mathbb{R}^5$ space. A simpler equation for this surface is

$$\Big(r_4\,\Big((r_5 - r_1)^2 - 2\,{r_2}^2\Big) - r_3\,r_2\,(r_5 - r_1)\Big)\,(r_5 - r_1)\,(r_2\,r_4 - r_3\,r_5) = 0\,.$$

Assuming that $\Big((r_5 - 3\,r_1)\,{r_2}^2 + r_1\,(r_5 - r_1)^2\Big)\,(r_5 - r_1) < 0$, and thus gear 2 drives gear 1, the ordinary efficiency of coupling C is given by

$$\eta_{21} = \frac{\mathcal{P}_1}{\mathcal{P}_2} = \frac{\$_C^{\mathbf{a}} \bullet^6 \$_1^{\mathbf{m}}}{\$_C^{\mathbf{a}} \bullet^6 \$_{2/3}^{\mathbf{m}}} \tag{89}$$

where equation (85) provides ${}^6\$_1^{\mathbf{m}}$ and ${}^6\$_{2/3}^{\mathbf{m}}$, and $\$_C^{\mathbf{a}}$ is taken from action matrix $\boldsymbol{A}$ written in terms of the primary variable and, this time, considering power loss. Equation (89) contains only one coefficient of friction, ζ_C.

Using the same action matrix $\boldsymbol{A}$ and the equation (85), the

ordinary efficiency of couplings D and E can be expressed as

$$\eta_{25} = \frac{\mathcal{P}_5}{\mathcal{P}_2} = \frac{\$_D^{\mathbf{a}} \bullet^6 \$_5^{\mathbf{m}}}{\$_D^{\mathbf{a}} \bullet^6 \$_{2/3}^{\mathbf{m}}} \tag{90}$$

$$\eta_{43} = \frac{\mathcal{P}_4}{\mathcal{P}_3} = \frac{\$_E^{\mathbf{a}} \bullet^6 \$_{2/3}^{\mathbf{m}}}{\$_E^{\mathbf{a}} \bullet^6 \$_4^{\mathbf{m}}} \tag{91}$$

and each one of these equations contains only one coefficient of friction.

Solving equations (89), (90), and (91) for ζ_C, ζ_D, and ζ_E leads to

$$\zeta_C = \frac{2\,a\,r_1\,r_2\,\left(b\,r_1 - e\,\left(r_5 - r_1\right)\right)\,\left(1 - \eta_{21}\right)}{e^2\,\left(r_5 - r_1\right) - b\,e\,r_1 + \eta_{21}\,b\,r_1\,\left(r_1\,\left(r_5 - r_1\right) + e\right)} \tag{92}$$

$$\zeta_D = \frac{2\,a\,r_2\,r_5\,\left(b\,r_5 + d\,\left(r_5 - r_1\right)\right)\,\left(1 - \eta_{25}\right)}{d^2\,\left(r_5 - r_1\right) + b\,d\,r_5 + \eta_{25}\,b\,r_5\,\left(r_5\,\left(r_5 - r_1\right) - d\right)} \tag{93}$$

$$\zeta_E = \frac{2\,c\,r_4\,\left(b\,r_4 + f\,\left(r_5 - r_1\right)\right)\,\left(1 - \eta_{43}\right)}{b\,r_4\,\left(f - r_4\,\left(r_5 - r_1\right)\right) - \eta_{43}\,f\,\left(b\,r_4 + f\,\left(r_5 - r_1\right)\right)} \tag{94}$$

where the constants a, b, c, d, e, and f are defined by equation (83).

The overall efficiency is computed by

$$\eta = \frac{\mathcal{P}_B}{\mathcal{P}_A} = \frac{\$_A^{\mathbf{a}} \bullet \$_A^{\mathbf{m}}}{\$_B^{\mathbf{a}} \bullet \$_B^{\mathbf{m}}} = \frac{\left(r_2\,r_4 - r_3\,r_5\right)\,\left(\eta_{21}\,r_1\,A - \eta_{25}\,r_5\,B\right)}{r_2\,\left(r_1 + r_5\right)\,\left(\eta_{21}\,r_4\,A + \eta_{21}\,\eta_{43}\,\eta_{25}\,r_5\,C\right)} \tag{95}$$

where $\$_A^{\mathbf{m}}$ and $\$_B^{\mathbf{m}}$ are taken from matrix $\boldsymbol{M}$, $\$_A^{\mathbf{a}}$ and $\$_B^{\mathbf{a}}$ from $\boldsymbol{A}$ considering power loss, and the constants are defined by

$$\begin{aligned} A &= {r_2}^2\,\left(r_1 - 3\,r_5\right) + r_5\,\left(r_5 - r_1\right)^2 \\ C &= {r_2}^2\,\left(r_5 - 3\,r_1\right) + r_1\,\left(r_5 - r_1\right)^2 \\ B &= r_4\,\left(2\,{r_2}^2 - \left(r_5 - r_1\right)^2\right) + r_2\,r_3\,\left(r_5 - r_1\right)\,. \end{aligned}$$

In deriving equation (95), four specific conditions were assumed to be true. The first one relates to knowledge of the input and output coupling. The other three relate to the power flow direction of each gear coupling and these assumptions are base on the relationship between the pitch radii. Before applying equation (95), Table 6 must be consulted and the modifications carried out if necessary.

Table 6 – Conditions for modifying equation (95)

Expression	Condition		Action	
	$T_A\, t_A > 0$	$T_A\, t_A < 0$	replace	by
$\left((r_5 - 3\, r_1)\ {r_2}^2 + r_1\ (r_5 - r_1)^2 \right)\ (r_5 - r_1)$	> 0	< 0	η_{21}	${\eta_{12}}^{-1}$
$\left((r_1 - 3\, r_5)\ {r_2}^2 + r_5\ (r_5 - r_1)^2 \right)\ (r_5 - r_1)\ (r_2\, r_4 - r_3\, r_5)$	> 0	< 0	η_{25}	${\eta_{52}}^{-1}$
$\left(r_4\ \left((r_5 - r_1)^2 - 2\, {r_2}^2 \right) - r_3\, r_2\ (r_5 - r_1) \right)\ (r_5 - r_1)\ (r_2\, r_4 - r_3\, r_5)$	> 0	< 0	η_{43}	${\eta_{34}}^{-1}$

3.5.1.2 Numerical example and comparison

Nelson and Cipra [7] applied a numerical method to calculate the efficiency of a Humpage bevel gear with the following numbers of teeth: $z_1 = 20$, $z_2 = 56$, $z_3 = 24$, $z_4 = 35$, and $z_5 = 76$. Coupling A was used as the input and coupling B as the output ($T_A\, t_A > 0$). Assuming that the module is the same for all gears, so the numbers of teeth can be used in the place of pitch radii, the expression in the first row of Table 6 is found to be positive and the other two negative. Therefore, η_{21} has to be replaced by ${\eta_{12}}^{-1}$ in equation (95). The ordinary efficiency of each gear pair is not given by Nelson and Cipra [7], but the power lost in each gear pair and the input power can be obtained from the available data. The power lost in each gear pair is given by

$$\begin{aligned} \mathcal{P}_C &= \$_C^{\mathbf{a}} \bullet \$_C^{\mathbf{m}} = 0.014\,\mathrm{W} \\ \mathcal{P}_D &= \$_D^{\mathbf{a}} \bullet \$_D^{\mathbf{m}} = 0.047\,\mathrm{W} \\ \mathcal{P}_E &= \$_E^{\mathbf{a}} \bullet \$_E^{\mathbf{m}} = 0.114\,\mathrm{W} \end{aligned} \tag{96}$$

where the action screws are taken from matrix $\boldsymbol{A}$ considering power loss and the motion screws are taken from matrix $\boldsymbol{M}$. Solving each equation of (96) for the respective coefficient of friction and replacing these coefficients in equations (89), (90), and (91) results in:

$$\begin{aligned} \eta_{12} &= 0.9725 \\ \eta_{25} &= 0.9983 \\ \eta_{43} &= 0.9958 \end{aligned}$$

which, when applied in the modified version of equation (95), verifies the result found by Nelson and Cipra [7]. Using the recommended [11] value for the external gearing efficiency of 0.98, the overall efficiency is estimated as 42.5 % indicating that Humpage bevel gear train requires exceedingly high manufacturing quality parts to function properly.

3.6 REMARKS

This section contains some general remarks on the efficiency and power flow computation of gear trains.

3.6.1 Number of teeth and transmission ratio

The use of the number of teeth instead of pitch radii is very common in the literature on gear train efficiency. When different modules can be used in different parts of a complex gear train, care should be taken particularly when the power flow turning conditions are evaluated (see Section 3.4.1.5 for an example).

The use of the transmission ratio is also deceiving. Probably, the most straightforward method for computing the efficiency of parallel axes gear trains of great complexity is that developed by Castillo Granado [17]. Using the transmission ratio, Castillo Granado [17] found four equations for efficiency in his first example and six in the second. If the pitch radii are replaced in the condition expressions, only two equations are proved to be possible for each example[10]. Depending on the convention adopted, transmission ratios can be positive or negative, making the reasoning process more difficult, in particular when power flow turning conditions are considered. Pitch radii, on the other hand, are always positive.

3.6.2 Validation of efficiency formula

The assumption that power loss is unlikely to change the power flow direction may sound risky. However, the overall efficiency expression obtained can be verified against the possible error caused should this assumption prove to be wrong. Since this assumption is used only in the determination of the turning condition and not in the overall efficiency derivation, the final expression should be correct, with the exception of the use of the ordinary efficiency in place of its reciprocal and vice-verse.

Since an increase in overall efficiency is expected from an increase in any ordinary efficiency, the partial derivative with respect to every ordinary efficiency must be positive when all variables and parameters assume their nominal value. Even so, this test can still produce a false result if the input and output are exchanged. Therefore, the overall efficiency equation must be chosen correctly regarding the input and output relationship.

In view of this simple procedure, the determination of the turning conditions presented in Section 3.5.1.1 seems to be overvalued.

[10] Interested readers should also note a small mistake in equation (13) of reference [17]. A quick fix for this is to swap the gear train input and output.

3.6.3 Primary variable selection

The primary kinematic and static variables can be chosen arbitrarily. It is not even necessary to select variables associated with the same coupling since these variables disappear in the final efficiency expression. It is however convenient to use variables related to the input or output because this allows for a simpler turning condition in terms of input/output and, in view of the considerations in the last section, this is crucial for the correct use of the formula obtained.

3.6.4 Multiple planets

Real epicyclic gear trains with cylindrical or bevel gears use multiple planets to split the transmitted actions. Under the hypothesis that ordinary efficiencies are load-independent, this splitting causes no impact on the overall efficiency. If, however, a more accurate model is needed, two courses of action can be adopted: the ordinary efficiencies can be adjusted to reflect the change in load or the multiple planets can be included in the model using the proposed approach. A function defining how the transmitted action is split among parallel planets will be required if the latter course of action is taken. The assumption that transmitted actions might be split evenly throughout collaborating planets may be inaccurate, but it is a good approximation nevertheless.

3.6.5 Multiple carriers

It is possible to have more than one carrier in a complex gear train. In this case, the absolute motion of the links belonging to each gear pair has to be computed with respect to the respective carrier. The inspection method of Section 3.5.1.1 can be computationally advantageous over the matrix method of Section 3.1.1.

3.6.6 Velocity Reference

Differently from most previous studies in the field, the network approach adopted herein employs relative motions. Absolute motions are needed only for power flow considerations. “Absolute” means that one link is used as a reference to specify the motions of all other links.

"Relative" means that the motion of one link is given with respect to an immediate neighbour in the network, i.e., with respect to a link directly connected to that link. The use of relative motions allows the application of the mechanical analogue of the Kirchhoff voltage law resulting in a systematic and theoretically correct procedure for kinematic analysis.

3.7 CONCLUSIONS

In this chapter a new method for efficiency determination based on graph and screw theories is presented. This method can be used for obtaining the analytical expression of any gear train where the gear axes are parallel (cylindrical gears, see the example in Section 3.4.1) or intersecting (bevel gears, see the example in Section 3.5). Losses in gear meshing and bearing can be included and complex friction model can be used (see the example in Section 3.3).

It is perhaps the first truly generic method made available: *ad-hoc* reasoning is avoided and extension to other areas of Mechanical Engineering is straightforward.

Three examples are presented (see Sections 3.3, 3.4.1, and 3.5) and, probably for the first time, an equation for Humpage bevel gear overall efficiency is published.

Beside these three examples, the proposed method was also applied to other gear trains described in the literature, particularly all of the examples in references [3, 17, 75] and many (cases 1, 2, 3, 4, 5, 13, 15, 18, and 30) from [11]. Several typographical mistakes were found in reference [11]. Notwithstanding, no methodological flaw was identified in the approach used by Glover [11]. The method was also applied to a two degree of freedom differential and it shall appear in a future publication.

The generally accepted notion that the action responsible for power loss is a pure torque is formalised and proved using screw theory (see Theorem 1 in Section 3.2).

A coefficient of torque friction is defined and related to the ordinary efficiency (see Section 3.2.1). Replacing these coefficients by the equivalent expression in terms of ordinary efficiency leads to an overall efficiency equation equivalent to those found in the literature, validating the method (see Sections 3.3, 3.4.1, and 3.5).

Real and virtual power flows are defined and compared with previous definitions in the literature. The notion of stationary

frame, in which other authors have based their definition, is refuted. The incidence of the input and output with the reference link is proposed as criterion for distinguishing real from virtual power flow (see Section 3.1). The main feature of the virtual power flow is to establish the driver/driven relationship for each gear pair transforming the non-linear system of equation in a linear system of ease solution (see Section 3.4).

A systematic method for (virtual) power flow computation is presented (see Section 3.1.1). It may be possible to extend the power flow concept to other applications.

In mechanical theory, efficiency is the ratio of work output to work input. The average idea is adapted from its analogous on electrical network theory to allow the use of average power in place of work. This conception leads to a more direct solution (see Section 3.2).

Since efficiency equations are dependent on the gear train input/output and gear dimensions (inducing the turning condition surface), a method for reuse the efficiency formula devised for one situation to obtain the formulae for the other situations was developed and presented (see Section 3.4.1).

In keeping with the scope limits, the gear trains analysed have only one degree of freedom. In future work, the method shall be applied to a two degree of freedom differential.

4 EFFICIENCY OF GENERAL MACHINES

Computers are useless. They can only give you answers.

Pablo Picasso

Efficiency of parallel robots has not received the deserved attention in the literature. The high load capacity of these machines indicates that there is a huge economical and environmental gain to be attained by efficiency improvement even considering that energy use is smaller than that of serial robots [23]. In this Chapter, a procedure for general machines efficiency determination is established. This method is considered more accurate than previous approach [1, 24, 26, 27] for the reasons given in the next section. Examples are presented in Sections 4.2 and 4.3.

4.1 FRICTION MODES AND MODELS

Under the rigid body assumption, it is possible to assume that forces are concentrated at a point on the respective lines of action. In actual practice, the concentrated forces do not exist and every external force which is applied mechanically to the body is distributed over the finite contact area. Frictional considerations require conciliation between these two concepts. For didactic reasons, planar geometry is assumed in this section. This assumption implies that the action screws belong to the 4^{th} special 3-system of screws, the screws of planar statics [52].

When an external force $\vec{Q}$ is applied to a slider moving with velocity $\vec{q}$ inside a guide, as shown in Figs. 12 and 13, a friction force $\vec{Q}_F$ can take place. This friction force is dependent upon the velocity $\vec{q}$, the normal reaction $\vec{Q}_N$, the material, and the contact surface. In Fig. 12a, the line of action of the external force $\vec{Q}$ and of the normal reaction $\vec{Q}_N$ passes through the centre of the contact area. The reaction $\vec{Q}_N$ is distributed across the contact area according to a distribution law; usually this law is assumed to be uniform for rigid body contact.

In Fig. 12b, the line of action of $\vec{Q}$ does not pass through the

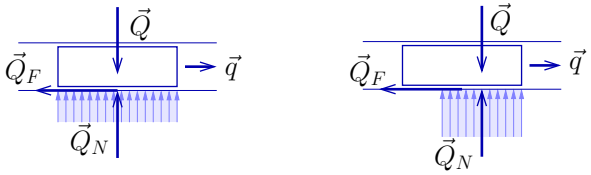

Figure 12 – Normal reaction $\vec{Q}_N$ and friction force $\vec{Q}_F$ when an external force $\vec{Q}$ is applied and its line of action intersects the contact area: (a) passing through the centre of the contact area, (b) dislocated from that centre

centre of the contact area, but it still intersects this area. Consequently, the normal reaction is distributed across a smaller area when compared with the situation in Fig. 12a. This fact has to be taken into account for friction models that are dependent on the contact area.

On the other hand, if the friction model is not dependent on the contact area, the situations depicted in Fig. 12 are considered equivalent. In both cases, the line of action of the friction force $\vec{Q}_F$ is located on the contact area and intersects with the line of action of the normal reaction $\vec{Q}_N$. The magnitude of the friction force $\vec{Q}_F$ is not dependent, in this case, on the location of the external force $\vec{Q}$ provided that the external force line of action intersects the contact area.

The force distributions of Fig. 12 are valid until the line of action of the external force $\vec{Q}$ is moved beyond the contact area. When the line of action of the external force $\vec{Q}$ reaches the edge of the contact area the effective contact area becomes a single point. Under the rigid body assumption, this causes no significant impact on the friction force model, unless this model is dependent on the contact area. Beyond the edge of the contact area, however, the change in the location of the external force $\vec{Q}$ line of action has a more dramatic impact upon the friction force model.

In Fig. 13a, the line of action of the external force $\vec{Q}$ passes by the right side of the contact area edge. If the clearance between the guide and slider is neglected, as when a small amount of flexibility is allowed, the normal reaction is distributed between two areas of the guide, respectively, on the upper and lower sides, respectively. Generally, it is assumed that the force distributions obey a triangular law and therefore the locations of the normal reactions $\vec{Q}_{N'}$ and $\vec{Q}_{N''}$

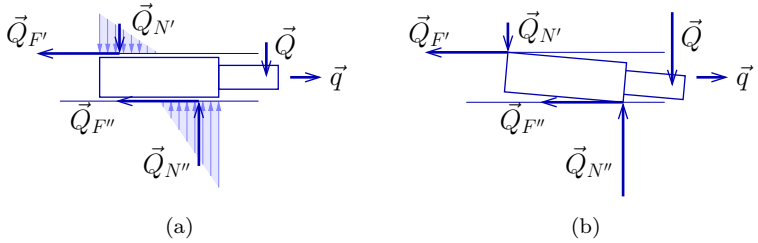

Figure 13 – Force $\vec{Q}$ applied far away from the centre of the contact area: (a) neglecting clearance between slider and guide, (b) considering that clearance

are known (they are at one third of the slider total length away from its centre). The magnitude of the normal reactions $\vec{Q}_{N'}$ and $\vec{Q}_{N''}$ can be computed in terms of the external force $\vec{Q}$, the slider length, and the moment produced by the external force $\vec{Q}$ at the slider centre. Once the normal reactions $\vec{Q}_{N'}$ and $\vec{Q}_{N''}$ are known, the friction forces $\vec{Q}_{F'}$ and $\vec{Q}_{F''}$ can be computed based on the some friction model.

One advantage of the network method used in this work is that the actions transmitted throughout the system are treated in the screw form, namely a force vector and a moment vector produced by this force at the origin. This moment vector can be computed at any point of interest by a change of coordinates.

If the clearance between the guide and slider is not neglected, the slider is expected to suffer a small rotation and two contact points are established as shown in Fig. 13b. Assuming that the clearance is small, so that the only appreciable effect produced by the rotation is the establishment of the contact points, the only noticeable difference between the situations describe in Figs. 13a and 13b is the location of the normal reactions $\vec{Q}_{N'}$ and $\vec{Q}_{N''}$. If, for example, Coulomb friction is used, a simple scaling of the coefficient of friction by 3/2 can make the results obtained from the two approaches compatible [72].

Two modes of operation have been identified. In the first mode, illustrated in Fig. 12, there is only one normal reaction sharing the same line of action with the external force. The second mode is illustrated in Fig. 13. In this mode, there are two normal reactions, for which the locations of the lines of action are independent of the external force location, but the magnitudes are dependent on the external force location and on the slider width.

The discrimination between these two modes is based on the external force location. Sometimes, this distinction can be made *a priori*. But in most cases, the possibility of two modes can make the modelling process unnecessarily complicated. When possible, simplification should be carried out to avoid these complications. A common simplifying factor is the relatively small dimensions of the contact area. Another possibility is to dismember a single coupling into two or more couplings acting in parallel.

4.1.1 Prismatic and cylindrical pair models

Passive cylindrical pairs, among other types, are used by Davies [21] to illustrate the use of equations (1-4). In static analysis, these pairs are regarded as capable of transmitting four independent actions: two forces and two torques. The locations of the forces are somewhat arbitrary, provided that they intersect the pair axis, since the torques compensate for the difference in location when equation (2) or (3) is solved.

Extending this reasoning to the planar case of Figs. 12 and 13, the normal reactions are represented by a single force, parallel to $\vec{Q}_N$ (or $\vec{Q}_{N'}$ and $\vec{Q}_{N''}$) but arbitrarily located, in addition to a torque. If the equivalent force and torque are known, a decision regarding the operation mode can be made and, consequently, the correct normal reaction applied. However, in a network problem, these equivalent actions are dependent on the friction force which, in turn, is dependent on the respective normal reaction.

To solve this dilemma, the slider can be split up into two small parallel sliders as shown in Fig. 14. Each slider is capable of transmitting one independent force. These forces correspond to the normal reactions of Fig. 13 or are equivalent to the single normal reaction of Fig. 12.

There is no need to determine the mode of operation with the split slider. Notwithstanding, the vertical location of the friction force is dependent on the direction of the respective normal reaction (compare $\vec{Q}_{F'}$ in Figs. 14a and 14b). If the height of the slider is small, this fact can be neglected, and in other case, the location of the friction forces is dependent on the sign of the corresponding normal reaction magnitude, i.e., the sign of the force transmitted by the coupling. Consequently, equations (2) and (3) become non-linear.

If the system is relatively small, in which only a few sign

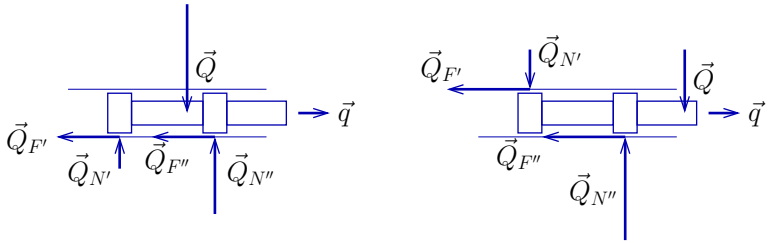

Figure 14 – Split slider equivalent to: (a) Fig. 12, (b) Fig. 13

functions appear, it would be possible to find a symbolic solution, as in Section 4.2. For larger problems, however, a numerical solution may be possible. Numerical solutions are discussed in Section 4.3.

Splitting up the slider into two parts has a second advantage. Usually, prismatic or cylindrical pairs are built in such a way that the distance between the split sliders is not constant, as shown in Fig. 15. Instead of considering one single coupling capable of transmitting two vertical forces, the locations of which are complicated to determine, it is more practical to consider two couplings in parallel capable of transmitting only one vertical force of easy location.

Care should be taken, however, in considering the other actions transmitted by the pair. For a prismatic pair, for instance, the torque around the pair axis can be considered as transmitted by any one of the parallel couplings, but not by both of them. If both couplings were capable of transmitting a torque, an undetermined torque could be locked in the circuit (loop) formed by the parallel couplings [29, 35]. This torque would be a new overconstraint which is unnecessary because it does not improve the description of the system and it is also unwanted because it requires an extra primary variable. An example of the use of prismatic pairs is given in Section 4.3.

4.2 SLIDER-CRANK

For the efficiency analysis, the slider-crank illustrated in Fig. 16 can be considered as being composed by four rigid links connected by three revolute joins and one cylindrical or prismatic joint. Herein, this latter pair is considered prismatic since the rotation of the pair D

Figure 15 – Variable-length split slider: (a) joint retreated, (b) joint advanced

(see Fig. 16) is completely prevented by the remaining member of the kinematic chain under the rigid link assumption. Assuming the coupling D as a prismatic pair decreases the dimension d and it is more of a convenience than a necessity.

Perfect linkage geometry is assumed implying that the actions related to any overconstraint, namely the forces parallel to z-axis and torques parallel to the plane $z = 0$, are neglected. In order to keep the example short, only friction in coupling D is modelled.

Normally, the location of a prismatic pair like coupling D is arbitrary. However, friction considerations suggest that simplification might be obtained by careful placement of such pairs. An external force aligned with the x-axis and a friction force parallel to the x-axis are applied to coupling D. The actual location of the friction force is dependent upon the direction of the vertical reaction on D. For now, the vertical offset of the friction force is neglected. Thus, it is convenient to locate coupling D coincident with C so that the torques at the origin produced by the vertical force in couplings C and D compensate each other. Moreover, coupling D behaves like the slider in Fig. 12 and only the first mode of operations discussed in Section 4.1 can take place.

The position of couplings B, C and D can be expressed in terms of θ, the crank angle (see Fig. 16), and the link lengths a_1 and a_2 as:

$$\begin{aligned} B_x &= a_1 \cos\theta \\ B_y &= a_1 \sin\theta \\ C_x = D_x &= B_x + \sqrt{{a_2}^2 - {a_1}^2 + {B_x}^2} \\ &= a_1 \cos\theta + \sqrt{{a_2}^2 - {a_1}^2 + {a_1}^2 \cos^2\theta}\,. \end{aligned} \tag{97}$$

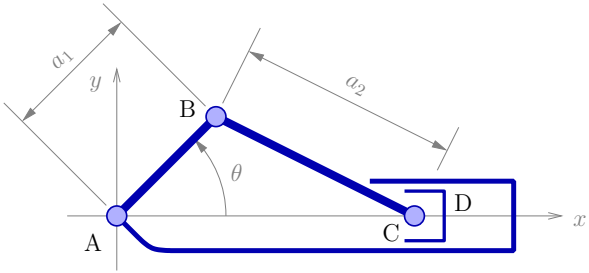

Figure 16 – RRRP or RRRC linkage

4.2.1 Screw systems and friction model

The motion screws of the coupling network shown in Fig. 16 belong to the 5^{th} special 3-system of screws according to Hunt's [52] classification. By orienting the z-axis parallel to the ISA of couplings labelled A, B and C, and the x-axis parallel to the ISA of coupling D, the motions can be spanned by the three motion screws $\{t;\, u,\, v\}$. The motion screws associated with the couplings are detailed in Table 7.

The action screws in the coupling network shown in Fig. 16 which can be spanned by $\{T;\, U,\, V\}$ belong to the 4^{th} special 3-system of screws, the screws of planar statics [52]. These action screws are described in Table 8. Note that in Table 8, T_A is the magnitude of an external torque and U_D is that of an external force, both applied to the network. U_{D_D} is the magnitude of the force due to friction given by

$$U_{D_D} = -\mu_D \ \text{sign}\,(V_D)\ V_D\ \text{sign}\,(u_D) \tag{98}$$

where V_D is the magnitude of the vertical force transmitted by coupling D (the normal force), μ_D is a dimensionless coefficient of friction in the classical sense, and u_D is the magnitude of translational velocity of coupling D (the speed of the slider with respect to the fixed frame). The minus sign in equation (98) is due to the fact that both screws $\$^{\mathbf{a}}_{U_{D_D}}$ and $\$^{\mathbf{m}}_{u_D}$ are orientated from left to right. Naturally, a more complex friction model can be adopted.

Table 7 – Motions spanning the systems of motions allowed by the couplings in Fig. 16

Coupling Label, type	Planar Location		Rotational or Translational Velocity (direction)	Magnitude	Unit motion screw coordinates in axis formation		
					Angular Velocity	Velocity of the point at the origin	
	x	y			t	u	v
A, revolute	0	0	Rotational (z)	t_A	1	0	0
B, revolute	B_x	B_y	Rotational (z)	t_B	1	B_y	$-B_x$
C, revolute	C_x	0	Rotational (z)	t_C	1	0	$-C_x$
D, prismatic	C_x	0	Translational (x)	u_D	0	1	0

Table 8 – Actions spanning the systems of actions that can be transmitted by the couplings in Fig. 16

Coupling Label, type	Planar Location		Force or Torque (direction)	Magnitude	Unit action screw coordinates in ray formation		
					Moment at origin	Force	
	x	y			T	U	V
A, revolute	0	0	Torque (z)	T_A	1	0	0
			Force (x)	U_A	0	1	0
			Force (y)	V_A	0	0	1
B, revolute	B_x	B_y	Force (x)	U_B	$-B_y$	1	0
			Force (y)	V_B	B_x	0	1
C, revolute	C_x	0	Force (x)	U_C	0	1	0
			Force (y)	V_C	C_x	0	1
D, prismatic	C_x	0	Torque (z)	T_D	1	0	0
			Force (x)	U_D	0	1	0
			Force (y)	V_D	C_x	0	1
			Force (x)	U_{D_D}	0	1	0

4.2.2 Motion analysis

The motion analysis of the single loop kinematic chain machine illustrated in Fig. 16 is a trivial matter since the network unit motion matrix $\hat{\boldsymbol{M}}_N$ is equal to the unit motion matrix of the direct couplings $\hat{\boldsymbol{M}}_D$ obtained from Table 7 as

$$\hat{\boldsymbol{M}}_N = \hat{\boldsymbol{M}}_D = \begin{array}{c} \\ t \\ u \\ v \end{array} \begin{array}{c} \begin{array}{cccc} t_A & t_B & t_C & u_D \end{array} \\ \begin{bmatrix} 1 & 1 & 1 & 0 \\ 0 & B_y & 0 & 1 \\ 0 & -B_x & -C_x & 0 \end{bmatrix} \end{array} . \tag{99}$$

where B_x, B_y, and C_x are given by equation (97). The null space, also called the kernel, of $\hat{\boldsymbol{M}}_N$ and $\hat{\boldsymbol{M}}_D$ is

$$\text{Null}\left(\hat{\boldsymbol{M}}_N\right) = \begin{array}{c} t_A \\ t_B \\ t_C \\ u_D \end{array} \begin{bmatrix} C_x - B_x \\ -C_x \\ B_x \\ B_y\, C_x \end{bmatrix} \tfrac{1}{C_x - B_x} . \tag{100}$$

The solution of equation (1) is proportional to the sole vector of Null $\left(\hat{\boldsymbol{M}}_N\right)$. Any variable listed in Table 7 can be chosen as the primary variable. Arbitrarily chosen t_A, the motion screw matrix that contains one screw per column, is given by

$$\boldsymbol{M} = \hat{\boldsymbol{M}}_D \ \text{diag}\left(\text{Null}\left(\hat{\boldsymbol{M}}_N\right)\right) \ t_A \tag{101}$$

which, using equations (99) and (100), leads to

$$\boldsymbol{M} = \begin{array}{c} \\ t \\ u \\ v \end{array} \begin{array}{c} \begin{array}{cccc} \$_A^{\mathbf{m}} & \$_B^{\mathbf{m}} & \$_C^{\mathbf{m}} & \$_D^{\mathbf{m}} \end{array} \\ \begin{bmatrix} B_x - C_x & C_x & -B_x & 0 \\ 0 & B_y\, C_x & 0 & -B_y\, C_x \\ 0 & -B_x\, C_x & B_x\, C_x & 0 \end{bmatrix} \end{array} \tfrac{t_A}{C_x - B_x} . \tag{102}$$

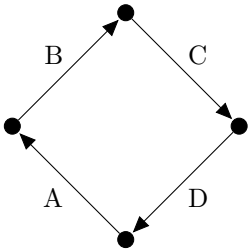

Figure 17 – Slider-crank coupling graphs G_C

4.2.3 Action analysis

The topology of the coupling network schematically shown in Fig. 16 is represented by the coupling graph of Fig. 17.

Using edges A, B, and C as branches, the fundamental cutset matrix[1] of G_C is obtained by inspection as

$$\boldsymbol{Q} = \begin{array}{c} \\ \mathrm{A} \\ \mathrm{B} \\ \mathrm{C} \end{array} \begin{array}{c} \begin{array}{cccc} \mathrm{A} & \mathrm{B} & \mathrm{C} & \mathrm{D} \end{array} \\ \begin{bmatrix} 1 & 0 & 0 & -1 \\ 0 & 1 & 0 & -1 \\ 0 & 0 & 1 & -1 \end{bmatrix} \end{array}. \tag{103}$$

In this case, any branch choice results in the same cutset matrix.

The fundamental cutset matrix of action graph G_A is obtained by means of column replication as

$$\boldsymbol{Q}_A = \begin{array}{c} \\ \mathrm{A} \\ \mathrm{B} \\ \mathrm{C} \end{array} \begin{array}{c} \begin{array}{ccccccccccc} \mathrm{A} & \mathrm{A} & \mathrm{A} & \mathrm{B} & \mathrm{B} & \mathrm{C} & \mathrm{C} & \mathrm{D} & \mathrm{D} & \mathrm{D} & \mathrm{D} \\ T_A & U_A & V_A & U_B & V_B & U_C & V_C & T_D & U_D & U_{D_D} & V_D \end{array} \\ \begin{bmatrix} 1 & 1 & 1 & 0 & 0 & 0 & 0 & -1 & -1 & -1 & -1 \\ 0 & 0 & 0 & 1 & 1 & 0 & 0 & -1 & -1 & -1 & -1 \\ 0 & 0 & 0 & 0 & 0 & 1 & 1 & -1 & -1 & -1 & -1 \end{bmatrix} \end{array} \tag{104}$$

where every column of $\boldsymbol{Q}$ was replicated a number of times equal to the number of independent actions transmitted by the respective coupling (see Table. 8). Alternatively, the action graph G_A can be drawn as in reference [21], then the matrix $\boldsymbol{Q}_A$ is assembled by inspection.

[1] For fundamental cutset matrix obtainment refer to any of the references [5, 20, 21, 73, 76, 77].

The unit action matrix of the direct couplings is assembled from Table 8 as

$$\boldsymbol{A}_D = \begin{array}{c} \\ T \\ U \\ V \end{array} \begin{array}{c} \begin{array}{cccccccccccc} T_A & U_A & V_A & U_B & V_B & U_C & V_C & T_D & U_D & U_{D_D} & V_D \end{array} \\ \left[\begin{array}{cccccccccccc} 1 & 0 & 0 & -B_y & B_x & 0 & C_x & 1 & 0 & C_x & 0 \\ 0 & 1 & 0 & 1 & 0 & 1 & 0 & 0 & 1 & 0 & 1 \\ 0 & 0 & 1 & 0 & 1 & 0 & 1 & 0 & 0 & 1 & 0 \end{array}\right] \end{array}. \tag{105}$$

The network unit action matrix is assembled using equation (19) from the data on equations (104) and (105) as

$$\hat{\boldsymbol{A}}_N = \begin{array}{c} \\ T \\ U \\ V \\ T \\ U \\ V \\ T \\ U \\ V \end{array} \begin{array}{c} \begin{array}{cccccccccccc} T_A & U_A & V_A & U_B & V_B & U_C & V_C & T_D & U_D & U_{D_D} & V_D \end{array} \\ \left[\begin{array}{cccccccccccc} 1 & 0 & 0 & 0 & 0 & 0 & 0 & -1 & 0 & -C_x & 0 \\ 0 & 1 & 0 & 0 & 0 & 0 & 0 & 0 & -1 & 0 & -1 \\ 0 & 0 & 1 & 0 & 0 & 0 & 0 & 0 & 0 & -1 & 0 \\ 0 & 0 & 0 & -B_y & B_x & 0 & 0 & -1 & 0 & -C_x & 0 \\ 0 & 0 & 0 & 1 & 0 & 0 & 0 & 0 & -1 & 0 & -1 \\ 0 & 0 & 0 & 0 & 1 & 0 & 0 & 0 & 0 & -1 & 0 \\ 0 & 0 & 0 & 0 & 0 & 0 & C_x & -1 & 0 & -C_x & 0 \\ 0 & 0 & 0 & 0 & 0 & 1 & 0 & 0 & -1 & 0 & -1 \\ 0 & 0 & 0 & 0 & 0 & 0 & 1 & 0 & 0 & -1 & 0 \end{array}\right] \end{array}. \tag{106}$$

Equation (106) carries only topological information; element characteristics are not present. Equations that express the element characteristics are called *constitutive equations* [71]. For instance, the single constitutive equation of this system is equation (98).

The augmented action matrix $\boldsymbol{D}_A$ that models action relationships in the network is obtained by appending equation (98) in matrix

form in equation (106) as

$$\boldsymbol{D}_A = \begin{array}{c} \\ T \\ U \\ V \\ T \\ U \\ V \\ T \\ U \\ V \\ c.e. \end{array} \begin{array}{c} \begin{array}{cccccccccccc} T_A & U_A & V_A & U_B & V_B & U_C & V_C & T_D & U_D & U_{D_D} & V_D \end{array} \\ \left[\begin{array}{cccccccccccc} 1 & 0 & 0 & 0 & 0 & 0 & 0 & -1 & 0 & -C_x & 0 \\ 0 & 1 & 0 & 0 & 0 & 0 & 0 & 0 & -1 & 0 & -1 \\ 0 & 0 & 1 & 0 & 0 & 0 & 0 & 0 & 0 & -1 & 0 \\ 0 & 0 & 0 & -B_y & B_x & 0 & 0 & -1 & 0 & -C_x & 0 \\ 0 & 0 & 0 & 1 & 0 & 0 & 0 & 0 & -1 & 0 & -1 \\ 0 & 0 & 0 & 0 & 1 & 0 & 0 & 0 & 0 & -1 & 0 \\ 0 & 0 & 0 & 0 & 0 & 0 & C_x & -1 & 0 & -C_x & 0 \\ 0 & 0 & 0 & 0 & 0 & 1 & 0 & 0 & -1 & 0 & -1 \\ 0 & 0 & 0 & 0 & 0 & 0 & 1 & 0 & 0 & -1 & 0 \\ \hdashline 0 & 0 & 0 & 0 & 0 & 0 & 0 & 0 & 0 & 1 & a\,\mu_D \end{array}\right] \end{array} \tag{107}$$

where $a = \text{sign}\,(V_D)\ \text{sign}\,(u_D)$, and the label *c.e.* indicates that the last row originates from a constitutive equation.

This matrix is used in place of $\hat{\boldsymbol{A}}_N$ in equation (2) and its null space is

$$\text{Null}\,(\boldsymbol{D}_A) = \begin{array}{c} T_A \\ U_A \\ V_A \\ U_B \\ V_B \\ T_C \\ T_C \\ T_D \\ U_D \\ V_D \\ U_{D_D} \end{array} \begin{array}{c} \left[\begin{array}{c} B_y\,C_x \\ B_x - C_x \\ B_y \\ B_x - C_x \\ B_y \\ B_x - C_x \\ B_y \\ 0 \\ B_x - C_x + a\,\mu_D\,B_y \\ B_y \\ -a\,\mu_D\,B_y \end{array}\right] \end{array} \frac{1}{B_y\,C_x} \tag{108}$$

where $a = \text{sign}\,(V_D)\ \text{sign}\,(u_D)$.

The vector of action magnitudes $\boldsymbol{\Psi}$ is proportional to the sole vector in $\text{Null}\,(\boldsymbol{D}_A)$. Thus, for any case T_D is zero because the location of coupling D was set coincident with C. If coupling D was located elsewhere, T_D may not be zero and V_D would have a different value requiring the modification of equation (98).

Any magnitude variable, with the exception of T_D, can be selected as the primary variable. Choosing T_A, the vector of the action magnitudes is given by

$$\boldsymbol{\Psi} = \text{Null}\,(\boldsymbol{D}_A)\; T_A \tag{109}$$

where $\text{Null}\,(\boldsymbol{D}_A)$ is given by equation (108).

It is possible to use another variable, other than T_D, as the primary variable by adapting equation (109) accordingly. For example, if it is desirable to use V_D as the primary variable, T_A is replaced by $C_x\, V_D$ and the last element of the vector $\text{Null}\,(\boldsymbol{D}_A)\; C_x\, V_D$ will be V_D alone.

The action matrix that contains one action screw per column can be computed by

$$\boldsymbol{A} = \hat{\boldsymbol{A}}_D\; \text{diag}\,(\boldsymbol{\Psi}) \tag{110}$$

where $\hat{\boldsymbol{A}}_D$ is given by equation (105) and $\boldsymbol{\Psi}$ by equation (109). In equation (110), each normalised action screw is multiplied by the respective magnitude resulting in the actual action screw.

Matrix $\boldsymbol{A}$ in equation (110) takes the form

$$\boldsymbol{A} = \left[\begin{array}{cccccccccccc} \$^{\mathbf{a}}_{T_A} & \$^{\mathbf{a}}_{U_A} & \$^{\mathbf{a}}_{V_A} & \$^{\mathbf{a}}_{U_B} & \$^{\mathbf{a}}_{V_B} & \$^{\mathbf{a}}_{U_C} & \$^{\mathbf{a}}_{V_C} & \$^{\mathbf{a}}_{T_D} & \$^{\mathbf{a}}_{U_D} & \$^{\mathbf{a}}_{U_{D_D}} & \$^{\mathbf{a}}_{V_D} \end{array}\right].$$

4.2.4 Power and efficiency

From equation (109), it follows that

$$V_D = \frac{T_A}{C_x}\,. \tag{111}$$

Since $a_2 > a_1$, otherwise a complete turn would not be possible, equation (97) reveals that $C_x > 0$ and $C_x > B_x$. Therefore

$$\text{sign}\,(V_D) = \text{sign}\,(T_A) \tag{112}$$

Also, from equations (100) and (101)

$$u_D = \frac{B_y\, C_x}{C_x - B_x}\, t_A \tag{113}$$

and, so

$$\text{sign}\left(\frac{B_y\, C_x}{C_x - B_x}\right) = \text{sign}\,(\sin\theta)$$

and $\text{sign}(\sin\theta) = \text{sign}(\theta)$ for $-\pi < \theta < \pi$. Thus

$$\text{sign}(u_D) = \text{sign}(t_A)\ \text{sign}(\theta) \tag{114}$$

in one cycle interval.

Two cases are possible depending on which coupling is the input.

4.2.4.1 Case 1: coupling A is the input

If coupling A is the input, the torque magnitude T_A and the angular speed magnitude t_A have the same sign:

$$\text{sign}(T_A) = \text{sign}(t_A) \tag{115}$$

and the input power is given by

$$\mathcal{P}_{\text{input}} = \$^{\mathbf{a}}_A \bullet \$^{\mathbf{m}}_A = T_A\, t_A \tag{116}$$

where $\$^{\mathbf{m}}_A$ is taken from equation (102) and $\$^{\mathbf{a}}_A = \$^{\mathbf{a}}_{T_A} + \$^{\mathbf{a}}_{U_A} + \$^{\mathbf{a}}_{V_A}$. Since $\$^{\mathbf{a}}_{U_A}$ and $\$^{\mathbf{a}}_{V_A}$ are both orthogonal with $\$^{\mathbf{m}}_A$, the only screw needed is $\$^{\mathbf{a}}_{T_A}$, and this screw is obtained upon evaluation of equation (110).

The output power is given by the inner product of the external action screw applied to coupling D by the motion screw of that coupling as

$$\mathcal{P}_{\text{output}} = \$^{\mathbf{a}}_{U_D} \bullet \$^{\mathbf{m}}_D = -T_A\, t_A \left(1 + \frac{\mu_D\, B_y\ \text{sign}(V_D)\ \text{sign}(u_D)}{B_x - C_x}\right) \tag{117}$$

where $\$^{\mathbf{m}}_D$ is taken from equation (102), and $\$^{\mathbf{a}}_{U_D}$ is obtained upon evaluation of equation (110).

Assuming that the input power is kept constant during one cycle, the input work during this cycle is computed integrating the input power as

$$\mathcal{W}_{\text{input}} = \int_{-\pi}^{\pi} \mathcal{P}_{\text{input}}\ d\theta = 2\,\pi\, T_A\, t_A \tag{118}$$

and the output work as

$$\mathcal{W}_{\text{output}} = -\int_{-\pi}^{\pi} \mathcal{P}_{\text{output}}\ d\theta$$

$$= T_A\, t_A \int_{-\pi}^{\pi} \left(1 + \mu_D \frac{a_1 \sin\theta}{\sqrt{{a_2}^2 - {a_1}^2 + {a_1}^2 \cos^2\theta}} \operatorname{sign}(\theta)\right) d\theta$$

$$= 2\,\pi\, T_A\, t_A - 2\,\mu_D\, T_A\, t_A \ln\left(\frac{a_1 + a_2}{a_2 - a_1}\right). \tag{119}$$

where equations (97), (112), (114), and (115) were applied to equation (117).

The average efficiency is given by the ratio of the output to the input work as

$$\eta = \frac{\mathcal{W}_{\text{output}}}{\mathcal{W}_{\text{input}}} = 1 - \frac{\mu_D}{\pi} \ln\left(\frac{a_1 + a_2}{a_2 - a_1}\right). \tag{120}$$

4.2.4.2 Case 2: coupling D is the input

If coupling D is the input, coupling A is the output, therefore

$$\operatorname{sign}(T_A) = -\operatorname{sign}(t_A) \tag{121}$$

and the input and output are reverted, thus

$$\mathcal{P}_{\text{output}} = \$_A^{\mathbf{a}} \bullet \$_A^{\mathbf{m}} = -T_A\, t_A$$

and

$$\mathcal{P}_{\text{input}} = \$_{U_D}^{\mathbf{a}} \bullet \$_D^{\mathbf{m}} = -T_A\, t_A \left(1 + \frac{\mu_D\, B_y \operatorname{sign}(V_D) \operatorname{sign}(u_D)}{B_x - C_x}\right). \tag{122}$$

and, in view of equation (121) the sign of the fraction in equation (122) will change after the substitution.

Assuming that the output power remains constant during one cycle, the output work

$$\mathcal{W}_{\text{output}} = -\int_{-\pi}^{\pi} \mathcal{P}_{\text{output}}\, d\theta = -2\,\pi\, T_A\, t_A$$

and the input work

$$\begin{aligned}\mathcal{W}_{\text{input}} &= \int_{-\pi}^{\pi} \mathcal{P}_{\text{input}}\, d\theta \\ &= T_A\, t_A \int_{-\pi}^{\pi} \left(1 - \mu_D \frac{a_1\, \sin\theta}{\sqrt{{a_2}^2 - {a_1}^2 + {a_1}^2\, \cos^2\theta}}\, \text{sign}\,(\theta)\right)\, d\theta \\ &= 2\,\pi\, T_A\, t_A + 2\,\mu_D\, T_A\, t_A\, \ln\left(\frac{a_1 + a_2}{a_2 - a_1}\right)\end{aligned}$$

give the efficiency as

$$\eta = \frac{\mathcal{W}_{\text{output}}}{\mathcal{W}_{\text{input}}} = \frac{\pi}{\pi + \mu_D\, \ln\left(\frac{a_1+a_2}{a_2-a_1}\right)}\,. \tag{123}$$

4.2.5 Remarks

The friction force, the magnitude of which is U_{D_D}, could be relocated to its correct position, which is dependent on the slider diameter and the sign of V_D, the vertical force transmitted by coupling D. This relocation would require modifications to the last row of Table 7 and, consequently, equations (105), (106), (107), and (108). However, the final result given by equations (120) and (123) would remain unaltered.

It could be argued that the assumption of constant power input and output during one cycle is unrealistic. Experimental data can be used with equations (116), (117) and (122) in which case numerical integration may be needed.

4.3 3-UPU

This section is dedicated to the friction analysis of a complex machine with parallel kinematic chain aiming to establish its efficiency. The machine selected as an example is called 3-UPU.

The 3-UPU [78] is a three-degrees-of-freedom spatial parallel manipulator composed of three limbs connected to a base and a platform by means of universal or Hooke joints as shown schematically in Fig. 18. Each limb has one actuated prismatic joint connected to

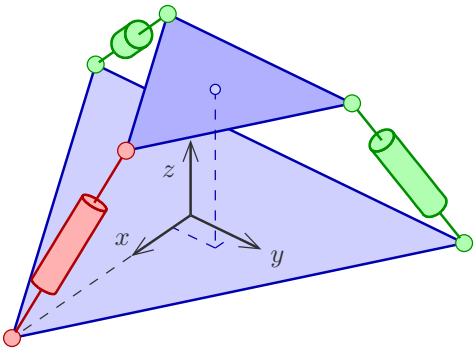

Figure 18 – 3-UPU manipulator – simplified perspective. The prismatic joints are represented by cylinders and the universal joints by spheres.

two universal joints. The limbs are assumed to be identical and their connections to the base and platform are symmetrically distributed (the centres of the universal joints form two equilateral triangles, one on the base and the another on the platform). The proposed method can be applied to machines in general, but symmetry is convenient because it allows a more concise description. Moreover, the system is assumed to be quasi-static and, accordingly, the inertia effects and control errors are neglected.

4.3.1 Inverse kinematics

Evaluation of the overall efficiency of the 3-UPU requires the computation of motions and actions during the execution of a task. Normally, the task is prescribed by the desired movement of the platform carrying a payload. Since the 3-UPU is only capable of translation[2], the description of the task is equivalent to the description of the motion of any point on the platform. The point at the centre of the platform is designed by M and an external load is applied to the platform at point M.

The coupling graph that represents how the links are connected together to form the whole 3-UPU is shown in Fig. 19.

A virtual coupling [45, 80], also labelled M, that directly couples the base and the platform, is included in the kinematic chain. The

[2]Under singular conditions, platform rotation may occur [79], but singularities are avoided under normal operation.

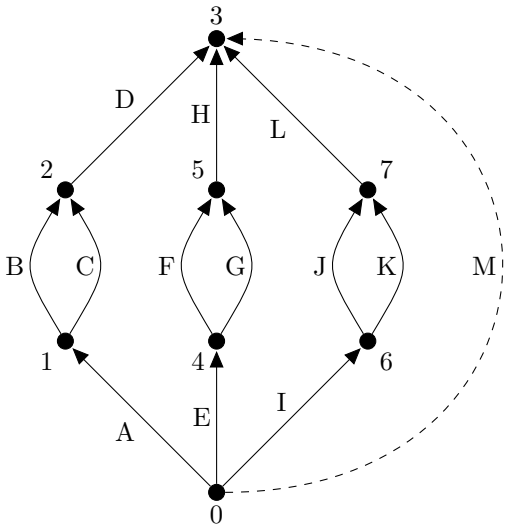

Figure 19 – Coupling graph of 3-UPU manipulator

purpose of this coupling is twofold: it allows the use of the platform-related variables as primary motion variables (inverse kinematics); and it internalises the external action applied to the platform (inverse dynamics), i.e., the external load. Coupling M, represented by a dashed line in Fig. 19, has six degrees of freedom and one degree of constrain. Thus, coupling M is an active coupling in the sense that power may be expended on it or provided by it.

4.3.1.1 Coupling location and orientation

Additional details needed for motion and action analyses include the position of the couplings and the orientation of the axes, all unambiguously written with respect to a reference frame.

The reference frame is located with the origin coincident to the centre of the connections of the three limbs to the base, with the z-axis orthogonal to the base plane and the x-axis pointing to a universal joint centre (see Fig. 18). This specific universal joint belongs to what is called the first limb. Since all limbs are identical, although placed at different locations, only this first limb, which is shown schematically in Fig. 20, is described herein. In Fig. 20, the coupling labelled A, of

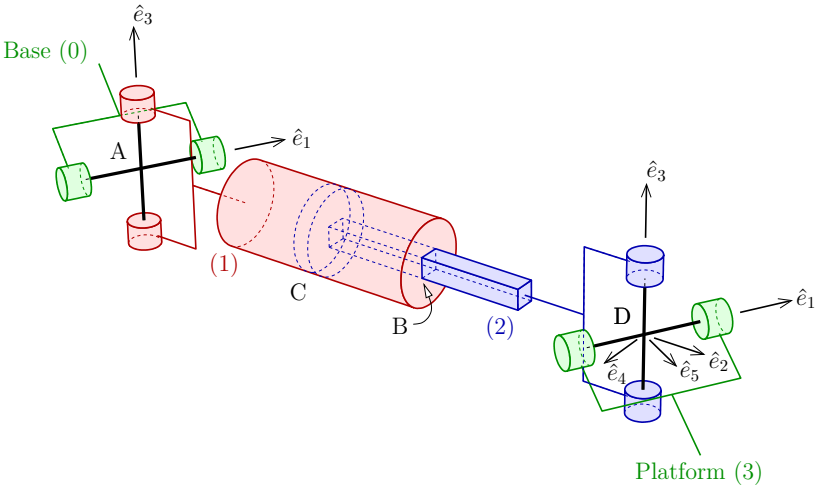

Figure 20 – 3-UPU representative limb, link labels are shown between parentheses

the universal kind, connects the base, labelled 0, to link 1. Link 1 is connected to link 2 by a prismatic joint modelled by the couplings B and C (for more details see Section 4.3.2). Finally, link 2 is connected to link 3, the platform, by another universal joint labelled D.

Point A is located at the universal joint centre with the same label. Link 2 stands on link 1 at point B and the distance between A and B is constant. A similar situation is found for points C and D.

The location of the base-connected universal joint centre (e.g., point A in Fig. 20) of each limb with respect to the reference frame is given by the position vector

$$\vec{e}_1 = \begin{matrix} x \\ y \\ z \end{matrix} \begin{bmatrix} \cos\alpha \\ \sin\alpha \\ 0 \end{bmatrix} r_b \tag{124}$$

where r_b is the distance from the base centre (the origin) to any universal joint centre connected to the base, and $\alpha = 0,\ 2\,\pi/3,\ -2\,\pi/3$ rad for first, second and third limbs, respectively. The orientation of the first axis of every universal joint, see Fig. 20, is given by the unity vector $\hat{e}_1$ of $\vec{e}_1$, since the platform rotation is prevented.

The vector pointing from the universal joint centre of the base

to that of the platform for each limb is given by

$$\vec{e}_2 = \begin{matrix} x \\ y \\ z \end{matrix} \begin{bmatrix} M_x + (r_t - r_b)\cos\alpha \\ M_y + (r_t - r_b)\sin\alpha \\ M_z \end{bmatrix} \tag{125}$$

where r_t is the distance from the platform centre to any universal joint centre connected to the platform; M_x, M_y, and M_z are the coordinates of the platform centre (point M) with respect to the reference frame; and r_b and α are defined for equation (124). It is worth noting that the vectors given by equation (125) are dependent on the current platform location, but those of equation (124) are constants. The direction (axis) of the prismatic joint of each limb is given by the unity vector $\hat{e}_2$ of $\vec{e}_2$.

The orientation of the second axis of every universal joint is given by the unity vector $\hat{e}_3$, orthogonal to $\hat{e}_1$ and $\hat{e}_2$. Couplings B and C transmit forces parallel to $\hat{e}_3$ and $\hat{e}_4$; $\hat{e}_4$ is orthogonal to $\hat{e}_2$ and $\hat{e}_3$. The universal joints transmit a torque around the unity vector $\hat{e}_5$, orthogonal to $\hat{e}_1$ and $\hat{e}_3$.

The five unity vectors $\hat{e}_i$, $(i = 1, 2, \ldots 5)$ are dependent on the location of the respective limb given by α. For the first limb, $\alpha = 0$, the $\hat{e}_i$ are shown in Fig. 20.

The location of the universal joint centres on the base (i.e. points A, E, and I) are given by $\vec{e}_1$, from equation (124), with a suitable angle α. Also, the location of the universal joint centres on the platform (i.e. points D, H, and L) are given by $\vec{e}_1 + \vec{e}_2$, from equations (124) and (125). Neglecting the radial length of the prismatic joints, the two contact points between links 1 and 2 are given by

$$\begin{aligned} \mathrm{B} &= \vec{e}_1 + l_B\,\hat{e}_2 \\ \mathrm{C} &= \vec{e}_1 + \vec{e}_2 - l_C\,\hat{e}_2 \end{aligned} \tag{126}$$

where l_B is the constant distance between points A and B, and l_C is that of points C and D. Equation (126) is also used to determine points F, G, J, and K using a suitable value of α.

4.3.2 Prismatic joints

As explained in Section 4.1.1, friction considerations require that the prismatic joint being split up into two couplings to simplify the placement of the transmitted forces. Thus, the prismatic joint of each limb is split up into two couplings, B and C (F-G and J-K for the second

and third limbs, respectively, see Fig. 19). Together, couplings B and C must behave like a prismatic pair; they must present one degree of freedom and five degrees of constraint. The challenge consists of selecting two coupling types that, when connected in parallel, allow only one translational movement without creating any overconstraint. This can be achieved by using a round and a square annulus joint.

A round annulus joint allows three rotations, two of which are infinitesimal, and one translation. Therefore, it transmits two forces. A square annulus joint allows two rotations, both of them infinitesimal, and one translation. Thus, it transmits two forces and one torque. Aligning the axes of the two annulus joints connected in parallel, only the translation is allowed and the assemblage behaves like a prismatic joint.

One square annulus joint is required to prevent the rotation around the joint axis. Nonetheless, it is not advisable to employ two square annuli because, in this case, a torque should be locked in the parallel sub-network which makes the action analysis unnecessarily more laborious.

The square annulus is placed at B and the round annulus at C. The assignment of the annulus kind to each point is completely arbitrary.

4.3.3 Analysis

The analysis described in Section 4.2 was carried out entirely symbolically with the help of a computer algebra system. The needs of the 3-UPU, however, are far beyond the available software and hardware capabilities. For this reason, a software program was written in C++ to simulate the execution of a task by the 3-UPU. The unit motion and action matrices of the direct couplings, $\hat{\boldsymbol{M}}_D$ and $\hat{\boldsymbol{A}}_D$, the fundamental cutset matrix $\boldsymbol{Q}_A$ of action graph G_A, and the fundamental circuit matrix $\boldsymbol{B}_M$ of motion graph G_M were assembled using a computer algebra system and hard coded in the software. In the following sections, the obtainment of the matrices, the friction model, and the software implementation are described.

4.3.3.1 Motion analysis

The motions allowed by the first limb couplings are linearly dependent on those depicted in Table 9. The first 33 columns of the unit motion matrix of the direct couplings $\hat{\boldsymbol{M}}_D$ are assembled based on the data in Table 9 in combination with the coupling locations given by equations (124), (125), and (126). The last 6 columns are related to coupling M and given by

$$\hat{\boldsymbol{M}}_{D_M} = \begin{array}{c} \\ r \\ s \\ t \\ u \\ v \\ w \end{array} \begin{array}{c} \begin{array}{cccccc} r_M & s_M & t_M & u_M & v_M & w_M \end{array} \\ \left[\begin{array}{cccccc} 1 & 0 & 0 & 0 & 0 & 0 \\ 0 & 1 & 0 & 0 & 0 & 0 \\ 0 & 0 & 1 & 0 & 0 & 0 \\ 0 & -M_z & M_y & 1 & 0 & 0 \\ M_z & 0 & -M_x & 0 & 1 & 0 \\ -M_y & M_x & 0 & 0 & 0 & 1 \end{array}\right] \end{array}.$$

The fundamental circuit matrix $\boldsymbol{B}$ of the coupling graph G_C is assembled by inspection of the graph in Fig. 19 using edges C, G, H, K, L, and M as chords. The fundamental circuit matrix $\boldsymbol{B}_M$ of the motion graph G_M is obtained replicating the columns of $\boldsymbol{B}$. A total of 36 linear equations in 39 variables are obtained from matrices $\hat{\boldsymbol{M}}_D$ and $\boldsymbol{B}_M$. Imposing the velocity magnitudes of point M, namely u_M, v_M, and w_M, the linear system of equations is solved for the remaining motion magnitudes.

4.3.3.2 Action analysis

The actions spanning the systems of actions transmitted by the couplings in the first limb of the 3-UPU are described in Table 10. The actuator of the first limb produces a force of magnitude Q_{C_A}. The friction forces, magnitudes of Q_{B_F} and Q_{C_F}, and the friction torques, magnitudes of $Q_{A_{F1}}$, $Q_{A_{F2}}$, $Q_{D_{F1}}$, and $Q_{D_{F2}}$, are described in Section 4.3.3.3. The remaining thirteen actions in Table 10 are related to the degrees of constraint of each coupling of the first limb.

Couplings A and D are capable of transmitting three independent forces. Normally, the screws used to span these forces would be aligned with canonical axes. However, the coefficients of friction ap-

Table 9 – Motions spanning the systems of motions allowed by the couplings in Fig. 20

Coupling	Magnitude	Motion	Direction
A	p_{A_1}	rotation	$\hat{e}_1$
	p_{A_2}	rotation	$\hat{e}_3$
B	q_B	translation	$\hat{e}_2$
	p_{B_1}	rotation	$\hat{e}_3$
	p_{B_2}	rotation	$\hat{e}_4$
C	q_C	translation	$\hat{e}_2$
	p_{C_1}	rotation	$\hat{e}_2$
	p_{C_2}	rotation	$\hat{e}_3$
	p_{C_3}	rotation	$\hat{e}_4$
D	p_{D_1}	rotation	$\hat{e}_1$
	p_{D_2}	rotation	$\hat{e}_3$

plied are dependent on the contact surface geometrical and material features. Thus, the directions of the forces spanning the force transmitted by the couplings A and D are those orthogonal to the cylindrical and flat surfaces, respectively.

The first 60 columns of the unit action matrix of the direct couplings $\hat{\boldsymbol{A}}_D$ are assembled based on the data in Table 10 in combination with the coupling locations given by equations (124), (125), and (126). The last column is related to coupling M and given by

$$\hat{\boldsymbol{A}}_{D_M} = \begin{array}{c} \\ R \\ S \\ T \\ U \\ V \\ W \end{array} \begin{array}{c} W_M \\ \left[\begin{array}{c} M_y \\ -M_x \\ 0 \\ 0 \\ 0 \\ 1 \end{array}\right] \end{array} .$$

The fundamental cutset matrix $\boldsymbol{Q}$ of the coupling graph G_C is assembled by inspection of the graph in Fig. 19 using edges A, B, D,

Table 10 – Actions spanning the systems of actions that can be transmitted by the couplings in Fig. 20

Coupling	Magnitude	Action	Direction
A	P_A	torque transmitted	$\hat{e}_5$
	$P_{A_{F1}}$	first friction torque	$\hat{e}_1$
	$P_{A_{F2}}$	second friction torque	$\hat{e}_3$
	Q_{A_1}	force transmitted	$\hat{e}_1$
	Q_{A_2}	force transmitted	$\hat{e}_3$
	Q_{A_3}	force transmitted	$\hat{e}_5$
B	P_B	torque transmitted	$\hat{e}_2$
	Q_{B_1}	first force transmitted	$\hat{e}_3$
	Q_{B_2}	second force transmitted	$\hat{e}_4$
	Q_{B_F}	friction force	$\hat{e}_2$
C	Q_{C_1}	first force transmitted	$\hat{e}_3$
	Q_{C_2}	second force transmitted	$\hat{e}_4$
	Q_{C_A}	actuation force	$\hat{e}_2$
	Q_{C_F}	friction force	$\hat{e}_2$
D	P_D	torque transmitted	$\hat{e}_5$
	$P_{D_{F1}}$	first friction torque	$\hat{e}_1$
	$P_{D_{F2}}$	second friction torque	$\hat{e}_3$
	Q_{D_1}	force transmitted	$\hat{e}_1$
	Q_{D_2}	force transmitted	$\hat{e}_3$
	Q_{D_3}	force transmitted	$\hat{e}_5$

E, F, I, and J as branches. The fundamental cutset matrix $\boldsymbol{Q}_A$ of the action graph G_A is obtained replicating the columns of $\boldsymbol{Q}$. A total of 42 linear equations in 61 variables are obtained from matrices $\hat{\boldsymbol{A}}_D$ and $\boldsymbol{Q}_A$.

4.3.3.3 Friction models

The focus of this study is the network effects of friction loss. The objective is the establishment of a general method easily adapted to any friction model. Therefore, the importance placed on the local friction model, despite the fact that it has a profound impact on the final result, is marginal since the proposed method can be straightforwardly adapted to all friction models. It is also important to keep the example as simple as possible, while maintaining the likelihood of the model. Hence, Coulomb friction is assumed.

A friction torque is assigned to each one of the universal joint rotation axes. The magnitudes of these torques are dependent on the actions transmitted by the joint and on the direction of the relative speed. Considering that the length of the central pin is small, the transmitted actions are forces that press the central pin against the insert. The contact surface can be cylindrical or flat, depending on the force direction. It is considered that the surfaces are old. For flat surfaces, equation (146) is used assuming that the inner radius is very small. It is also considered that the contact angle on the cylindrical surfaces is $2\,\beta = \pi\,\text{rad}$. According to Table 16, the coefficient of friction is multiplied by $4/\pi$ for cylindrical surfaces.

The first axis of coupling A is aligned with $\hat{e}_1$; thus Q_{A_1} pushes against a flat surface and Q_{A_2} and Q_{A_3} push against a cylindrical surface. Therefore, the magnitude of the friction torque of the first axis is estimated by

$$P_{A_{F\,1}} = -\mu_A\, r_A\, \text{sign}\,(p_{A_1}) \left(|Q_{A_1}| + \frac{4}{\pi}\, |Q_{A_2}| + \frac{4}{\pi}\, |Q_{A_3}| \right) \qquad (127)$$

where r_A is the shaft radius.

The second axis of coupling A is aligned with $\hat{e}_3$; thus Q_{A_1} and Q_{A_3} push against a cylindrical surface and Q_{A_2} pushes against a flat surface (see Table. 10). The magnitude of the friction torque of the second axis is given by

$$P_{A_{F\,2}} = -\mu_A\, r_A\, \text{sign}\,(p_{A_2}) \left(\frac{4}{\pi}\, |Q_{A_1}| + |Q_{A_2}| + \frac{4}{\pi}\, |Q_{A_3}| \right). \qquad (128)$$

Equations (127) and (128) are also used for coupling D by replacing index A with D.

The friction forces acting on the prismatic joint of the first limb are split up into couplings B and C. The magnitude of the force friction

Algorithm 2 – 3-UPU efficiency simulation procedure

1. compute the coordinates of point M and its linear velocity;
2. assemble the network unit motion matrix $\hat{\boldsymbol{M}}_N$;
3. solve equation (1) for $\boldsymbol{\psi}$;
4. assemble the network unit action matrix $\hat{\boldsymbol{A}}_N$;
5. assemble the constitutive equations (see Section 4.3.3.3) and append them to $\hat{\boldsymbol{A}}_N$;
6. solve equation (2) for $\boldsymbol{\Psi}$;
7. compute the instantaneous power.

on coupling B is given by

$$Q_{B_F} = -\mu_B \operatorname{sign}(q_B) \left(|Q_{B_1}| + |Q_{B_2}|\right) \tag{129}$$

and equation (129) is also used for coupling C replacing index B with C. The friction torque in coupling C, the round annulus, is not modelled since its rotation is prevented by coupling B, the square annulus.

A total of 18 constitutive equations are obtained from equations (127), (128), and (129). These equations are non-linear due to the use of the absolute value operator (the sign function is used only on already known motion variables). Together with the 42 network linear equations obtained from matrices $\boldsymbol{Q}_A$ and $\hat{\boldsymbol{A}}_N$, a system of 60 equations in 61 variables is assembled.

4.3.3.4 Software implementation

A software program was implemented in C++ specifically to simulate the behaviour of the 3-UPU during the execution of a task with emphasis on the power loss computation. For every discrete instant of time, the steps carried by the software are described by the Algorithm 2.

In Algorithm 2, step 3 is performed by LU-factorization. Step 6 is more complex and requires the solution of a system of non-linear equations. The specific solution used herein differs from that used in

other research [26].

The traditional approach to solving an otherwise linear system of equations that contains absolute value operators consists of assuming all possible combination of the sign of the variables and then solving the linear system. When the solution contradicts the assumption, the solution is discarded. Multiple solutions should be expected.

For the 3-UPU action analysis, the signs of 30 variables are needed: Q_{A_1}, Q_{A_2}, Q_{A_2}, Q_{B_1}, Q_{B_2}, Q_{C_1}, Q_{C_2}, Q_{D_1}, Q_{D_2}, Q_{D_2}, Q_{E_1}, Q_{E_2}, Q_{E_3}, Q_{F_1}, Q_{F_2}, Q_{G_1}, Q_{G_2}, Q_{H_1}, Q_{H_2}, Q_{H_3}, Q_{I_1}, Q_{I_2}, Q_{I_3}, Q_{J_1}, Q_{J_2}, Q_{K_1}, Q_{K_2}, Q_{L_1}, Q_{L_2}, and Q_{L_3}. Using the traditional approach, a linear system of 60 equations should be solved 2^{30} times which is not practical. Moreover, it is reasonable to expect that more than one of the attained solutions is valid but only one of them should be adopted. Hence, a less traditional method, called the homotopy continuation method [81], was used herein.

The homotopy continuation method involves numerically finding the solution of a problem by starting from the solution of a known problem and continuing the solution as the known problem is homotoped, i.e. gradually deformed, to the given problem [81].

In this case, for the first instant, the solution starts by finding the action magnitudes disregarding friction and proceeds by gradually increasing the coefficients of friction until a solution is found. Disregarding friction turns the problem into a linear problem with trivial solution. During homotoping, the signs of 30 variables are needed before their actual values are known. These signs are taken from the values that corresponding variables had at the end of the known problem (neglecting friction) and are stored in the variables; sign variables that can assume only the values in $\{-1, 0, +1\}$. If during the process any variable switches its sign, the sign variable is updated and the process restarted. For the next instant, the known problem is the previously completed problem, i.e., the position is gradually deformed to the current position.

The process is time consuming, but it is certainly faster than attempting to find the 2^{30} possible solutions. Furthermore, a verisimilar result is found. In next section, the result obtained using this software is discussed.

4.3.4 Simulation results

The execution of a specific task was used for the efficiency evaluation of the 3-UPU. A second task is used to appraise the software performance and accuracy. The two tasks employed are: lifting and translation through an elliptical path of a payload.

4.3.4.1 Physical description of the simulated 3-UPU

Both tasks were simulated using a 3-UPU with dimensions of

$$\begin{aligned} r_b &= 1.0\,\mathrm{m} \\ r_t &= 0.5\,\mathrm{m} \\ l_B = l_F = l_J &= 0.6\,\mathrm{m} \\ l_C = l_G = l_K &= 0.6\,\mathrm{m} \end{aligned}$$

and the pin radius of the universal joints is $r_i = 15\,\mathrm{mm}$, $i = A,\ D,\ E,\ H,\ I,$ and L. The coefficient of friction was adopted as $\mu_i = 0.11$, $i = A, \ldots, L$, as suggested by Shigley and Mischke [65] for lubricated steel-to-steel contact.

4.3.4.2 Efficiency

The task used to determine the 3-UPU efficiency is the lifting of a constant payload at constant speed in 1 s. The total load applied at point M is $W_M = 10\,000\,\mathrm{N}$, constant. The parametric equations for point M are

$$\begin{aligned} M_x &= 0.1\,\mathrm{m} \\ M_y &= 0.2\,\mathrm{m} \\ M_z &= 0.5 + 0.4\,t\,[\mathrm{m}] \end{aligned} \tag{130}$$

where t is the time in seconds. Differentiating equation (130) with respect to time, leads to

$$\begin{aligned} u_M &= 0 \\ v_M &= 0 \\ w_M &= 0.4\,\mathrm{m/s}\,. \end{aligned}$$

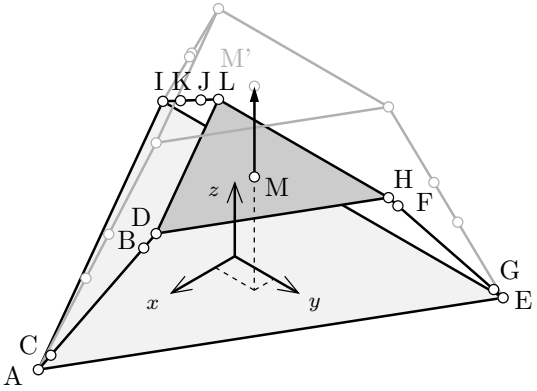

Figure 21 – 3-UPU schematic perspective representation. The coupling locations are denoted by small circles. The test path is a straight line from M to M'

This trajectory was selected because it is simple, the work done is of easy computation so validation is straightforward, and, most importantly, no motion changes direction during its execution.

In Fig. 21, plotted using simulated data, the initial and final configurations of the 3-UPU are illustrated with emphasis on the location of each coupling.

The time step adopted is 5 ms. As expected, the power expended at the load, $\mathcal{P}_M$, is constant as shown in Fig. 22. In Fig. 22, the power provided by each actuator and the total power are also shown.

Integrating the total power, the energy supplied by the actuators is found to be 6 146.83 J. The amount of energy supplied to coupling M is 4 000 J and this amount corresponds to the increase in the gravitational potential energy. The mechanical efficiency given by the ratio of these two amounts is computed as $\eta = 0.6517$.

Note that, $\eta = 0.6517$ is the efficiency associated with executing this specific task only. In the case of a different task, the efficiency might be different. For instance, lifting the same payload through half the length, in half the time, starting from the same position the efficiency is found to be $\eta = 0.7372$.

For the original task, the prismatic couplings are responsible for 98.55 % of the losses. In the universal joints, small friction torques combined with low speeds result in relatively low power losses.

The effects produced by a reversal of motion are discussed in the next section.

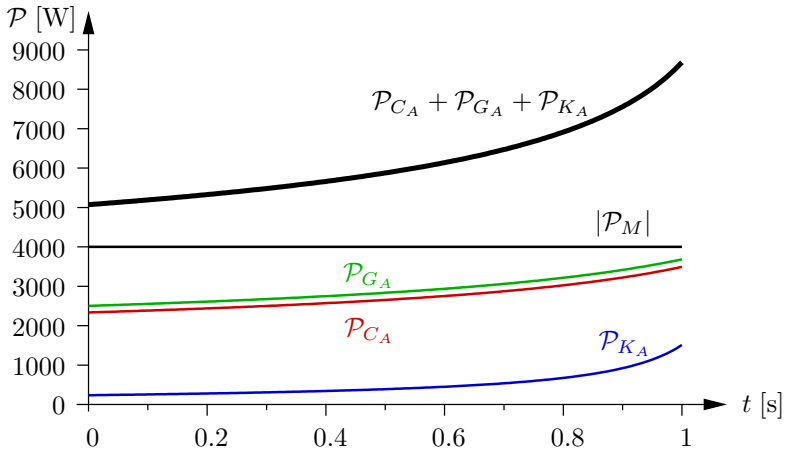

Figure 22 – Instantaneous power supplied by the actuator ($\mathcal{P}_{C_A}$, $\mathcal{P}_{G_A}$, $\mathcal{P}_{K_A}$, and total) and expended at the payload ($|\mathcal{P}_M|$) during the payload lifting at constant speed in 1 s, overall efficiency $\eta = 0.6517$

4.3.4.3 Elliptical path

The task described in Section 4.3.4.2 is suitable for the efficiency determination. However, the effects of motion reversal, an important feature for demonstrating the correctness of the approach, are not present in that task. Thus, to appraise such effects a second task is used. This task consists in moving a payload through an elliptical path described by the parametric equations

$$\begin{aligned} M_x &= 0.2\,\cos(2\,\pi\,t) \\ M_y &= 0.2\,\sin(2\,\pi\,t) \\ M_z &= 0.2\,\sin(2\,\pi\,t) + 0.7 \end{aligned} \tag{131}$$

which are given in meters, and t in seconds. After differentiation with respect to time, equation (131) produces

$$\begin{aligned} u_M &= -0.4\,\pi\,\sin(2\,\pi\,t) \\ v_M &= 0.4\,\pi\,\cos(2\,\pi\,t) \\ w_M &= 0.4\,\pi\,\cos(2\,\pi\,t) \end{aligned} \tag{132}$$

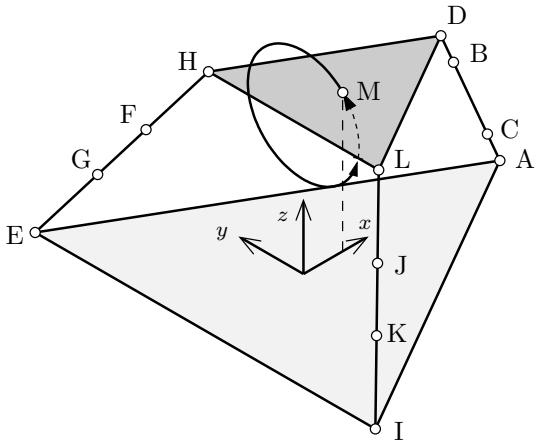

Figure 23 – 3-UPU schematic perspective representation. The coupling locations are denoted by small circles. The test path is elliptical

which are given in meters per second. The initial configuration of the 3-UPU and the elliptical path are illustrated in Fig. 23.

In Fig. 24, the total power $\mathcal{P}_{C_A} + \mathcal{P}_{G_A} + \mathcal{P}_{K_A}$ provided by the actuators and the power $\mathcal{P}_M$ expended at the payload are shown. At the beginning of the task, the sign of $\mathcal{P}_M$ is negative in Fig. 24 indicating that power is leaving the 3-UPU. In other words, the payload is been lifted.

Motion reversal causes sudden changes in friction actions requiring abrupt power income adjustments. These abrupt adjustments are seen in the power graph as discontinuities or tendency changes. The first noticeable discontinuity occurs at $t \approx 66.43\,\text{ms}$ when the angle formed between the base and the first limb (links 1 and 2 in Figs. 19 and 20) is minimal. As a consequence, the signs of p_{A_2} and p_{D_2} change reverting the friction torque directions and requiring a sudden increase in the actuator force (Q_{K_A} increases by 4.13 %). Another two discontinuities occur just before this one (at $t \approx 43.54\,\text{ms}$ caused by p_{E_1} and p_{H_1} and at $t \approx 47.57\,\text{ms}$ caused by p_{I_2} and p_{L_2}), but they are barely noticeable due to the smoothing algorithm used to plot Fig. 24.

A subtle change in tendency is caused, for instance, by the reversal in the actuator B-C movement when $t \approx 0.33275\,\text{s}$.

Examining the actuator force evolution in comparison with the case where friction is ignored, not only are higher magnitudes found, but also discontinuities and cuspidal points. In Fig. 25 the force applied

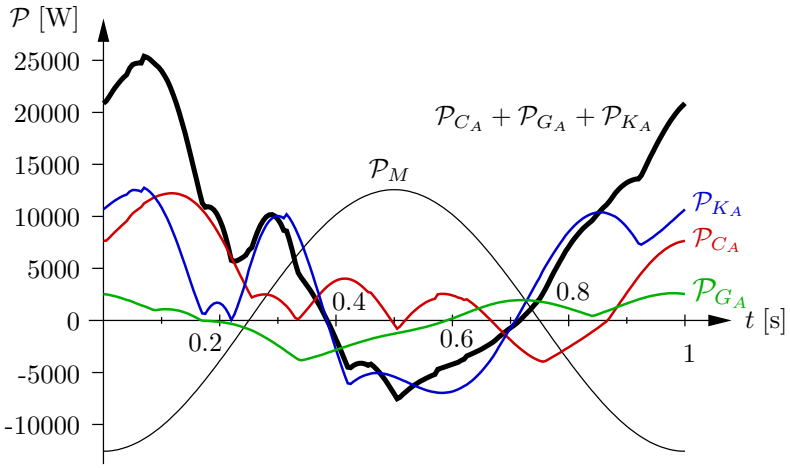

Figure 24 – Instantaneous power $\mathcal{P}_{C_A} + \mathcal{P}_{G_A} + \mathcal{P}_{K_A}$ supplied by the actuator and expended at the payload ($\mathcal{P}_M$) during an elliptical movement

by the actuator of the first limb, Q_{C_A}, is shown in two situations: considering and ignoring friction. Without friction, the actuators have only to support the payload weight and a smooth trajectory requies smooth forces from the actuators. When friction is taken into account, the cause of the aforementioned change in the tendency of the input power behaviour at $t \approx 0.33275\,\mathrm{s}$ is clearly identified as a sharp discontinuity in the actuation force. Fig. 25 also shows small discontinuities and cuspidal points caused in response to motion reversal in other parts of the machine.

The behaviour shown in Figs. 24 and 25 is exactly what would be expected for a complex system with non-linear friction.

4.3.4.4 Comparison with other approaches

As explained in the introduction, in general, researchers do not include the transmitted torque in their friction models neglecting its influence in the actual contact force magnitudes [1, 24, 25, 26, 27]. To appraise the consequence of this exclusion, the annular couplings of each limb were replaced by a single prismatic coupling. Three locations were considered for these prismatic joints: on each extremity and the middle

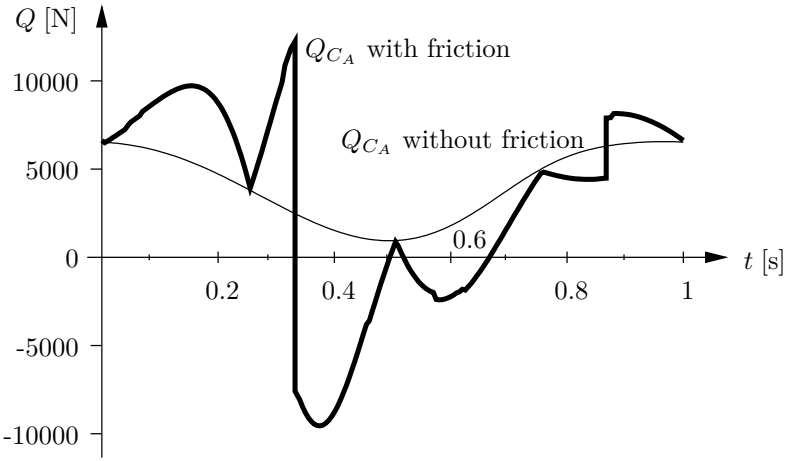

Figure 25 – Instantaneous force supplied by the actuator of the first limb (Q_{C_A}) with (thick line) and without (thin line) friction when following an elliptical path

point of the respective limb. The difference in location is compensated by the torque transmitted through the coupling and the transmitted force must be the same for all three locations.

The friction force magnitude was estimated using equation (129) and, consequently, the torque transmitted by the prismatic coupling was disregarded.

The efficiency found in the execution of the first task (see Section 4.3.4.2) and under the same considerations was $\eta = 0.9904$, regardless of the location of the prismatic joint. This value is close to unity because the contact force, computed using only the transmitted force, is much smaller than the actual value.

As expected, the transmitted force has the same value for different joint locations which explains why the efficiency is the same in all three situations.

4.3.5 Remarks

The friction force acting on round annuli (couplings C, G, and K) can be considered proportional to the normal forces (magnitudes of which are Q_{B_1} and Q_{B_2}) resultant instead of the sum of these force

magnitudes due to the axial symmetry. Thus, the friction would be given by

$$Q_{C_F} = -\mu_C \operatorname{sign}(q_C) \sqrt{{Q_{C_1}}^2 + {Q_{C_2}}^2} \tag{133}$$

instead of by equation (129). The use of equation (133) introduces quadratic equations into the system. These equations, however, are easier to solve than equations containing absolute value operators.

For the same reason, equations (127) and (128), which estimate the friction torque acting on the universal joints, can be modified.

Noteworthily, no significant impact on the overall efficiency was observed after these changes.

4.4 CONCLUSIONS

In complex machines the efficiency is dependent on the specific task. The concept of an overall efficiency valid for all situations is futile. If efficiency is to be used as a criterion to rank different machines, the task has to be specified as part of the criterion (see Section 4.3.4).

The non-linear system of equations is solved using the homotopy continuation method. The method showed a good performance in the solution of the actions in the analysis of the 3-UPU. In the worst case, only six iterations were needed. The amount of time for numerical solution is considered acceptable[3]: around 2 minutes for the evaluation of 200 time steps (see Section 4.3.4).

Friction in prismatic and cylindrical pairs can be straightforwardly modelled by splitting up the joint into two sliders (see Section 4.1.1). These sliders can be modelled as two round annuli for cylindrical pairs or a combination of a round and a square annulus for prismatic pairs (see Section 4.3.2). More detailed models are also possible if information of the joint constructions is available. Two common ways of implementing actuated prismatic joints employ a hydraulic ram and screw. The use of friction model of the hydraulic ram is reported by Bonchis, Corke and Rye [82] and a screw by Dupont [1].

For the 3-UPU simulated task, prismatic couplings are responsible for 98.55 % (straight line path) and 97.71 % (elliptical path) of the losses. Any attempt to replace the journal bearings in the universal joints with rolling element bearings appears to be of little benefit (see

[3]Naturally, the amount of time needed for computation is highly dependent on the hardware used to run the program. The time mentioned herein was obtained using a HP G61 laptop.

Section 4.3.4).

There are 275 possible spanning trees for the coupling graph in Fig. 19. The same arbitrarily selected spanning tree was used in Sections 4.3.3.1 and 4.3.3.2.

5 CONCLUSIONS

Success is never final.

Winston Churchill

In Chapter 3 a new method for efficiency determination based on graph and screw theories is presented. This method was developed through modifying and improving the well known Davies' Method and it can be used for obtaining the analytical expression of any gear train. Losses in gear meshing and bearing can be included and complex friction model can be used fulfilling the objectives stated in Chapter 1.

In general, the couplings in a machine are lower pairs or complex subsystems that can be modelled as lower pairs. One exception is the gear meshing, a higher pair in which it is possible to have more than one contact point (or line) at the same time. The contact point (or line) changes during meshing causing the friction action to change, but keeping its average value.

The main particularities of gear train modelling intending the efficiency determination are:

- The average magnitudes of the friction actions are consider instead of their instantaneous value.
- Multiple paths created by the presence of multiple planets may be ignored.
- Customarily, the overall efficiency is expressed in terms of the ordinary efficiency of each gear pair.
- The dimension d is usually low (2 or 3) requiring special screw system considerations.

Beside the three examples presented in Chapter 3, the proposed method was also applied to other gear trains described in the literature, particularly all of the examples in references [3,17,75] and many (cases 1, 2, 3, 4, 5, 13, 15, 18, and 30) from [11]. The method was also applied to a two degree of freedom differential and it shall appear in a future publication.

The generally accepted notion that the action responsible for power loss is a pure torque is formalised and proved using screw theory (see Theorem 1 in Section 3.2).

The most important findings of Chapter 3 were reported in technical article format submitted to the international journal of Mechanism and Machine Theory [83].

It is remarkable that the greater deal of effort is expended replacing the coefficient of friction by the ordinary efficiency. This replacement alone requires the definition and use of virtual power flow and the judicious use of ordinary efficiency. The procedure would be much more direct if the global efficiency were to be expressed in terms of coefficient of frictions as it is in Chapter 4.

In Chapter 4 the method presented in Chapter 3 is applied to determine the efficiency of complex machines. In complex machines, the efficiency is dependent on the specific task and the concept of an overall efficiency valid for all situations is futile. The application of the method in Chapter 4 is more straightforward than in Chapter 3, but even so care should be taken in modelling the actions transmitted by the couplings and the friction actions. A useful technique consists in splitting up the coupling into two parts such that the friction force locations are known *a priori*, possibly with multiples solutions. The method presented herein is considered more accurate than previous approach [1, 24, 26, 27] because all transmitted actions are taken into count even if they cause the model to become non-linear.

This method consists of an adaptation of Davies' Method that allows power to enter and leave to coupling network through ports or dissipative elements. The dissipative elements, analogous to electrical resistors, are included in the coupling network to model friction, an exclusive dissipative feature. The ports are analogous to the electrical current sources that normally provide power to the network, but can also absorb power from the network. These elements are included in the coupling network to model actuators and external loads, which can sometimes act as inputs, sometimes as outputs. This approach simplifies the modelling of complex machines when power losses are to be considered. The developed method achieves the objective stated in Chapter 1: it is a general purpose method easily adapted to any friction model.

The method presented in this thesis widens the application of the equations presented by Davies [20,21] to the case where power lost has to be considered. It represents an option to the use of energy and variational methods in the closed kinematic chain mechanics. The high

number of variables disfavour the used of these equations for dynamics however.

5.1 SUGGESTIONS FOR FUTURE WORK

The suggestions for future work are:

- The action related to friction is not a pure torque if the shaft axes are skew. This case shall be addressed in a future publication. Noteworthily, equation (5) is still valid for this case.
- The method was applied to the two degrees of freedom differential studied by Pennestrì and Freudenstein; Pennestrì and Valentini; Chen and Liang [4,12,84], but it remains unpublished. A detailed comparison between theirs method in the method presented herein shall be prepared.
- The method proposed by Chen and Angeles [3] and improved by Chen and Liang [4] can benefit from a graph theory approach. It may possible to extend the use of virtual power ratio leading to a simplified method without approximation and viable for automation.
- The possibility of extending of the method proposed by Castillo Granado [17] to bevel gear trains shall be addressed.
- The use of clutches and breaks in multi-speed transmission modelled by elements analogous to electrical switches might result in advantages yet to be determined.
- A comparison between the efficiency of different robot models, as example of the work conducted by Li and Bone [23], might be produced.
- The utilisation of method proposed in Chapter 4 into friction compensation control may result in practical advantage. The main obstacle is the computation time, too high for real time application.

REFERENCES

1 DUPONT, P. Friction modeling in dynamic robot simulation. In: *1990 IEEE International Conference on Robotics and Automation, 1990. Proceedings*. Cincinnati: IEEE, 1990. p. 1370 –1376 vol.2. Available from Internet: http://ieeexplore.ieee.org/xpls/abs_all.jsp?arnumber=126193.

2 ARMSTRONG-HÉLOUVRY, B.; DUPONT, P.; WIT, C. C. D. A survey of models, analysis tools and compensation methods for the control of machines with friction. *Automatica*, v. 30, n. 7, p. 1083–1138, 1994. ISSN 0005-1098. Available from Internet: http://www.sciencedirect.com/science/article/B6V21-47TG070-1N/2/0444a186a9e7597364e65b8c97c9cf51.

3 CHEN, C.; ANGELES, J. Virtual-power flow and mechanical gear-mesh power losses of epicyclic gear trains. *Journal of Mechanical Design*, v. 129, n. 1, p. 107–114, Jan 2007. Available from Internet: http://dx.doi.org/10.1115/1.2359473.

4 CHEN, C.; LIANG, T. T. Theoretic study of efficiency of two-dofs of epicyclic gear transmission via virtual power. *Journal of Mechanical Design*, v. 133, p. 031007, 2011. Available from Internet: http://dx.doi.org/10.1115/1.4003568.

5 DAVIES, T. H. Kirchhoff's circulation law applied to multi-loop kinematic chains. *Mechanism and Machine Theory*, v. 16, n. 3, p. 171–183, 1981. Available from Internet: http://www.sciencedirect.com/science/article/B6V46-482GN4J-PC/2/da424f56be0f7c29e7ddec5c95a7a7e7.

6 WHITE, G. Derivation of high efficiency two-stage epicyclic gears. *Mechanism and Machine Theory*, v. 38, n. 2, p. 149–159, 2003. ISSN 0094-114X. Available from Internet: http://www.sciencedirect.com/science/article/B6V46-47F0N9J-3/2/6da1effb048f967b70bf30c68959f56f.

7 NELSON, C. A.; CIPRA, R. J. Simplified kinematic analysis of bevel epicyclic gear trains with application to power-flow and efficiency analyses. *Journal of Mechanical Design*, ASME, v. 127, n. 2, p. 278–286, 2005. Available from Internet: http://link.aip.org/link/?JMD/127/278/1.

8 BUCKINGHAM, E. *Analytical mechanics of gears*. New York: Dover, 1963. First published by McGraw-Hill in 1949.

9 MACMILLAN, R. H. Epicyclic gear efficiencies. *The Engineer*, v. 188, p. 727–728, 1949.

10 TUPLIN, W. Designing compound epicyclic gear trains for maximum speed at high velocity ratios. *Machine Design*, v. 29, n. 7, p. 100–104, 1957.

11 GLOVER, J. Efficiency and speed ratio formulas for planetary gear systems. *Product Engineering*, v. 27, p. 72–79, 1965.

12 PENNESTRÌ, E.; FREUDENSTEIN, F. The mechanical efficiency of epicyclic gear trains. *Journal of Mechanical Design*, ASME, v. 115, n. 3, p. 645–651, 1993. Available from Internet: http://link.aip.org/link/?JMD/115/645/1.

13 POLDER, J. W. *A network theory for variable epicyclic gear trains*. Tese (Doctoral degree thesis) — Technische Hogeschool Eindhoven, Eindhoven, 1969. Hans Blok, Supervisor, Department of Electrical Engineering. Available from Internet: http://repository.tue.nl/104190.

14 BUCHSBAUM, F.; FREUDENSTEIN, F. Synthesis of kinematic structure of geared kinematic chains and other mechanisms. *Journal of Mechanisms*, v. 5, n. 3, p. 357–392, 1970. ISSN 0022-2569. Available from Internet: http://www.sciencedirect.com/science/article/B756S-47YDRRN-6/2/dc8b298add0bdd53a0844c9d0bce356b.

15 FREUDENSTEIN, F.; YANG, A. T. Kinematics and statics of a coupled epicyclic spur-gear train. *Mechanism and Machine Theory*, v. 7, n. 2, p. 263–275, 1972. ISSN 0094-114X. Available from Internet: http://www.sciencedirect.com/science/article/B6V46-482GS1H-CC/2/be95e233d14742e2ad15dbd9a6342e98.

16 SAGGERE, L.; OLSON, D. Simplified approach for force and power-flow analysis of compound epicyclic spur-gear trains. In: HOELTZEL, D. A. (Ed.). *Conference of* 18^{th} *Annual ASME Design Automation Conference Advances in Design Automation*. New York: ASME, 1992. v. 44 pt 2, p. 83–89.

17 CASTILLO GRANADO, J. M. d. The analytical expression of the efficiency of planetary gear trains. *Mechanism and Machine Theory*, v. 37, n. 2, p. 197–214, 2002. ISSN 0094-114X. Available

from Internet: http://www.sciencedirect.com/science/article/B6V46-44MG4B4-1/2/c74cdfa6a41e06dece938c8163d5d047.

18 TISCHLER, C. R.; SAMUEL, A. E.; HUNT, K. H. Selecting multi-freedom multi-loop kinematic chains to suit a given task. *Mechanism and Machine Theory*, v. 36, n. 8, p. 925–938, 2001. ISSN 0094-114X. Available from Internet: http://www.sciencedirect.com/science/article/B6V46-43T2F9D-3/2/c941e0e0d85168349d36d36bd14402ee.

19 MANTRIOTA, G.; PENNESTRÌ, E. Theoretical and experimental efficiency analysis of multi-degrees-of-freedom epicyclic gear trains. *Multibody System Dynamics*, Springer Netherlands, v. 9, n. 4, p. 389–408, 2003. ISSN 1384-5640. Available from Internet: http://www.springerlink.com/content/r85t80pq57762228/.

20 DAVIES, T. H. The 1887 committee meets again. Subject: freedom and constraint. In: UNIVERSITY OF CAMBRIDGE. *Ball 2000 Conference, University of Cambridge, Cambridge University Press, Trinity College Proceedings of a Symposium commemorating the Legacy, Works, and Life of Sir Robert Stawell Ball upon the* 100^{th} *Anniversary of A Treatise on the Theory of Screws*. Trinity College, 2000. p. 1–56. Available from Internet: http://hdl.handle.net/2134/700.

21 DAVIES, T. H. Freedom and constraint in coupling networks. *Proceedings of the Institution of Mechanical Engineers, Part C: Journal of Mechanical Engineering Science*, v. 220, n. 7, p. 989–1010, 2006. ISSN 0954-4062. Available from Internet: http://hdl.handle.net/2134/5892.

22 CRAIG, J. J. *Introduction to robotics : mechanics and control*. 2^{nd}. Reading, Massachusetts: Prentice Hall, 1989.

23 LI, Y.; BONE, G. M. Are parallel manipulators more energy efficient? In: *Proceedings of the 2001 IEEE International Symposium on Computational Intelligence in Robotics and Automation*. IEEE, 2001. p. 41–46. Available from Internet: http://ieeexplore.ieee.org/xpls/abs_all.jsp?arnumber=1013170.

24 TISCHLER, C. R.; LUCAS, S. R.; SAMUEL, A. E. Modelling friction in multi-loop linkages. In: *Experimental Robotics VI*. Berlin / Heidelberg: Springer, 2000, (Lecture Notes in Control and

Information Sciences, v. 250). p. 465–474. Available from Internet: http://www.springerlink.com/content/a31308400r322523.

25 DMITRY, V. *Component-oriented method for simulation of multibody dynamics*. Tese (Accepted dissertation) — Otto von Guericke University, Magdeburg, Jan 2006. Available from Internet: http://www.vlasenko.name/articles/vlasenko_dissertation.pdf.

26 FARHAT, N. et al. Dynamic simulation of a parallel robot: Coulomb friction and stick-slip in robot joints. *Robotica*, Cambridge University Press, New York, NY, USA, v. 28, n. 1, p. 35–45, 2010. ISSN 0263-5747. Available from Internet: http://dx.doi.org/10.1017/S0263574709005530.

27 FARHAT, N. et al. Identification of dynamic parameters of a 3-DOF RPS parallel manipulator. *Mechanism and Machine Theory*, v. 43, n. 1, p. 1–17, 2008. ISSN 0094-114X. Available from Internet: http://www.sciencedirect.com/science/article/pii/S0094114X07000079.

28 DAVIES, T. H. Couplings, coupling networks and their graphs. *Mechanism and Machine Theory*, v. 30, n. 7, p. 991–1000, 1995. ISSN 0094-114X. Graphs and Mechanics First International Conference, Zakopane, Poland, 1993. Available from Internet: http://www.sciencedirect.com/science/article/B6V46-3YMFRH1-N/2/af193277f5af381883e4b8be6a26e94f.

29 DAVIES, T. H.; LAUS, L. P. Tellegen's theorem applied to machinery. 13th *World Congress in Mechanism and Machine Science, Guanajuato, México, 19–25 June, 2011*, jun 2011. Paper number A8-295.

30 GOGU, G. Mobility of mechanisms: a critical review. *Mechanism and Machine Theory*, v. 40, n. 9, p. 1068–1097, 2005. ISSN 0094-114X. Available from Internet: http://www.sciencedirect.com/science/article/B6V46-4FKYDN2-D/2/027d02d1a70c75132e9216c59de9e170.

31 DAVIES, T. H. Mechanical networks – I Passivity and redundancy. *Mechanism and Machine Theory*, v. 18, n. 2, p. 95–101, 1983a. ISSN 0094-114X. Available from Internet: http://www.sciencedirect.com/science/article/B6V46-482GNP1-60/2/99ec936b4d627c7dbc29fbd976b5e2db.

32 DAVIES, T. H. Mechanical networks – II Formulae for the degrees of mobility and redundancy. *Mechanism and Machine Theory*, v. 18, n. 2, p. 103–106, 1983b. ISSN 0094-114X. Available from Internet: http://www.sciencedirect.com/science/article/B6V46-482GNP1-61/2/43272edab6520402afa74c3e38f2f2b0.

33 DAVIES, T. H. Mechanical networks – III Wrenches on circuit screws. *Mechanism and Machine Theory*, v. 18, n. 2, p. 107–112, 1983c. ISSN 0094-114X. Available from Internet: http://www.sciencedirect.com/science/article/B6V46-482GNP1-62/2/552c343d2c11876fc4be30f6673a3710.

34 DAVIES, T. H. Dual coupling networks. *Proceedings of the Institution of Mechanical Engineers, Part C: Journal of Mechanical Engineering Science*, v. 220, n. 8, p. 1237–1247, 2006. Available from Internet: http://hdl.handle.net/2134/4667.

35 DAVIES, T. H.; LAUS, L. P. Coupling networks dual with planar revolute coupled linkages in critical configurations. 13^{th} *World Congress in Mechanism and Machine Science, Guanajuato, México, 19–25 June, 2011*, jun 2011. Paper number A11-305.

36 BAKER, J. E. On mobility and relative freedoms in multiloop linkages and structures. *Mechanism and Machine Theory*, v. 16, n. 6, p. 583–597, 1981. ISSN 0094-114X. Available from Internet: http://www.sciencedirect.com/science/article/B6V46-482GN8J-SD/2/5c8814867e0fe149b54dd4b78b3f58e2.

37 BAKER, J. E.; HON-CHEUNG, Y. Re-examination of a Kempe linkage. *Mechanism and Machine Theory*, v. 18, n. 1, p. 7–22, 1983. ISSN 0094-114X. Available from Internet: http://www.sciencedirect.com/science/article/B6V46-482GMKC-F8/2/acdf89c564648eeca3441c325eb8293c.

38 BAKER, J. E. An analysis of Goldberg's anconoidal linkage. *Mechanism and Machine Theory*, v. 18, n. 5, p. 371–376, 1983. ISSN 0094-114X. Available from Internet: http://www.sciencedirect.com/science/article/B6V46-482GSTP-P5/2/b76453fd3ee5719e371ed68d7fe68bce.

39 BAKER, J. E. Limiting positions of a Bricard linkage and their possible relevance to the cyclohexane molecule. *Mechanism and Machine Theory*, v. 21, n. 3, p. 253–260, 1986. ISSN 0094-114X. Available from Internet:

http://www.sciencedirect.com/science/article/B6V46-482GRS9-75/2/12e36f18db6a082b8c163d487d4c4114.

40 HUANG, Z.; TAO, W. S.; FANG, Y. F. Study on the kinematic characteristics of 3 dof in-parallel actuated platform mechanisms. *Mechanism and Machine Theory*, v. 31, n. 8, p. 999–1007, 1996. ISSN 0094-114X. Available from Internet: http://www.sciencedirect.com/science/article/B6V46-3VTW8VY-1/2/bde5a2a576d213724c614505ebb1a610.

41 BULCA, F. *The kinematics and workspace analysis of platform mechanisms*. Tese (PhD Thesis) — McGill University, Department of Mechanical Engineering, Montréal, 1998. Available from Internet: http://www.collectionscanada.gc.ca/obj/s4/f2/dsk1/tape11/PQDD_0006/NQ44374.pdf.

42 ZOPPI, M.; ZLATANOV, D.; MOLFINO, R. On the velocity analysis of interconnected chains mechanisms. *Mechanism and Machine Theory*, v. 41, n. 11, p. 1346–1358, 2006. ISSN 0094-114X. Available from Internet: http://www.sciencedirect.com/science/article/B6V46-4J90VVD-1/2/aa66475f11ca7b0050e3266f7dd975f2.

43 MARTINS, D.; GUENTHER, R. Hierarchical kinematic analysis of robots. *Mechanism and Machine Theory*, v. 38, p. 497–518, 2003. Available from Internet: http://www.sciencedirect.com/science/article/pii/S0094114X03000053.

44 MARTINS, D. *Análise cinemática hierárquica de robôs manipuladores*. Tese (Tese de Doutorado) — Universidade Federal de Santa Catarina – UFSC, Florianópolis, SC, Fevereiro 2002. Em inglês.

45 CAMPOS BONILLA, A. A. *Cinemática diferencial de manipuladores empregando cadeias virtuais*. Tese (Tese de Doutorado) — Universidade Federal de Santa Catarina – UFSC, Florianópolis, 2004.

46 DOURADO, A. O. *Cinemática de robôs cooperativos*. Dissertação (Dissertação de Mestrado) — Universidade Federal de Santa Catarina – UFSC, Florianópolis, Abril 2005.

47 SANTOS, C. H. F. dos. *Movimento coordenado de sistemas veículo-manipulador submarinos utilizando técnicas de inteligência artificial e sistemas híbridos*. Tese (Tese de Doutorado) — Universidade Federal de Santa Catarina – UFSC, Florianópolis, 2006.

48 CRUZ, D. F. M. da. *Implementação da cinemática inversa de robôs redundantes operando em ambientes confinados no projeto ROBOTURB*. Dissertação (Dissertação de Mestrado) — Universidade Federal de Santa Catarina – UFSC, Florianópolis, Setembro 2007.

49 SIMAS, H. *Planejamento de trajetórias e evitamento de colisão em tarefas de manipuladores redundantes operando em ambiantes confinados*. Tese (Tese de Doutorado) — Universidade Federal de Santa Catarina – UFSC, Florianópolis, Fevereiro 2008.

50 CAZANGI, H. R. *Aplicação da ortogonalidade ao Método de Davies para análise cinemática e estática de mecanismos de múltiplos graus de liberdade*. Dissertação (Dissertação de Mestrado) — Universidade Federal de Santa Catarina – UFSC, Florianópolis, setembro 2007.

51 ERTHAL, J. L. *Modelo cinestático para análise de rolagem em veículos*. Tese (Tese de Doutorado) — Universidade Federal de Santa Catarina – UFSC, Florianópolis, Março 2007.

52 HUNT, K. H. *Kinematic geometry of mechanisms*. Oxford: Clarendon Press, 1990. (The Oxford engineering science series, v. 7). Reprinted with corrections [from the 1978 edition].

53 GALVAGNO, E.; VELARDOCCHIA, M.; VIGLIANI, A. Dynamic and kinematic model of a dual clutch transmission. *Mechanism and Machine Theory*, v. 46, n. 6, p. 794–805, 2011. ISSN 0094-114X. Available from Internet: http://www.sciencedirect.com/science/article/B6V46-526KFB1-1/2/6ce13f7f67894cd7af851924630c8835.

54 KAHRAMAN, A. et al. A kinematics and power flow analysis methodology for automatic transmission planetary gear trains. *Journal of Mechanical Design*, ASME, v. 126, n. 6, p. 1071–1081, 2004. Available from Internet: http://link.aip.org/link/?JMD/126/1071/1.

55 MATHIS, R.; REMOND, Y. Kinematic and dynamic simulation of epicyclic gear trains. *Mechanism and Machine Theory*, v. 44, n. 2, p. 412–424, 2009. ISSN 0094-114X. Available from Internet: http://www.sciencedirect.com/science/article/B6V46-4SBHD7M-1/2/0277d41eb27df88309bb598dfb2ba4ad.

56 PENNESTRÌ, E.; FREUDENSTEIN, F. A systematic approach to power-flow and static-force analysis in epicyclic

spur-gear trains. *Journal of Mechanical Design*, ASME, v. 115, n. 3, p. 639–644, 1993. Available from Internet: http://link.aip.org/link/?JMD/115/639/1.

57 PENNESTRÌ, E.; VALENTINI, P. P. Dynamic analysis of epicyclic gear trains by means of computer algebra. *Multibody System Dynamics*, Springer, v. 7, n. 3, p. 249–264, 2002. ISSN 1384-5640. Available from Internet: http://www.springerlink.com/content/nu67tmp3dwh9u1ma/.

58 SALGADO, D. R.; CASTILLO GRANADO, J. M. d. Selection and design of planetary gear trains based on power flow maps. *Journal of Mechanical Design*, ASME, v. 127, n. 1, p. 120–134, 2005. Available from Internet: http://link.aip.org/link/?JMD/127/120/1.

59 SANGER, D. J. The determination of power flow in multiple-path transmission systems. *Mechanism and Machine Theory*, v. 7, n. 1, p. 103–109, 1972. ISSN 0094-114X. Available from Internet: http://www.sciencedirect.com/science/article/B6V46-482GN85-13/2/934fe3cdd70010729b913ec539c4f25a.

60 FANGHELLA, P. A computational approach for the evaluation of single d.o.f. planetary gear efficiency. In: KECSKEMÉTHY, A.; MÜLLER, A. (Ed.). *Computational Kinematics*. Springer Berlin Heidelberg, 2009. p. 367–374. ISBN 978-3-642-01947-0. Available from Internet: http://www.springerlink.com/content/q53510621246u178.

61 PENFIELD JR., P.; SPENCE, R.; DUINKER, S. *Tellegen's theorem and electrical networks. Research Monograph No. 58.* Massachusetts: The MIT Press Cambridge, 1970.

62 BAPAT, R. B. *Graphs and matrices*. London: Springer, 2010. ISBN 978-1-84882-980-0.

63 RADZIMOVSKY, E. I. A simplified approach for determining power losses and efficiency of planetary gear drives. *Machine Design*, v. 28, n. 3, p. 101–110, 1956.

64 RADZIMOVSKY, E. I. How to find efficiency, speed, and power in planetary gear drives. *Machine Design*, v. 31, n. 12, p. 144–153, 1959.

65 SHIGLEY, J. E.; MISCHKE, C. R. *Mechanical engineering design*. 5th. New York: McGraw Hill, 1989. 779 p. (McGraw-Hill series in mechanical engineering). ISBN 0070568995.

66 PHILLIPS, J. *General spatial involute gearing*. Berlin: Springer, 2003. 498 p. (Mechanical Engineering, XVIII). ISBN 978-3-540-44204-2. Available from Internet: http://www.springer.com/engineering/mechanical+eng/book/978-3-540-44204-2.

67 STACHEL, H. On Jack Phillip's spatial involute gearing. In: CITESEER. *Proceeding of the* 11^{th} *International Conference on Geometry and Graphics*. Guangzhou, China, 2004. p. 1–5. Available from Internet: http://www.geometrie.tuwien.ac.at/stachel/guangzhou.pdf.

68 PHILLIPS, J. *Freedom in Machinery*. Cambridge University, 2007. Volume 1 (1984) and volume 2 (1990) combined. ISBN 978-0-521-67331-0. Available from Internet: http://ebooks.cambridge.org/ebook.jsf?bid=CBO9780511751745.

69 FRAZER, R. C.; FISH, M.; PALMER, D. *Optimizing gear geometry for minimum transmission error, mesh friction losses and scuffing risk through computer-aided engineering*. Alexandria, Virginia, Aug 2010. Internet. Gear Technology. Available from Internet: http://www.geartechnology.com/issues/0810x/frazer.pdf.

70 LITVIN, F. L.; FUENTES, A. *Gear Geometry and Applied Theory*. 2^{nd}. Cambridge: Cambridge University, 2004. 816 p. Available from Internet: http://www.cambridge.org/9780521815178.

71 MUROTA, K. *Matrices and matroids for systems analysis*. Berlin: Springer, 2000. 483 p. (Algorithms and Combinatorics, v. 20). ISBN 978-3-642-03993-5.

72 BARANOV, G. G. *Curso de la teoría de mecanismos y máquinas*. 2^{nd}. Moscow: Mir, 1985. 524 p. Spanish translation from Russian original.

73 BALABANIAN, N.; BICKART, T. A. *Electrical network theory*. New York: John Wiley & Sons, 1969. 931 p.

74 HARARY, F. *Graph theory*. Reading, MA: Addison-Wesley, 1969. (Addsison-Wesley Seriais in Mathematics).

75 RAVIGNEAUX, P. *Speed changing device*. Patent no. 2,220,174. Available from Internet: http://www.freepatentsonline.com/2220174.html.

76 BALABANIAN, N. *Fundamentals of circuit theory*. Boston: Allyn and Bocon, 1964. 555 p. (Electrical Engineering Series).

77 SESHU, S.; REED, M. B. *Linear graphs and electrical networks*. Reading-MA: Addison-Wesley, 1961. 315 p. (Engineering Sciences, Electrical and Control Systems).

78 MERLET, J.-P. *Parallel robots*. 2nd. Dordrecht: Springer, 2006. 394 p. (Solid mechanics and its applications, v. 128).

79 WOLF, A.; SHOHAM, M.; PARK, F. C. Investigation of singularities and self-motions of the 3-UPU robot. *Advances in Robot Kinematics*, p. 165–174, Jun 2002. J. Lenarcic and F. Thomas, eds. Available from Internet: http://brml.technion.ac.il/publications_files/1195633931.pdf.

80 SIMAS, H. et al. A new method to solve robot inverse kinematics using assur virtual chains. *Robotica*, v. 27, n. 7, p. 1017–1026, 2009. Available from Internet: http://dx.doi.org/10.1017/S0263574709005426.

81 ALEXANDER, J. C.; YORKE, J. A. The homotopy continuation method: numerically implementable topological procedures. *Transactions of the American Mathematical Society*, American Mathematical Society, v. 242, p. 271–284, 1978. ISSN 00029947. Available from Internet: http://www.jstor.org/stable/1997737.

82 BONCHIS, A.; CORKE, P. I.; RYE, D. C. A pressure-based, velocity independent, friction model for asymmetric hydraulic cylinders. In: *1999 IEEE International Conference on Robotics and Automation*. IEEE, 1999. v. 3, p. 1746–1751. Available from Internet: http://ieeexplore.ieee.org/xpls/abs_all.jsp?arnumber=770361.

83 LAUS, L. P.; MARTINS, D. Efficiency of gear trains using graph and screw theories. *Mechanism and Machine Theory*, to appear.

84 PENNESTRÌ, E.; VALENTINI, P. P. A review of formulas for the mechanical efficiency analysis of two degrees-of-freedom epicyclic gear trains. *Journal of Mechanical Design*, v. 125, n. 3, p. 602–609, 2003. Available from Internet: http://www.ingegneriameccanica.org/papers/review.pdf.

85 RESHETOV, L. *Self-aligning mechanisms*. 2nd revised edition. Moscow: Mir, 1986. 528 p. Translated from Russian by Leo M. Sachs.

APPENDIX A – Efficiency of involute spur gears

Men have become tools of their tools.

Henry David Thoreau

This appendix presents the efficiency analysis of an involute spur gear train. This gear train is similar to the more generic gear train illustrated schematically in Fig. 5. The friction forces are shown in Fig. 26c and these action screws belong to a 4^{th} special 3-system of screws [52] in the form $\{T;\, U,\, V\}$. The relative velocities, shown in Fig. 26b, belong to a 5^{th} special 3-system of screws in the form $\{t;\, u,\, v\}$; thus $d = 3$.

In this analysis it is assumed that:

- the geometry of the gear teeth is perfect;
- the driver angular velocity and torque are constant;
- when two or more pairs of teeth carry the load simultaneously, the normal pressure is shared equally between them.

Variable ρ is used to describe the distance (coordinate over the contact line) from the pitch point P to the contact point. Assuming that, gear 1 drives gear 2 which implies that $t_A,\, T_A > 0$ as shown in Fig. 27a, the approach length $\rho_a = \text{DP}$ can be determined in terms of the approach angle $\beta_{a\,1}$ remembering that, for the involute gear, the distance between two points on the contact line is equal to the difference between the corresponding arc lengths. Thus, from Fig. 27a:

$$\begin{aligned}
\beta_2 &= \alpha + \alpha' + \beta_{a\,2} \\
\beta_2\, r_{b\,2} &= r_{b\,2}\ (\alpha + \alpha') + \rho_a \\
\beta_{a\,2} &= \beta_{a\,1}\, \frac{r_1}{r_2} \\
\rho_a &= r_{b\,2}\ (\beta_2 - \alpha - \alpha') \\
&= r_{b\,2}\, \beta_{a\,2} = r_{b\,2}\, \beta_{a\,1}\, \frac{r_1}{r_2} \\
&= r_{b\,1}\, \beta_{a\,1}
\end{aligned}$$

where $r_{b\,1}$ and $r_{b\,2}$ are the base radii given by

$$\begin{aligned}
r_{b\,1} &= r_1\ \cos\alpha \\
r_{b\,2} &= r_2\ \cos\alpha\,.
\end{aligned}$$

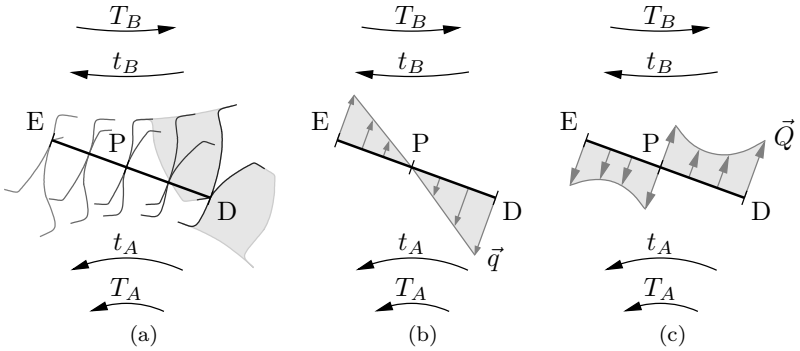

Figure 26 – Gear meshing where t_A and t_B are gear angular velocity magnitudes and T_A and T_B are torques (z-axis perpendicular to the figure), (a) contact line DE, (b) relative velocity for every contact point, (c) friction force for every contact point

Similarly, considering Fig. 27b, the recess length ρ_r = EP and the recess angle $\beta_{r\,1}$ are related by:

$$\begin{aligned} \beta_1 &= \alpha + \alpha' + \beta_{r\,1} \\ \beta_1\, r_{b\,1} &= r_{b\,1}\ (\alpha + \alpha') + \rho_r \\ \rho_r &= r_{b\,1}\ (\beta_1 - \alpha - \alpha') \\ &= r_{b\,1}\, \beta_{r\,1}\,. \end{aligned}$$

Using the fact that the pressure line segment is delimited by the intersection of the pressure line with the addendum circles, the approach and recess lengths can be written as:

$$\mathrm{EP} = \rho_r = -r_1\, \sin\alpha + \sqrt{{r_{a\,1}}^2 - {r_1}^2\, \cos^2\alpha} = r_1\, \cos\alpha\, \beta_{r\,1} \qquad (134)$$

$$\mathrm{DP} = \rho_a = -r_2\, \sin\alpha + \sqrt{{r_{a\,2}}^2 - {r_2}^2\, \cos^2\alpha} = r_1\, \cos\alpha\, \beta_{a\,1} \qquad (135)$$

where $r_{a\,1}$ and $r_{a\,2}$ are the addendum radii usually given by

$$\begin{aligned} r_{a\,1} &= r_1 + m \\ r_{a\,2} &= r_2 + m \end{aligned}$$

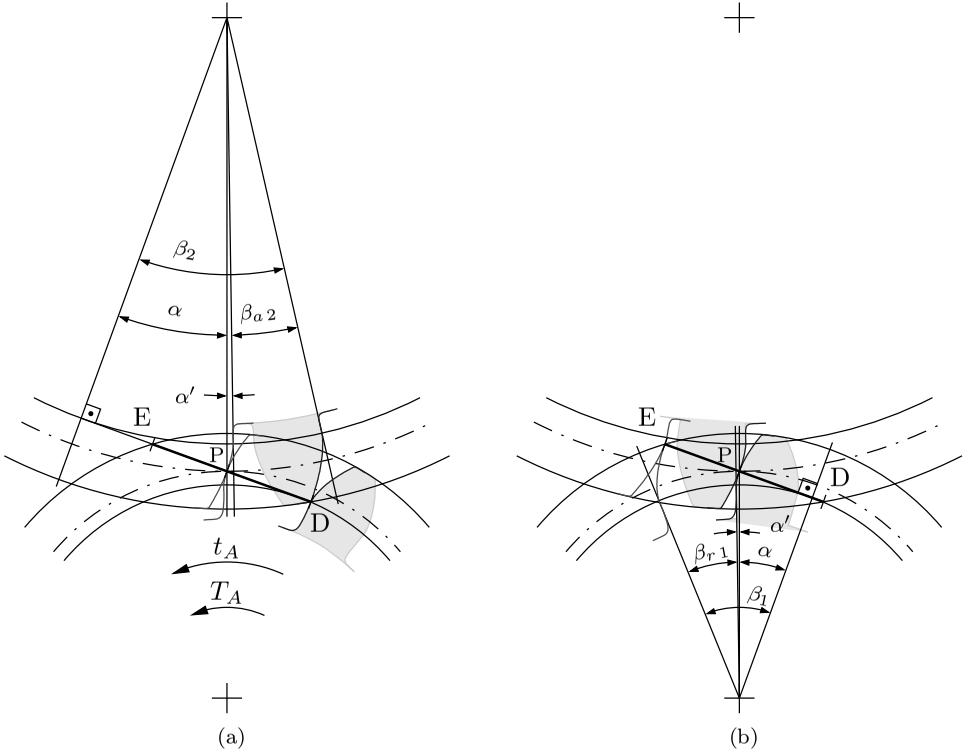

Figure 27 – Relationship between (a) approach and (b) recess angles of the respective contact point lengths

where m is the module.

A.1 MOTION ANALYSIS

The motion analysis is identical to $d = 2$ case (see Section 3.3) and the motion screw of coupling C passes through the pitch point, so

$$\$_C^{\mathbf{m}} = -t_A \left(\frac{r_1}{r_2} + 1\right) \begin{bmatrix} 1 \\ r_1 \\ 0 \end{bmatrix}$$

is the motion screw taken from the last column of the matrix in equation (16) with a zero appended to it.

A.2 ACTION ANALYSIS

The reaction forces acting on bearings A and B are now four: U_A, V_A, U_B and V_B. The external torque on these bearings still being T_A and T_B. The contact point C is shifted to:

$$\mathrm{C} = \begin{bmatrix} \rho \cos\alpha \\ r_1 - \rho \sin\alpha \\ 0 \end{bmatrix}.$$

The normal force direction at contact point C is

$$\hat{Q}_{C_N} = \begin{bmatrix} -\cos\alpha \\ \sin\alpha \\ 0 \end{bmatrix}$$

and the direction of the friction force on C is

$$\hat{Q}_{C_F} = \begin{bmatrix} \sin\alpha \\ \cos\alpha \\ 0 \end{bmatrix}.$$

The actions spanning the systems of actions that can be transmitted

Table 11 – Actions spanning the systems of actions that can be transmitted by the couplings of Fig. 5 when force friction is considered

Coupling Label, type	Planar Location		Force or Torque (direction)	Magnitude	Unit action screw coordinates in ray formation		
					Moment at origin	Force	
	x	y			T	U	V
A, bearing	0	0	Torque (z)	T_A	1	0	0
			Force (x)	U_A	0	1	0
			Force (y)	V_A	0	0	1
B, bearing	0	$r_1 + r_2$	Torque (z)	T_B	1	0	0
			Force (x)	U_B	$-r_1 - r_2$	1	0
			Force (y)	V_B	0	0	1
C, gear	$\rho \cos\alpha$	$r_1 - \rho \sin\alpha$	Force (Q)	Q_{C_F}	$\rho - r_1 \sin\alpha$	$\sin\alpha$	$\cos\alpha$
			Force (Q)	Q_{C_N}	$r_1 \cos\alpha$	-$\cos\alpha$	$\sin\alpha$

by couplings of Fig. 5 when force friction is considered are given in Table 11.

Considering that the friction force magnitude is dependent on the normal force:

$$Q_{C_F} = \mathfrak{g}\,(\rho)\; Q_{C_N}$$

where $\mathfrak{g}\,(\rho)$ is a friction function that is dependent explicitly on contact point position ρ and implicitly on the power flow sense.

For the Coulomb friction model

$$\mathfrak{g}\,(\rho) = \begin{cases} \mu & \text{if } \rho > 0 \wedge T_A\, t_A > 0 \\ -\mu & \text{if } \rho < 0 \wedge T_A\, t_A > 0 \end{cases}$$

where μ is the coefficient of friction, assumed constant. $T_A\, t_A > 0$ is a direct consequence of the fact that gear 1 drives gear 2.

The instantaneous magnitudes of the normal and friction forces are given by:

$$Q_{C_N} = \frac{T_A}{\mathfrak{g}\,\rho + r_1\;(\cos\alpha - \mathfrak{g}\,\sin\alpha)}$$
$$Q_{C_F} = \frac{T_A\,\mathfrak{g}}{\mathfrak{g}\,\rho + r_1\;(\cos\alpha - \mathfrak{g}\,\sin\alpha)}$$

and, therefore, the respective action screws are given by

$$\$^{\mathbf{a}}_{Q_{C_N}} = \frac{T_A}{\mathfrak{g}\,\rho + r_1\,\cos\alpha - \mathfrak{g}\,r_1\,\sin\alpha} \begin{bmatrix} r_1\,\cos\alpha \\ -\cos\alpha \\ \sin\alpha \end{bmatrix}$$

$$\$^{\mathbf{a}}_{Q_{C_F}} = \frac{g\,T_A}{\mathfrak{g}\,\rho + r_1\,\cos\alpha - \mathfrak{g}\,r_1\,\sin\alpha} \begin{bmatrix} \rho - r_1\,\sin\alpha \\ \sin\alpha \\ \cos\alpha \end{bmatrix}.$$

Note that

$$\$^{\mathbf{a}}_{Q_{C_N}} \bullet \$^{\mathbf{m}}_{C} = 0$$

$$\$^{\mathbf{a}}_{Q_{C_F}} \bullet \$^{\mathbf{m}}_{C} = \$^{\mathbf{a}}_{C} \bullet \$^{\mathbf{m}}_{C} = -t_A\, T_A \left(\frac{r_1}{r_2} + 1\right) \frac{\mathfrak{g}\,\rho}{\mathfrak{g}\,\rho + r_1\;(\cos\alpha - \mathfrak{g}\,\sin\alpha)}$$

which means that the normal force does not do any work on coupling C.

A.3 INSTANTANEOUS POWER AND EFFICIENCY

The instantaneous power loss is

$$\mathsf{p}_C = \$_C^{\mathbf{a}} \bullet \$_C^{\mathbf{m}} = \begin{cases} -t_A\, T_A \left(\frac{r_1}{r_2}+1\right) \frac{-\mu\,\rho}{-\mu\,\rho + r_1\,(\cos\alpha + \mu\,\sin\alpha)} & \text{if } \rho < 0 \wedge T_A\, t_A > 0 \\ -t_A\, T_A \left(\frac{r_1}{r_2}+1\right) \frac{\mu\,\rho}{\mu\,\rho + r_1\,(\cos\alpha - \mu\,\sin\alpha)} & \text{if } \rho > 0 \wedge T_A\, t_A > 0 \end{cases}$$

where Coulomb friction is assumed.

Defining the constants

$$\kappa_1 = -r_1 \left(\sin\alpha + \frac{\cos\alpha}{\mu}\right)$$
$$\kappa_2 = -r_1 \left(\sin\alpha - \frac{\cos\alpha}{\mu}\right)$$

the instantaneous power loss can be rewritten as

$$\mathsf{p}_C = \begin{cases} -t_A\, T_A \left(\frac{r_1}{r_2}+1\right) \frac{\rho}{\rho+\kappa_1} & \text{if } \rho < 0 \wedge T_A\, t_A > 0 \\ -t_A\, T_A \left(\frac{r_1}{r_2}+1\right) \frac{\rho}{\rho+\kappa_2} & \text{if } \rho > 0 \wedge T_A\, t_A > 0 \end{cases}$$

Assuming that coupling A is the input, which is the same as saying that gear 1 drives gear 2, the instantaneous input power is $\mathsf{p}_A = t_A\, T_A$ and the instantaneous efficiency

$$\begin{aligned} \eta_A &= 1 - \frac{|\mathsf{p}_C|}{\mathsf{p}_A} \\ &= \begin{cases} \frac{\kappa_1 - \frac{r_1}{r_2}\,\rho}{\kappa_1 + \rho} & \text{if } \rho < 0 \wedge T_A\, t_A > 0 \\ \frac{\kappa_2 - \frac{r_1}{r_2}\,\rho}{\kappa_2 + \rho} & \text{if } \rho > 0 \wedge T_A\, t_A > 0 \end{cases} \end{aligned}$$

The gear efficiency η_{12} is the average of the instantaneous efficiency during one gear mating interval:

$$\eta_{12} = \frac{1}{\mathsf{t}_r - \mathsf{t}_a} \int_{\mathsf{t}_a}^{\mathsf{t}_r} \eta_A \; d\mathsf{t}$$

where t_a is the approach time and t_r is the recess time.

For involute tooth form

$$\rho = -r_{b\,1}\, t_A\, \mathsf{t} = -r_1\, \cos\alpha\, t_A\, \mathsf{t}$$

thus

$$d\rho = -r_1 \cos\alpha\, t_A \; dt$$
$$dt = \frac{d\rho}{-r_1 \cos\alpha\, t_A}\,.$$

Note that ρ_r given by the above equation is the length from P to E, thus the sign of ρ_r is positive and it must be preceded by a minus sign when used in the efficiency equations, so

$$\rho = \rho_a \rightarrow t = t_a = -\frac{\rho_a}{r_1 \cos\alpha\, t_A}$$
$$\rho = -\rho_r \rightarrow t = t_r = \frac{\rho_r}{r_1 \cos\alpha\, t_A}$$

note that $t = 0 \rightarrow \rho = 0$ meaning that at this time the contact point coincides with the pitch point. For the integration interval

$$t = t_a \rightarrow \rho = \rho_a$$
$$t = t_r \rightarrow \rho = -\rho_r$$

then

$$\begin{aligned}
\eta_{12} &= \frac{1}{t_r - t_a} \int_{t_a}^{t_r} \eta_A \; dt \\
&= \frac{r_1 \cos\alpha\, t_A}{\rho_r + \rho_a} \int_{\rho_a}^{-\rho_r} \eta_A \frac{d\rho}{-r_1 \cos\alpha\, t_A} \\
&= \frac{1}{\rho_a + \rho_r} \int_{-\rho_r}^{\rho_a} \eta_A \; d\rho \\
&= \frac{1}{\rho_a + \rho_r} \left(\int_{-\rho_r}^{0} \frac{\kappa_1 - \frac{r_1}{r_2}\rho}{\kappa_1 + \rho} \; d\rho + \int_{0}^{\rho_a} \frac{\kappa_2 - \frac{r_1}{r_2}\rho}{\kappa_2 + \rho} \; d\rho \right) \\
&= \frac{1}{\rho_a + \rho_r} \left(\frac{r_1}{r_2} + 1 \right) \left(\kappa_2 \ln\left(1 + \frac{\rho_a}{\kappa_2} \right) - \kappa_1 \ln\left(1 - \frac{\rho_r}{\kappa_1} \right) \right) - \frac{r_1}{r_2}\,.
\end{aligned} \tag{136}$$

A.4 NUMERIC EXAMPLE

The following numerical data were extracted from reference [8, p. 401] and the notation was adapted as required.

$$\begin{aligned} m &= 1/3\,\text{in} \\ \beta_a &= 0.3691\,\text{rad} \\ \beta_r &= 0.3045\,\text{rad} \\ z_1 &= 18 \\ z_2 &= 48 \\ r_1 &= 3\,\text{in} \\ r_2 &= 8\,\text{in} \\ \alpha &= 14.5^\circ \\ \mu &= 0.0272 \\ \bar{\eta}_{12} &= 0.9936 \end{aligned} \tag{137}$$

So, applying equations (135), (134), and (136)

$$\begin{aligned} \rho_a &= 1.072029882\,\text{in} \\ \rho_r &= 0.8844028695\,\text{in} \\ \eta_{12} &= 0.9936745104 \end{aligned}$$

and there is no significant difference between the efficiency obtained by Buckingham [8, p. 401] and the approach developed herein. It is worth noting that the value of $\bar{\eta}_{12}$ in equation (137) was calculated based on an approximated equation and without resorting to any modern digital calculators. A more exact equation, also deduced by Buckingham [8, p. 399],

$$\begin{aligned} \bar{\eta}_{12} &= \frac{\beta_{a\,1} + \beta_{r\,1} - \mu\,\tan(\alpha)\,(\beta_{a\,1} - \beta_{r\,1}) - \frac{\mu\,r_1}{2\,r_2}\left({\beta_{a\,1}}^2 + {\beta_{r\,1}}^2\right)}{\beta_{a\,1} + \beta_{r\,1} - \mu\,\tan(\alpha)\,(\beta_{a\,1} - \beta_{r\,1}) + \frac{\mu}{2}\left({\beta_{a\,1}}^2 + {\beta_{r\,1}}^2\right)} \\ &= 0.993668909 \end{aligned}$$

renders a result that differs by one thousandth of a percent from the approach devised herein.

There are far more complex methods available in the literature. The interested read should refer, for instance, to Tooth Contact Analysis (TCA) [69, 70].

A.5 COEFFICIENT OF FRICTION

To perform the efficiency analysis, it is possible to replace the instantaneous friction action with an average action that produces the same average power loss in the coupling keeping the statics relationship unaltered. Such an equivalent average action can be split into a pure torque action $\$^{\mathbf{a}}_{C\,t}$ and a pure force action $\$^{\mathbf{a}}_{C\,f}$ given by

$$\$^{\mathbf{a}}_{C\,f} = \frac{\varrho^{\mathbf{a}}_{C\,t}}{\zeta_C \cos\alpha} \begin{bmatrix} r_1 \cos\alpha \\ -\cos\alpha \\ \sin\alpha \end{bmatrix}$$

$$\$^{\mathbf{a}}_{C\,t} = \varrho^{\mathbf{a}}_{C\,t} \begin{bmatrix} 1 \\ 0 \\ 0 \end{bmatrix}$$

$$\varrho^{\mathbf{a}}_{C\,t} = \zeta_C \cos\alpha\, \varrho^{\mathbf{a}}_{C\,f}$$

where the coefficient of friction ζ_C is the average or equivalent value of μ, the coefficient of friction in a classical sense. Note that the force action $\$^{\mathbf{a}}_{C\,f}$ does not do any work at coupling C since

$$\$^{\mathbf{a}}_{C\,f} \bullet \$^{\mathbf{m}}_{C} = 0$$

moreover, this action can be disregarded unless bearing losses are to be considered.

The average power loss is

$$\mathcal{P}_C = \frac{1}{t_r - t_a} \int_{t_a}^{t_r} p_C \, dt$$

but it is also

$$\mathcal{P}_C = \$^{\mathbf{a}}_{C\,t} \bullet \$^{\mathbf{m}}_{C} = -t_A \left(\frac{r_1}{r_2} + 1\right) \varrho^{\mathbf{a}}_{C\,t} = -T_A\, t_A \left(\frac{r_1}{r_2} + 1\right) \frac{\zeta_C}{\zeta_C + r_1}$$

so

$$\varrho^{\mathbf{a}}_{C\,t} = T_A \frac{\zeta_C}{\zeta_C + r_1}$$

and also

$$\begin{aligned}\zeta_C &= r_1 \frac{\frac{1}{\rho_a+\rho_r}\left(\int\limits_{-\rho_r}^{0} \frac{\rho}{\rho+\kappa_1}\,d\rho + \int\limits_{0}^{\rho_a} \frac{\rho}{\rho+\kappa_2}\,d\rho\right)}{1-\frac{1}{\rho_a+\rho_r}\left(\int\limits_{-\rho_r}^{0} \frac{\rho}{\rho+\kappa_1}\,d\rho + \int\limits_{0}^{\rho_a} \frac{\rho}{\rho+\kappa_2}\,d\rho\right)} \\ &= r_1 \frac{\rho_a+\rho_r}{\kappa_2\,\ln\left(1+\frac{\rho_a}{\kappa_2}\right)-\kappa_1\,\ln\left(1-\frac{\rho_r}{\kappa_1}\right)}\end{aligned}$$

and this result agrees with equation (33) when η_{12} is estimated by equation (136). Also note that the action magnitude is

$$\begin{aligned}\varrho^{\mathbf{a}}_{C\,t} &= T_A \frac{1}{\rho_a+\rho_r}\left(\int\limits_{-\rho_r}^{0} \frac{\rho}{\rho+\kappa_1}\,d\rho + \int\limits_{0}^{\rho_a} \frac{\rho}{\rho+\kappa_2}\,d\rho\right) \\ &= T_A\left(1+\frac{1}{\rho_a+\rho_r}\left(\kappa_1\,\ln\left(1-\frac{\rho_r}{\kappa_1}\right)-\kappa_2\,\ln\left(1+\frac{\rho_a}{\kappa_2}\right)\right)\right)\end{aligned}$$

and thus it has been referred to as the average torque.

APPENDIX B – Epicyclic Gear Train

In this world there are only two tragedies. One is not getting what one wants, and the other is getting it.

Oscar Wilde

This appendix presents motion and action spanning the systems of motions and actions allowed and transmitted by the couplings in Fig. 7

T_A and T_B are external torques, T_C and T_D are friction torques, U_A, U_B and U_E are reaction forces related to the sole degree of constraint of the coupling, and U_C and U_D are forces transmitted by the gear couplings. The location $z = 0$ is somewhat arbitrary since none of the motions in Table 12 nor actions in Table 13 are affected by this choice.

Table 12 – Motions spanning the systems of motions allowed by the couplings of Fig. 7

Coupling Label, type	Planar Location		Rotational or Translational Velocity (direction)	Magnitude	Unit motion screw coordinates in axis formation	
					Angular Velocity	Velocity of the point at the origin
	y	z			t	u
A, revolute	0	0	Rotational (z)	t_A	1	0
B, revolute	0	0	Rotational (z)	t_B	1	0
C, gear	r_1	0	Rotational (z)	t_C	1	r_1
D, gear	r_2	0	Rotational (z)	t_D	1	r_2
E, revolute	$r_1 - r_3$	0	Rotational (z)	t_E	1	$r_1 - r_3$

Table 13 – Actions spanning the systems of actions that can be transmitted by the couplings of Fig. 7

Coupling Label, type	Planar Location		Force or Torque (direction)	Magnitude	Unit action screw coordinates in ray formation	
					Moment at origin	Force
	y	z			T	U
A, revolute	0	0	Torque (z)	T_A	1	0
			Force (x)	U_A	0	1
B, revolute	0	0	Torque (z)	T_B	1	0
			Force (x)	U_B	0	1
C, gear	r_1	0	Torque (z)	T_C	1	0
			Force (x)	U_C	$-r_1$	1
D, gear	r_2	0	Torque (z)	T_D	1	0
			Force (x)	U_D	$-r_2$	1
E, revolute	$r_1 - r_3$	0	Force (x)	U_E	$r_3 - r_1$	1

APPENDIX C – Humpage Bevel Gear Train

One machine can do the work of fifty ordinary men. No machine can do the work of one extraordinary man.

Elbert Hubbard

This appendix presents motion and action spanning the systems of motions and actions allowed and transmitted by the couplings in Fig. 9 and some geometrical consideration used to obtain these screws.

All of the geometrical relationships in Fig. 9 can be determined in terms of the pitch radii r_i $(i = 1, \ldots, 5)$. The cosine of β, angle between the carrier axis and y-axis in Fig. 28, is given by

$$\cos\beta = \frac{r_5 - r_1}{2\,r_2}\,.$$

Therefore, the coordinates of pitch points C, D and E in the plane $x = 0$ are given by

$$\begin{aligned}
E_y &= r_4 \\
D_y &= r_5 \\
C_y &= r_1 \\
E_z &= \frac{r_3}{\sin\beta} - \frac{r_4}{\tan\beta} \\
&= \frac{2\,r_2\,r_3 - r_4\,(r_5 - r_1)}{\sqrt{4\,{r_2}^2 - (r_5 - r_1)^2}} = \frac{f}{\sqrt{b}} \\
D_z &= \frac{r_2}{\sin\beta} - \frac{r_5}{\tan\beta} \\
&= \frac{2\,{r_2}^2 - r_5\,(r_5 - r_1)}{\sqrt{4\,{r_2}^2 - (r_5 - r_1)^2}} = \frac{d}{\sqrt{b}} \\
C_z &= D_z - 2\,r_2\,\sin\beta \\
&= -\frac{2\,{r_2}^2 + r_1\,(r_5 - r_1)}{\sqrt{4\,{r_2}^2 - (r_5 - r_1)^2}} = -\frac{e}{\sqrt{b}}
\end{aligned} \tag{138}$$

where a, b, c, d, e, and f are given by equation (83).

Couplings C, D, and E are of the gear type and their motion ISAs pass through the origin O and have orientation parallel to the

unit vectors:

$$\hat{p}_C = \hat{P}_C = \begin{matrix} x \\ y \\ z \end{matrix} \begin{bmatrix} 0 \\ r_1\sqrt{b} \\ -e \end{bmatrix} \frac{1}{2\,r_2\,a} \tag{139}$$

$$\hat{p}_D = \hat{P}_D = \begin{matrix} x \\ y \\ z \end{matrix} \begin{bmatrix} 0 \\ r_5\sqrt{b} \\ d \end{bmatrix} \frac{1}{2\,r_2\,a} \tag{140}$$

$$\hat{p}_E = \hat{P}_E = \begin{matrix} x \\ y \\ z \end{matrix} \begin{bmatrix} 0 \\ r_4\sqrt{b} \\ f \end{bmatrix} \frac{1}{2\,c} \tag{141}$$

at the instant of time that the coupling network is found as shown in Fig. 9.

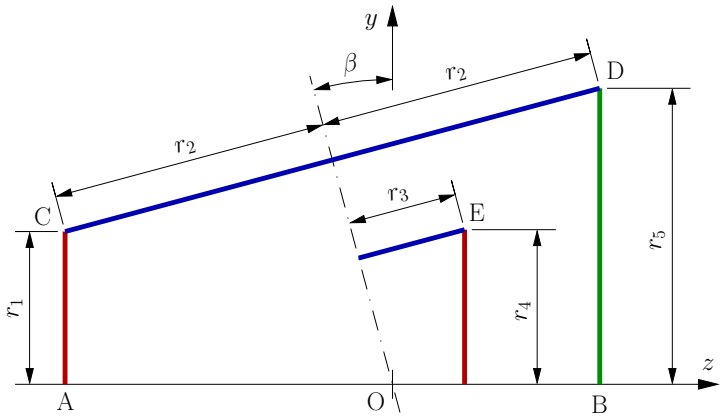

Figure 28 – Geometrical relationship for Humpage bevel gear

Tables 14 and 15 bring the screws which span the system of actions and motions for the Humpage bevel gear. The constants used in these tables are given by equations (83) and (138).

Table 14 – Motions spanning the systems of motions allowed by the couplings of Fig. 9

Coupling Label, type	Planar Location		Rotational or Translational Velocity (direction)	Magnitude	Unit motion screw coordinates in axis formation		
					Angular Velocity		Velocity of the point at the origin
	y	z			s	t	u
A, revolute	0	0	Rotational (z)	t_A	0	1	0
B, revolute	0	0	Rotational (z)	t_B	0	1	0
C, gear	C_y	C_z	Rotational $(\vec{p}_C)$	p_C	$\frac{\sqrt{b}\, r_1}{2\, a\, r_2}$	$-\frac{e}{2\, a\, r_2}$	0
D, gear	D_y	D_z	Rotational $(\vec{p}_D)$	p_D	$\frac{\sqrt{b}\, r_5}{2\, a\, r_2}$	$\frac{d}{2\, a\, r_2}$	0
E, gear	E_y	E_z	Rotational $(\vec{p}_E)$	p_E	$\frac{\sqrt{b}\, r_4}{2\, c}$	$\frac{f}{2\, c}$	0
F, revolute	0	0	Rotational (z)	t_F	0	1	0
G, revolute	0	0	Rotational $(\vec{p}_G)$	p_G	$\frac{r_1 - r_5}{2\, r_2}$	$\frac{\sqrt{b}}{2\, r_2}$	0

Table 15 – Actions spanning the systems of actions that can be transmitted by the couplings of Fig. 9

Coupling Label, type	Planar Location		Force or Torque (direction)	Magnitude	Unit action screw coordinates in ray formation		
					Moment at origin		Force
	y	z			S	T	U
A, revolute	0	0	Torque (y)	S_A	1	0	0
			Torque (z)	T_A	0	1	0
			Force (x)	U_A	0	0	1
B, revolute	0	0	Torque (y)	S_B	1	0	0
			Torque (z)	T_B	0	1	0
			Force (x)	U_B	0	0	1
C, gear	C_y	C_z	Torque $\left(\vec{P}_C\right)$	P_C	$\frac{\sqrt{b}\,r_1}{2\,a\,r_2}$	$-\frac{e}{2\,a\,r_2}$	0
			Force (x)	U_C	$-\frac{e}{\sqrt{b}}$	$-r_1$	1
D, gear	D_y	D_z	Torque $\left(\vec{P}_D\right)$	P_D	$\frac{\sqrt{b}\,r_5}{2\,a\,r_2}$	$\frac{d}{2\,a\,r_2}$	0
			Force (x)	U_D	$\frac{d}{\sqrt{b}}$	$-r_5$	1
E, gear	E_y	E_z	Torque $\left(\vec{P}_E\right)$	P_E	$\frac{\sqrt{b}\,r_4}{2\,c}$	$\frac{f}{2\,c}$	0
			Force (x)	U_E	$\frac{f}{\sqrt{b}}$	$-r_4$	1
F, revolute	0	0	Torque (y)	S_F	1	0	0
			Force (x)	U_F	0	0	1
G, revolute	0	0	Torque $\left(\vec{P}_G\right)$	P_G	$\frac{\sqrt{b}}{2\,r_2}$	$-\frac{r_1-r_5}{2\,r_2}$	0
			Force (x)	U_G	0	0	1

APPENDIX D – Friction in cylindrical journal bearings

Why are our days numbered and not, say, lettered.

Woody Allen

In this appendix, friction on cylindrical journal bearings is discussed and modelled.

D.1 NORMAL REACTION ON CYLINDRICAL CONTACT SURFACES

The contact surface geometry influences the normal reaction distribution and, consequently, the normal reaction and friction force magnitudes. In Fig. 29, the normal reaction distribution for an external applied force $\vec{Q}$ that passes through the pair axis is illustrated. The angle of engagement of the pin with the insert is denoted by $2\,\beta$.

The common approach is to adjust the coefficient of friction according to the normal reaction distribution law. Baranov [72] recommends the use of two laws: constant, to be used for new pairs; and cosine, to be used for old pairs that have worn and accommodated. In Table 16, the coefficient of friction multipliers is shown for the two laws. For friction models that are dependent on normal reaction, the appropriate coefficient of friction is obtained multiplying the coefficient of friction for the planar case coefficient by a suitable value selected from Table 16. The procedure is the same for both force and torque friction.

D.2 TORQUE FRICTION IN AN ANNUAL PIVOT BEARING UPON A PLANE

In revolute pairs, sometimes the contact is made in the form of an annual pivot bearing upon a plane. In this case, the Coulomb friction torque is dependent on the normal contact force, the coefficient of friction μ, and the normal force distribution law. Reshetov [85] recommends the use of two laws. For a new pivot the normal pressure

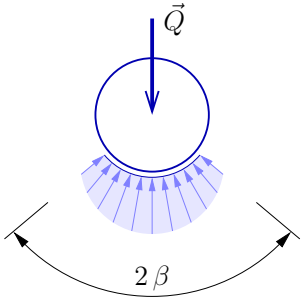

Figure 29 – Cylindrical contact and normal reaction distribution

Table 16 – Coefficient of friction multipliers for cylindrical contact surfaces

	Constant	Cosine
any β	$\dfrac{\beta}{\sin\beta}$	$\dfrac{4\,\sin\beta}{2\,\beta+\sin 2\,\beta}$
$\beta=\dfrac{\pi}{2}$	$\dfrac{\pi}{2}$	$\dfrac{4}{\pi}$

$\mathcal{N}$ is uniformly distributed over the contact area and it is given by

$$\mathcal{N}=\frac{Q_N}{\pi\,({r_2}^2-{r_1}^2)} \tag{142}$$

where Q_N is the normal force magnitude, and r_1 and r_2 are the inner and outer radii of the annular pivot, respectively. For an old pivot the normal pressure is not constant,

$$\mathcal{N}=\frac{Q_N}{\pi\,(r_2-r_1)\,\rho} \tag{143}$$

where ρ is the distance from the pivot centre to the point on the contact surface where $\mathcal{N}$ is measured.

The friction torque P_F is obtained by integration as

$$P_F=\int_{-\pi}^{\pi}\int_{r_1}^{r_2}\mu\,\mathcal{N}\,\rho^2\;d\rho\,d\theta \tag{144}$$

resulting in

$$P_F = \frac{2\,\mu\,\left({r_1}^2 + r_1\,r_2 + {r_2}^2\right)}{3\,\left(r_1 + r_2\right)}\,Q_N \tag{145}$$

for a new pivot and

$$P_F = \mu\,\left(r_1 + r_2\right)\,Q_N \tag{146}$$

for a old pivot.

APPENDIX E – Insight into Davies' Equations

From error to error, one discovers the entire truth.

Sigmund Freud

This appendix explores the dual relationship between equations (56) and (19), renumbered herein to (148) and (150), the available alternatives for assembling the network unit motion and action matrices ($\hat{\boldsymbol{M}}_N$ and $\hat{\boldsymbol{A}}_N$), and the topological relationships that allow the determination of all network motion and actions from a minimal set.

E.1 MOTION AND ACTIONS EQUATIONS

The following text is developed in two columns. The left column regards the motion equations and the right one the actions equations. The matrices for the mechanism illustrated in Fig. 30 are provided as example. In Fig. 31 the coupling graph of the mechanism in Fig. 30 is shown. In this coupling graph, the spanning tree used for both motion and action analysis is indicated by thick lines. The symbol $\times$ is used to indicate matrix dimensions and the comma to separate matrix index.

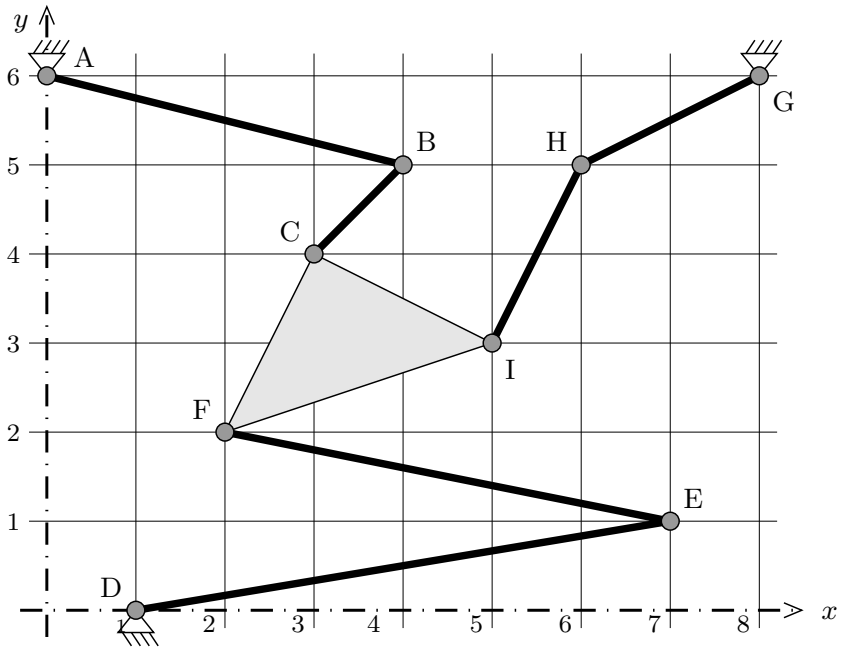

Figure 30 – 3-RRR, a 3-dof planar parallel manipulator

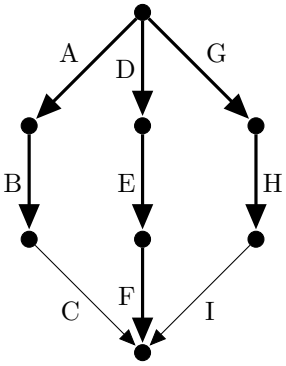

Figure 31 – 3-RRR, 3-dof planar parallel manipulator coupling graphs G_C

The analogous of Kirchhoff voltage law for a mechanical system [20, 21] is given by:

$$\left[\hat{\boldsymbol{M}}_N\right]_{d\,l\times F}[\boldsymbol{\psi}]_F = [\boldsymbol{0}]_{d\,l} \tag{147}$$

where $[\boldsymbol{\psi}]_F$ is the vector of F generalised motion magnitudes (angular or translational velocity), F is the gross degree of freedom of the coupling network equal in number to the sum of the gross degrees of freedom f_j of the direct couplings ($j = 1, 2, \ldots e$). $\left[\hat{\boldsymbol{M}}_N\right]_{d\,l\times F}$ is the network unit motion matrix where l is the number of independent circuits (loops) of the coupling graph. This matrix is given by:

$$\left[\hat{\boldsymbol{M}}_N\right]_{d\,l\times F} = \begin{bmatrix} \left[\hat{\boldsymbol{M}}_D\right]_{d\times F}[\boldsymbol{B}_1]_{F\times F} \\ \left[\hat{\boldsymbol{M}}_D\right]_{d\times F}[\boldsymbol{B}_2]_{F\times F} \\ \vdots \\ \left[\hat{\boldsymbol{M}}_D\right]_{d\times F}[\boldsymbol{B}_l]_{F\times F} \end{bmatrix}_{d\,l\times F} \tag{148}$$

where $\left[\hat{\boldsymbol{M}}_D\right]_{d\times F}$ is the unit motion matrices of the direct couplings of a coupling network, and $[\boldsymbol{B}_i]_{F\times F} = \mathrm{diag}\left([\boldsymbol{B}_M]_i\right)$ are diagonal matrices ($i = 1, 2, \ldots, l$).

The analogous of Kirchhoff current law for a mechanical system [20, 21] is given by:

$$\left[\hat{\boldsymbol{A}}_N\right]_{d\,k\times C}[\boldsymbol{\Psi}]_C = [\boldsymbol{0}]_{d\,k} \tag{149}$$

where $[\boldsymbol{\Psi}]_C$ is the vector of C generalised action magnitudes (torque or force), C is the gross degree of constraint of the coupling network equal in number to the sum of the gross degrees of constraint c_j of the direct couplings ($j = 1, 2, \ldots e$). $\left[\hat{\boldsymbol{A}}_N\right]_{d\,k\times C}$ is the network unit action matrix where k is the number of independent cutsets of the coupling graph. This matrix is given by:

$$\left[\hat{\boldsymbol{A}}_N\right]_{d\,k\times C} = \begin{bmatrix} \left[\hat{\boldsymbol{A}}_D\right]_{d\times C}[\boldsymbol{Q}_1]_{C\times C} \\ \left[\hat{\boldsymbol{A}}_D\right]_{d\times C}[\boldsymbol{Q}_2]_{C\times C} \\ \vdots \\ \left[\hat{\boldsymbol{A}}_D\right]_{d\times C}[\boldsymbol{Q}_k]_{C\times C} \end{bmatrix}_{d\,k\times C} \tag{150}$$

where $\left[\hat{\boldsymbol{A}}_D\right]_{d\times C}$ is the unit action matrix of the direct couplings of a coupling network, and $[\boldsymbol{Q}_i]_{C\times C} = \mathrm{diag}\left([\boldsymbol{Q}_A]_i\right)$ are diagonal matrices ($i = 1, 2, \ldots, k$).

The diagonal elements of $[\boldsymbol{B}_i]_{F\times F}$ are those of row i of $[\boldsymbol{B}_M]_{l\times F}$, the fundamental circuit matrix of motion graph G_M. The matrix $[\boldsymbol{B}_M]_{l\times F}$ correspond to the fundamental circuit matrix $[\boldsymbol{B}]_{l\times e}$ with the column j replicated f_j times.

The structure of matrix in equation (148) is

$$\left[\hat{\boldsymbol{M}}_N\right]_{d\,l\times F} = \begin{bmatrix} \text{circuit 1}\left\{\begin{matrix} \bullet & \bullet & \cdots & \bullet \end{matrix}\right\}\text{dimension 1} \\ \left\{\begin{matrix} \bullet & \bullet & \cdots & \bullet \end{matrix}\right\}\text{dimension 2} \\ \vdots \\ \left\{\begin{matrix} \bullet & \bullet & \cdots & \bullet \end{matrix}\right\}\text{dimension } d \\ \text{circuit 2}\left\{\begin{matrix} \bullet & \bullet & \cdots & \bullet \end{matrix}\right\}\text{dimension 1} \\ \left\{\begin{matrix} \bullet & \bullet & \cdots & \bullet \end{matrix}\right\}\text{dimension 2} \\ \vdots \\ \left\{\begin{matrix} \bullet & \bullet & \cdots & \bullet \end{matrix}\right\}\text{dimension } d \\ \vdots \\ \text{circuit } l\left\{\begin{matrix} \bullet & \bullet & \cdots & \bullet \end{matrix}\right\}\text{dimension 1} \\ \left\{\begin{matrix} \bullet & \bullet & \cdots & \bullet \end{matrix}\right\}\text{dimension 2} \\ \vdots \\ \left\{\begin{matrix} \bullet & \bullet & \cdots & \bullet \end{matrix}\right\}\text{dimension } d \end{bmatrix}$$

The diagonal elements of $[\boldsymbol{Q}_i]_{C\times C}$ are those of row i of $[\boldsymbol{Q}_A]_{k\times C}$, the fundamental cutset matrix of action graph G_A. The matrix $[\boldsymbol{Q}_A]_{k\times C}$ correspond to the fundamental cutset matrix $[\boldsymbol{Q}]_{k\times e}$ with the column j replicated c_j times.

The structure of matrix in equation (150) is

$$\left[\hat{\boldsymbol{A}}_N\right]_{d\,k\times C} = \begin{bmatrix} \text{cutset 1}\left\{\begin{matrix} \bullet & \bullet & \cdots & \bullet \end{matrix}\right\}\text{dimension 1} \\ \left\{\begin{matrix} \bullet & \bullet & \cdots & \bullet \end{matrix}\right\}\text{dimension 2} \\ \vdots \\ \left\{\begin{matrix} \bullet & \bullet & \cdots & \bullet \end{matrix}\right\}\text{dimension } d \\ \text{cutset 2}\left\{\begin{matrix} \bullet & \bullet & \cdots & \bullet \end{matrix}\right\}\text{dimension 1} \\ \left\{\begin{matrix} \bullet & \bullet & \cdots & \bullet \end{matrix}\right\}\text{dimension 2} \\ \vdots \\ \left\{\begin{matrix} \bullet & \bullet & \cdots & \bullet \end{matrix}\right\}\text{dimension } d \\ \vdots \\ \text{cutset } k\left\{\begin{matrix} \bullet & \bullet & \cdots & \bullet \end{matrix}\right\}\text{dimension 1} \\ \left\{\begin{matrix} \bullet & \bullet & \cdots & \bullet \end{matrix}\right\}\text{dimension 2} \\ \vdots \\ \left\{\begin{matrix} \bullet & \bullet & \cdots & \bullet \end{matrix}\right\}\text{dimension } d \end{bmatrix}$$

meaning that each layer, corresponding to a circuit, is divided in sublayers for each screw dimension consisting of every row of the matrix.

Applying equation (148),

$$\left[\hat{\boldsymbol{M}}_N\right]_{6\times 9} = \left[\begin{array}{ccccccccc} 1 & 1 & 1 & -1 & -1 & -1 & 0 & 0 & 0 \\ 6 & 5 & 4 & 0 & -1 & -2 & 0 & 0 & 0 \\ 0 & -4 & -3 & 1 & 7 & 2 & 0 & 0 & 0 \\ \hdashline 0 & 0 & 0 & -1 & -1 & -1 & 1 & 1 & 1 \\ 0 & 0 & 0 & 0 & -1 & -2 & 6 & 5 & 3 \\ 0 & 0 & 0 & 1 & 7 & 2 & -8 & -6 & -5 \end{array}\right]$$

It is possible to compute a different form of

meaning that each layer, corresponding to a cutset, is divided in sublayers for each screw dimension consisting of every row of the matrix.

Applying equation (150),

$$\left[\hat{\boldsymbol{A}}_N\right]_{21\times 18} = \left[\begin{array}{cccccccccccccccccc} -6 & 0 & 0 & 0 & 4 & -3 & 0 & 0 & 0 & 0 & 0 & 0 & 0 & 0 & 0 & 0 & 0 & 0 \\ 1 & 0 & 0 & 0 & -1 & 0 & 0 & 0 & 0 & 0 & 0 & 0 & 0 & 0 & 0 & 0 & 0 & 0 \\ 0 & 1 & 0 & 0 & 0 & -1 & 0 & 0 & 0 & 0 & 0 & 0 & 0 & 0 & 0 & 0 & 0 & 0 \\ \hdashline 0 & 0 & -5 & 4 & 4 & -3 & 0 & 0 & 0 & 0 & 0 & 0 & 0 & 0 & 0 & 0 & 0 & 0 \\ 0 & 0 & 1 & 0 & -1 & 0 & 0 & 0 & 0 & 0 & 0 & 0 & 0 & 0 & 0 & 0 & 0 & 0 \\ 0 & 0 & 0 & 1 & 0 & -1 & 0 & 0 & 0 & 0 & 0 & 0 & 0 & 0 & 0 & 0 & 0 & 0 \\ \hdashline 0 & 0 & 0 & 0 & -4 & 3 & 0 & 1 & 0 & 0 & 0 & 0 & 0 & 0 & 0 & 0 & -3 & 5 \\ 0 & 0 & 0 & 0 & 1 & 0 & 1 & 0 & 0 & 0 & 0 & 0 & 0 & 0 & 0 & 0 & 1 & 0 \\ 0 & 0 & 0 & 0 & 0 & 1 & 0 & 1 & 0 & 0 & 0 & 0 & 0 & 0 & 0 & 0 & 0 & 1 \\ \hdashline 0 & 0 & 0 & 0 & -4 & 3 & 0 & 0 & -1 & 7 & 0 & 0 & 0 & 0 & 0 & 0 & -3 & 5 \\ 0 & 0 & 0 & 0 & 1 & 0 & 0 & 0 & 1 & 0 & 0 & 0 & 0 & 0 & 0 & 0 & 1 & 0 \\ 0 & 0 & 0 & 0 & 0 & 1 & 0 & 0 & 0 & 1 & 0 & 0 & 0 & 0 & 0 & 0 & 0 & 1 \\ \hdashline 0 & 0 & 0 & 0 & -4 & 3 & 0 & 0 & 0 & 0 & -2 & 2 & 0 & 0 & 0 & 0 & -3 & 5 \\ 0 & 0 & 0 & 0 & 1 & 0 & 0 & 0 & 0 & 0 & 1 & 0 & 0 & 0 & 0 & 0 & 1 & 0 \\ 0 & 0 & 0 & 0 & 0 & 1 & 0 & 0 & 0 & 0 & 0 & 1 & 0 & 0 & 0 & 0 & 0 & 1 \\ \hdashline 0 & 0 & 0 & 0 & 0 & 0 & 0 & 0 & 0 & 0 & 0 & 0 & -6 & 8 & 0 & 0 & 3 & -5 \\ 0 & 0 & 0 & 0 & 0 & 0 & 0 & 0 & 0 & 0 & 0 & 0 & 1 & 0 & 0 & 0 & -1 & 0 \\ 0 & 0 & 0 & 0 & 0 & 0 & 0 & 0 & 0 & 0 & 0 & 0 & 0 & 1 & 0 & 0 & 0 & -1 \\ \hdashline 0 & 0 & 0 & 0 & 0 & 0 & 0 & 0 & 0 & 0 & 0 & 0 & 0 & 0 & -5 & 6 & 3 & -5 \\ 0 & 0 & 0 & 0 & 0 & 0 & 0 & 0 & 0 & 0 & 0 & 0 & 0 & 0 & 1 & 0 & -1 & 0 \\ 0 & 0 & 0 & 0 & 0 & 0 & 0 & 0 & 0 & 0 & 0 & 0 & 0 & 0 & 0 & 1 & 0 & -1 \end{array}\right]$$

It is possible to compute a different form of

matrix $\left[\hat{\boldsymbol{M}}_N\right]_{d\,l\times F}$ by

$$\left[\hat{\boldsymbol{M}}_N\right]_{d\,l\times F} = \begin{bmatrix} [\boldsymbol{B}_M]_{l\times F}\left[\hat{\boldsymbol{M}}_1\right] \\ [\boldsymbol{B}_M]_{l\times F}\left[\hat{\boldsymbol{M}}_2\right] \\ \vdots \\ [\boldsymbol{B}_M]_{l\times F}\left[\hat{\boldsymbol{M}}_d\right] \end{bmatrix}_{d\,l\times F} \tag{151}$$

where $\left[\hat{\boldsymbol{M}}_i\right] = \text{diag}\left(\left[\hat{\boldsymbol{M}}_D\right]_i\right)$ is a diagonal matrices with $i = 1, 2, \ldots, d$. This matrix $\left[\hat{\boldsymbol{M}}_N\right]_{d\,l\times F}$ is different that the matrix given by equation (148). However, the difference regards only the row order so equation (147) holds for $\left[\hat{\boldsymbol{M}}_N\right]_{d\,l\times F}$ given by both equations (148) and (151).

matrix $\left[\hat{\boldsymbol{A}}_N\right]_{d\,k\times C}$ by

$$\left[\hat{\boldsymbol{A}}_N\right]_{d\,k\times C} = \begin{bmatrix} [\boldsymbol{Q}_A]_{k\times C}\left[\hat{\boldsymbol{A}}_1\right] \\ [\boldsymbol{Q}_A]_{k\times C}\left[\hat{\boldsymbol{A}}_2\right] \\ \vdots \\ [\boldsymbol{Q}_A]_{k\times C}\left[\hat{\boldsymbol{A}}_d\right] \end{bmatrix}_{d\,k\times C} \tag{152}$$

where $\left[\hat{\boldsymbol{A}}_i\right] = \text{diag}\left(\left[\hat{\boldsymbol{A}}_D\right]_i\right)$ is a diagonal matrices with $i = 1, 2, \ldots, d$. This matrix $\left[\hat{\boldsymbol{A}}_N\right]_{d\,k\times C}$ is different that the matrix given by equation (150). However, the difference regards only the row order so equation (147) holds for $\left[\hat{\boldsymbol{A}}_N\right]_{d\,k\times C}$ given by both equations (150) and (152).

The structure of matrix in equation (151) is

$$\left[\hat{\boldsymbol{M}}_N\right]_{d\,l\times F} = \begin{bmatrix} \text{dimension 1} \left\{ \begin{matrix} \bullet & \bullet & \cdots & \bullet \\ \bullet & \bullet & \cdots & \bullet \\ & & \vdots & \\ \bullet & \bullet & \cdots & \bullet \end{matrix} \right. \begin{matrix} \} \text{ circuit 1} \\ \} \text{ circuit 2} \\ \\ \} \text{ circuit } l \end{matrix} \\ \text{dimension 2} \left\{ \begin{matrix} \bullet & \bullet & \cdots & \bullet \\ \bullet & \bullet & \cdots & \bullet \\ & & \vdots & \\ \bullet & \bullet & \cdots & \bullet \end{matrix} \right. \begin{matrix} \} \text{ circuit 1} \\ \} \text{ circuit 2} \\ \\ \} \text{ circuit } l \end{matrix} \\ \vdots \\ \text{dimension } d \left\{ \begin{matrix} \bullet & \bullet & \cdots & \bullet \\ \bullet & \bullet & \cdots & \bullet \\ & & \vdots & \\ \bullet & \bullet & \cdots & \bullet \end{matrix} \right. \begin{matrix} \} \text{ circuit 1} \\ \} \text{ circuit 2} \\ \\ \} \text{ circuit } l \end{matrix} \end{bmatrix}$$

and, in this case, each layer corresponding to a dimension is composed by sublayer corresponding to each circuit (one per matrix row).

In this case, using equation (151) instead of (148), the motions matrix is

The structure of matrix in equation (152) is

$$\left[\hat{\boldsymbol{A}}_N\right]_{d\,k\times C} = \begin{bmatrix} \text{dimension 1} \left\{ \begin{matrix} \bullet & \bullet & \cdots & \bullet \\ \bullet & \bullet & \cdots & \bullet \\ & & \vdots & \\ \bullet & \bullet & \cdots & \bullet \end{matrix} \right. \begin{matrix} \} \text{ cutset 1} \\ \} \text{ cutset 2} \\ \\ \} \text{ cutset } k \end{matrix} \\ \text{dimension 2} \left\{ \begin{matrix} \bullet & \bullet & \cdots & \bullet \\ \bullet & \bullet & \cdots & \bullet \\ & & \vdots & \\ \bullet & \bullet & \cdots & \bullet \end{matrix} \right. \begin{matrix} \} \text{ cutset 1} \\ \} \text{ cutset 2} \\ \\ \} \text{ cutset } k \end{matrix} \\ \vdots \\ \text{dimension } d \left\{ \begin{matrix} \bullet & \bullet & \cdots & \bullet \\ \bullet & \bullet & \cdots & \bullet \\ & & \vdots & \\ \bullet & \bullet & \cdots & \bullet \end{matrix} \right. \begin{matrix} \} \text{ cutset 1} \\ \} \text{ cutset 2} \\ \\ \} \text{ cutset } k \end{matrix} \end{bmatrix}$$

and, in this case, each layer corresponding to a dimension is composed by sublayer corresponding to each cutset (one per matrix row).

In this case, using equation (152) instead of (150), the actions matrix is

$$\left[\hat{\boldsymbol{M}}^{\star}_{N}\right]_{6\times 9} = \left[\begin{array}{ccccccccc} 1 & 1 & 1 & -1 & -1 & -1 & 0 & 0 & 0 \\ 0 & 0 & 0 & -1 & -1 & -1 & 1 & 1 & 1 \\ \hdashline 6 & 5 & 4 & 0 & -1 & -2 & 0 & 0 & 0 \\ 0 & 0 & 0 & 0 & -1 & -2 & 6 & 5 & 3 \\ \hdashline 0 & -4 & -3 & 1 & 7 & 2 & 0 & 0 & 0 \\ 0 & 0 & 0 & 1 & 7 & 2 & -8 & -6 & -5 \end{array}\right]$$

Each element of $\left[\hat{\boldsymbol{M}}_{N}\right]_{d\,l\times F}$ in equations (148) and (151) can be expressed by

$$\begin{aligned} \left[\hat{M}_{N}\right]_{\beta+d\,(i-1),\,\alpha} &= \left[\hat{M}_{D}\right]_{\beta,\,\alpha}\,[B_{M}]_{i,\,\alpha} \\ \left[\hat{M}_{N}\right]_{i+l\,(\beta-1),\,\alpha} &= \left[\hat{M}_{D}\right]_{\beta,\,\alpha}\,[B_{M}]_{i,\,\alpha}\ , \end{aligned}$$

respectively, where $\beta = 1,\, 2, \ldots\, d$, $\alpha = 1,\, 2\,\ldots,\, F$, and $i = 1,\, 2, \ldots,\, l$.

$$\left[\hat{\boldsymbol{A}}^{\star}_{N}\right]_{21\times 19} = \left[\begin{array}{ccccccccccccccccccc} -6 & 0 & 0 & 0 & 4 & -3 & 0 & 0 & 0 & 0 & 0 & 0 & 0 & 0 & 0 & 0 & 0 & 0 & 0 \\ 0 & 0 & -5 & 4 & 4 & -3 & 0 & 0 & 0 & 0 & 0 & 0 & 0 & 0 & 0 & 0 & 0 & 0 & 0 \\ 0 & 0 & 0 & 0 & -4 & 3 & 0 & 1 & 0 & 0 & 0 & 0 & 0 & 0 & 0 & 0 & 0 & -3 & 5 \\ 0 & 0 & 0 & 0 & -4 & 3 & 0 & 0 & -1 & 7 & 0 & 0 & 0 & 0 & 0 & 0 & 0 & -3 & 5 \\ 0 & 0 & 0 & 0 & -4 & 3 & 0 & 0 & 0 & 0 & -2 & 2 & 0 & 0 & 0 & 0 & 0 & -3 & 5 \\ 0 & 0 & 0 & 0 & 0 & 0 & 0 & 0 & 0 & 0 & 0 & 0 & -6 & 8 & 0 & 0 & 0 & 3 & -5 \\ 0 & 0 & 0 & 0 & 0 & 0 & 0 & 0 & 0 & 0 & 0 & 0 & 0 & 0 & -5 & 6 & 3 & 0 & -5 \\ \hdashline 1 & 0 & 0 & 0 & -1 & 0 & 0 & 0 & 0 & 0 & 0 & 0 & 0 & 0 & 0 & 0 & 0 & 0 & 0 \\ 0 & 0 & 1 & 0 & -1 & 0 & 0 & 0 & 0 & 0 & 0 & 0 & 0 & 0 & 0 & 0 & 0 & 0 & 0 \\ 0 & 0 & 0 & 0 & 1 & 0 & 1 & 0 & 0 & 0 & 0 & 0 & 0 & 0 & 0 & 0 & 0 & 1 & 0 \\ 0 & 0 & 0 & 0 & 1 & 0 & 0 & 0 & 1 & 0 & 0 & 0 & 0 & 0 & 0 & 0 & 0 & 1 & 0 \\ 0 & 0 & 0 & 0 & 1 & 0 & 0 & 0 & 0 & 0 & 1 & 0 & 0 & 0 & 0 & 0 & 0 & 1 & 0 \\ 0 & 0 & 0 & 0 & 0 & 0 & 0 & 0 & 0 & 0 & 0 & 0 & 1 & 0 & 0 & 0 & 0 & -1 & 0 \\ 0 & 0 & 0 & 0 & 0 & 0 & 0 & 0 & 0 & 0 & 0 & 0 & 0 & 0 & 1 & 0 & 0 & -1 & 0 \\ \hdashline 0 & 1 & 0 & 0 & 0 & -1 & 0 & 0 & 0 & 0 & 0 & 0 & 0 & 0 & 0 & 0 & 0 & 0 & 0 \\ 0 & 0 & 0 & 1 & 0 & -1 & 0 & 0 & 0 & 0 & 0 & 0 & 0 & 0 & 0 & 0 & 0 & 0 & 0 \\ 0 & 0 & 0 & 0 & 0 & 1 & 0 & 1 & 0 & 0 & 0 & 0 & 0 & 0 & 0 & 0 & 0 & 0 & 1 \\ 0 & 0 & 0 & 0 & 0 & 1 & 0 & 0 & 0 & 1 & 0 & 0 & 0 & 0 & 0 & 0 & 0 & 0 & 1 \\ 0 & 0 & 0 & 0 & 0 & 1 & 0 & 0 & 0 & 0 & 0 & 1 & 0 & 0 & 0 & 0 & 0 & 0 & 1 \\ 0 & 0 & 0 & 0 & 0 & 0 & 0 & 0 & 0 & 0 & 0 & 0 & 0 & 1 & 0 & 0 & 0 & 0 & -1 \\ 0 & 0 & 0 & 0 & 0 & 0 & 0 & 0 & 0 & 0 & 0 & 0 & 0 & 0 & 0 & 1 & 0 & 0 & -1 \end{array}\right]$$

Each element of $\left[\hat{\boldsymbol{A}}_{N}\right]_{d\,k\times C}$ in equations (150) and (152) can be expressed by

$$\begin{aligned} \left[\hat{A}_{N}\right]_{\beta+d\,(i-1),\,\alpha} &= \left[\hat{A}_{D}\right]_{\beta,\,\alpha}\,[Q_{A}]_{i,\,\alpha} \\ \left[\hat{A}_{N}\right]_{i+l\,(\beta-1),\,\alpha} &= \left[\hat{A}_{D}\right]_{\beta,\,\alpha}\,[Q_{A}]_{i,\,\alpha}\ , \end{aligned}$$

respectively, where $\beta = 1,\, 2, \ldots\, d$, $\alpha = 1,\, 2\,\ldots,\, C$, and $i = 1,\, 2, \ldots,\, k$.

The matrix equation (147) can be expressed by the following $d\,l$ equations

$$\sum_{\alpha=1}^{F} \left[\hat{M}_D\right]_{\beta,\,\alpha} [\psi]_\alpha \, [B_M]_{i,\,\alpha} = 0 \tag{153}$$

where $\beta = 1,\, 2, \ldots\, d$, $i = 1,\, 2, \ldots,\, l$.

Comparing the motion graph G_M with the coupling graph G_C, one can infer that matrix $[\boldsymbol{B}_M]_{l\times F}$ can be built based on matrix $[\boldsymbol{B}]_{l\times e}$ replicating the column j a number of times equal to the degree of freedom of the direct coupling corresponding to the edge j in the coupling graph. It is also possible to express this relationship in matrix form by

$$[\boldsymbol{B}_M]_{l\times F} = [\boldsymbol{B}]_{l\times e} \, [\boldsymbol{X}_M]_{e\times F}$$

where $[\boldsymbol{X}_M]_{e\times F}$ is a motion index matrix defined by

$$[X_M]_{j,\,\alpha} = \begin{cases} 1 & \text{if } \psi_\alpha \text{ is a magnitude of a montion in edge } j \\ 0 & \text{otherwise} \end{cases}$$

where $j = 1,\, 2,\, \ldots,\, e$ and $\alpha = 1,\, 2,\, \ldots,\, F$. The motion index matrix has an interesting property:

$$[\boldsymbol{X}_M]_{e\times F} \, \left([\boldsymbol{X}_M]_{e\times F}\right)^T = \operatorname{diag}\left(\begin{bmatrix} f_1 & \cdots & f_e \end{bmatrix}\right)$$

where f_j with $j = 1,\, 2,\, \ldots,\, e$ is the degree of freedom

The matrix equation (149) can be expressed by the following $d\,k$ equations

$$\sum_{\alpha=1}^{C} \left[\hat{A}_D\right]_{\beta,\,\alpha} [\Psi]_\alpha \, [Q_A]_{i,\,\alpha} = 0 \tag{154}$$

where $\beta = 1,\, 2, \ldots\, d$, $i = 1,\, 2, \ldots,\, k$.

Comparing the action graph G_A with the coupling graph G_C, one can infer that matrix $[\boldsymbol{Q}_A]_{k\times C}$ can be built based on matrix $[\boldsymbol{Q}]_{k\times e}$ replicating the column j a number of times equal to the degree of constraint of the direct coupling corresponding to the edge j in the coupling graph. It is also possible to express this relationship in matrix form by

$$[\boldsymbol{Q}_A]_{k\times C} = [\boldsymbol{Q}]_{k\times e} \, [\boldsymbol{X}_A]_{e\times C}$$

where $[\boldsymbol{X}_A]_{e\times C}$ is an action index matrix defined by

$$[X_A]_{j,\,\alpha} = \begin{cases} 1 & \text{if } \Psi_\alpha \text{ is a magnitude of an action in edge } j \\ 0 & \text{otherwise} \end{cases}$$

where $j = 1,\, 2,\, \ldots,\, e$ and $\alpha = 1,\, 2,\, \ldots,\, C$. The action index matrix has an interesting property:

$$[\boldsymbol{X}_A]_{e\times C} \, \left([\boldsymbol{X}_A]_{e\times C}\right)^T = \operatorname{diag}\left(\begin{bmatrix} c_1 & \cdots & c_e \end{bmatrix}\right)$$

where c_j with $j = 1,\, 2,\, \ldots,\, e$ is the degree of constraint

of coupling j.

If the motion magnitudes vector is organised in a matrix $[\boldsymbol{\psi}]_{F\times e}$ like

$$[\boldsymbol{\psi}]_{F\times e} = \mathrm{diag}\left([\boldsymbol{\psi}]_F\right)\ \left([\boldsymbol{X}_M]_{e\times F}\right)^T$$

the motion matrix of a coupling network can be expressed as

$$[\boldsymbol{M}]_{d\times e} = \left[\hat{\boldsymbol{M}}_D\right]_{d\times F}\ [\boldsymbol{\psi}]_{F\times e}$$

with one column for each coupling. Therefore

$$\begin{aligned}[\boldsymbol{M}]_{d\times e} &= \left[\hat{\boldsymbol{M}}_D\right]_{d\times F}\ [\boldsymbol{\psi}]_{F\times e}\\ &= \left[\hat{\boldsymbol{M}}_D\right]_{d\times F}\ \mathrm{diag}\left([\boldsymbol{\psi}]_F\right)\ \left([\boldsymbol{X}_M]_{e\times F}\right)^T\end{aligned}$$

A evident equivalent of Kirchhoff voltage law is

$$[\boldsymbol{M}]_{d\times e}\ \left([\boldsymbol{B}]_{l\times e}\right)^T = [\boldsymbol{0}]_{d\times l} \tag{155}$$

can be obtained by multiplying

$$[\boldsymbol{M}]_{d\times e} = \left[\hat{\boldsymbol{M}}_D\right]_{d\times F}\ [\boldsymbol{\psi}]_{F\times e}$$

of coupling j.

If the action magnitudes vector is organised in a matrix $[\boldsymbol{\Psi}]_{C\times e}$ like

$$[\boldsymbol{\Psi}]_{C\times e} = \mathrm{diag}\left([\boldsymbol{\Psi}]_C\right)\ \left([\boldsymbol{X}_A]_{e\times C}\right)^T$$

the action matrix of a coupling network can be expressed as

$$[\boldsymbol{A}]_{d\times e} = \left[\hat{\boldsymbol{A}}_D\right]_{d\times C}\ [\boldsymbol{\Psi}]_{C\times e}$$

with one column for each coupling. Therefore

$$\begin{aligned}[\boldsymbol{A}]_{d\times e} &= \left[\hat{\boldsymbol{A}}_D\right]_{d\times C}\ [\boldsymbol{\Psi}]_{C\times e}\\ &= \left[\hat{\boldsymbol{A}}_D\right]_{d\times C}\ \mathrm{diag}\left([\boldsymbol{\Psi}]_C\right)\ \left([\boldsymbol{X}_A]_{e\times C}\right)^T\end{aligned}$$

A evident equivalent of Kirchhoff current law is

$$[\boldsymbol{A}]_{d\times e}\ \left([\boldsymbol{Q}]_{k\times e}\right)^T = [\boldsymbol{0}]_{d\times k} \tag{156}$$

can be obtained by multiplying

$$[\boldsymbol{A}]_{d\times e} = \left[\hat{\boldsymbol{A}}_D\right]_{d\times C}\ [\boldsymbol{\Psi}]_{C\times e}$$

by $\left([\boldsymbol{B}]_{l\times e}\right)^T$ such that

$$\begin{aligned}
& [\boldsymbol{M}]_{d\times e}\ \left([\boldsymbol{B}]_{l\times e}\right)^T \\
= & \left[\hat{\boldsymbol{M}}_D\right]_{d\times F}\ [\boldsymbol{\psi}]_{F\times e}\ \left([\boldsymbol{B}]_{l\times e}\right)^T \\
= & \left[\hat{\boldsymbol{M}}_D\right]_{d\times F}\ \mathrm{diag}\left([\boldsymbol{\psi}]_F\right)\ \left([\boldsymbol{X}_M]_{e\times F}\right)^T\ \left([\boldsymbol{B}]_{l\times e}\right)^T \\
= & \left[\hat{\boldsymbol{M}}_D\right]_{d\times F}\ \mathrm{diag}\left([\boldsymbol{\psi}]_F\right)\ \left([\boldsymbol{B}]_{l\times e}\ [\boldsymbol{X}_M]_{e\times F}\right)^T \\
= & \left[\hat{\boldsymbol{M}}_D\right]_{d\times F}\ \mathrm{diag}\left([\boldsymbol{\psi}]_F\right)\ \left([\boldsymbol{B}_M]_{l\times F}\right)^T \\
= & \ [\boldsymbol{0}]_{d\times l}\ .
\end{aligned}$$

Therefor the equation (147) can be expressed as

$$\left[\hat{\boldsymbol{M}}_D\right]_{d\times F}\ \mathrm{diag}\left([\boldsymbol{\psi}]_F\right)\ \left([\boldsymbol{B}_M]_{l\times F}\right)^T = [\boldsymbol{0}]_{d\times l}$$

and the scalar form of this equation is identical to equation (153). Then the equation (153) can be rewritten as

$$\sum_{j=1}^{e} [B]_{i,\,j}\ [M]_{\beta,\,j} = 0 \tag{157}$$

where $\beta = 1,\, 2,\, \ldots\, d,\ i = 1,\, 2,\, \ldots,\, l$ and $[B]_{i,\,j}$ is an element of the circuit matrix of coupling graph, $[\boldsymbol{B}]_{l\times e}$.

by $\left([\boldsymbol{Q}]_{k\times e}\right)^T$ such that

$$\begin{aligned}
& [\boldsymbol{A}]_{d\times e}\ \left([\boldsymbol{Q}]_{k\times e}\right)^T \\
= & \left[\hat{\boldsymbol{A}}_D\right]_{d\times C}\ [\boldsymbol{\Psi}]_{C\times e}\ \left([\boldsymbol{Q}]_{k\times e}\right)^T \\
= & \left[\hat{\boldsymbol{A}}_D\right]_{d\times C}\ \mathrm{diag}\left([\boldsymbol{\Psi}]_C\right)\ \left([\boldsymbol{X}_A]_{e\times C}\right)^T\ \left([\boldsymbol{Q}]_{k\times e}\right)^T \\
= & \left[\hat{\boldsymbol{A}}_D\right]_{d\times C}\ \mathrm{diag}\left([\boldsymbol{\Psi}]_C\right)\ \left([\boldsymbol{Q}]_{k\times e}\ [\boldsymbol{X}_A]_{e\times C}\right)^T \\
= & \left[\hat{\boldsymbol{A}}_D\right]_{d\times C}\ \mathrm{diag}\left([\boldsymbol{\Psi}]_C\right)\ \left([\boldsymbol{Q}_A]_{l\times C}\right)^T \\
= & \ [\boldsymbol{0}]_{d\times l}\ .
\end{aligned}$$

Therefor the equation (149) can be expressed as

$$\left[\hat{\boldsymbol{A}}_D\right]_{d\times C}\ \mathrm{diag}\left([\boldsymbol{\Psi}]_C\right)\ \left([\boldsymbol{Q}_A]_{l\times C}\right)^T = [\boldsymbol{0}]_{d\times l}$$

and the scalar form of this equation is identical to equation (154). Then the equation (154) can be rewritten as

$$\sum_{j=1}^{e} [Q]_{i,\,j}\ [A]_{\beta,\,j} = 0 \tag{158}$$

where $\beta = 1,\, 2,\, \ldots\, d,\ i = 1,\, 2,\, \ldots,\, k$ and $[Q]_{i,\,j}$ is an element of the cutset matrix of coupling graph, $[\boldsymbol{Q}]_{k\times e}$.

The mechanical counterpart of a transformation from cutset voltages to edge voltages in an electrical network is

$$[\boldsymbol{M}]_{d\times e} = [\boldsymbol{M}_k]_{d\times k}\,[\boldsymbol{Q}]_{k\times e} \tag{159}$$

where $[\boldsymbol{M}]_{d\times l}$ is a condensed version of motion matrix of a coupling network with one column for each coupling, $[\boldsymbol{M}_k]_{d\times k}$ is the $d\times k$ motion system components for all k cutsets, and $[\boldsymbol{Q}]_{k\times e}$ is the cutset matrix of the coupling graph G_C. Equation (159) allows the computation of all network motion from a minimal set of cutset motions.

Note that, contrary to what the name suggests, the cutset motion is not the motion of a cutset, but the motion of the coupling that gives name to a cutset. Equation (155) can be obtained by multiplying equation (159) by $[\boldsymbol{B}_{l\times e}]^T$ such that

$$\begin{aligned}[\boldsymbol{M}]_{d\times e}\,\left([\boldsymbol{B}]_{l\times e}\right)^T &= \\ [\boldsymbol{M}_k]_{d\times k}\,[\boldsymbol{Q}]_{k\times e}\,\left([\boldsymbol{B}]_{l\times e}\right)^T &= [\boldsymbol{0}]_{d\times l}\end{aligned}$$

since $[\boldsymbol{Q}]_{k\times e}$ and $[\boldsymbol{B}]_{l\times e}$ are orthogonal, thus

The mechanical counterpart of a transformation from loop currents to edge currents in an electrical network is

$$[\boldsymbol{A}]_{d\times e} = [\boldsymbol{A}_l]_{d\times l}\,[\boldsymbol{B}]_{l\times e} \tag{160}$$

where $[\boldsymbol{A}]_{d\times l}$ is a condensed version of action matrix of a coupling network with one column for each coupling, $[\boldsymbol{A}_l]_{d\times l}$ is the $d\times l$ action system components for all l circuits, and $[\boldsymbol{B}]_{l\times e}$ is the circuit matrix of the coupling graph G_C. Equation (160) allows the computation of all network action from a minimal set of circuit actions.

Note that, as the name suggests, the circuit action is the action locked into a circuit. Equation (156) can be obtained by multiplying equation (160) by $\left[\boldsymbol{Q}_{k\times e}\right]^T$ such that

$$\begin{aligned}[\boldsymbol{A}]_{d\times e}\,\left([\boldsymbol{Q}]_{k\times e}\right)^T &= \\ [\boldsymbol{A}_l]_{d\times l}\,[\boldsymbol{B}]_{l\times e}\,\left([\boldsymbol{Q}]_{k\times e}\right)^T &= [\boldsymbol{0}]_{d\times k}\end{aligned}$$

since $[\boldsymbol{Q}]_{k\times e}$ and $[\boldsymbol{B}]_{l\times e}$ are orthogonal, thus

$$[\boldsymbol{Q}]_{k\times e}\left([\boldsymbol{B}]_{l\times e}\right)^T=[\mathbf{0}]_{k\times l}\ .$$

$$[\boldsymbol{B}]_{l\times e}\left([\boldsymbol{Q}]_{k\times e}\right)^T=[\mathbf{0}]_{l\times k}\ .$$